UNIVERSITY OF OKLAHOMA

GRADUATE COLLEGE

A NOVEL METHOD FOR THE CHARACTERIZATION OF ANISOTROPIC MATERIALS

A THESIS

SUBMITTED TO THE GRADUATE FACULTY

in partial fulfillment of the requirements for the

Degree of

MASTER OF SCIENCE

By

ALEXANDER STRINGER
Norman, Oklahoma
2018

A NOVEL METHOD FOR THE CHARACTERIZATION OF ANISOTROPIC MATERIALS

A THESIS APPROVED FOR THE
SCHOOL OF ELECTRICAL AND COMPUTER ENGINEERING

BY

Dr. Jorge Salazar-Cerreño, Chair

Dr. Mark Yeary

Dr. Binbin Weng

Acknowledgments

I would like to begin by thanking everyone who contributed directly to this thesis. First and foremost, I am grateful to Dr. Salazar for all of his guidance, support, and assitance over the past year. I am also grateful to my committee as a whole for their time and input. I appreciate all of the assisstance I received from the other members of the PAARD team. Special thanks to Zeeshan, Alessio, and Jose, all of whom were central in the development of this project. My gratitude also goes to Redmond, Jonathan, and the other members of the ARRC engineering team. Their input during the design process and assisstance during assembly of the system were invaluable.

I would also like to express my sincerest thanks to my wife, Eileen. She has been my greatest source of strength and joy for the past 13 years, and her unwavering support during my time in graduate school has helped to make this possible. In addition, I owe much of my academic success to my mother, Dr. Gillian Bond. She instilled in me a deep respect for education and hard work, and has consistently served as an example of everything an engineer should be.

Finally, I would like to thank my good friends and colleagues Andrew, Brian, and Lacey, with whom I got to share to the graduate school experience. Working alongside them in my classes has helped me to grow as an engineer, and spending time with them outside of class has helped me to grow as a person. I know they will all go far in life.

Table of Contents

List Of Figures

Abstract

This thesis details the successful conceptualization, development, and proof of concept testing of a novel system for the characterization of a material's electromagnetic properties. In particular, the proposed system was designed to allow for the future wideband characterization of the permittivity and permeability of anisotropic solids at oblique angles of incidence. The characterization of these properties is crucial to understanding how a material will perform as a substrate in electronics and RF applications. Various techniques have been developed to characterize these properties for the case of normal incidence based the test material's inductive/capactive, resonant, and transmission/reflection characteristics. For isotropic materials, the electromagnetic parameters have no angle dependence and normal incidence testing is sufficient. However, the increasingly widespread development and use of inhomogenous composites and artificial dielectrics/diamagnetics has necessitated the development of methods to characterize materials over a range of incidence angles. The proposed system accomplishes this without the limitations of currently existing methods (such as the need for multiple sample configurations or the assumption of non-magnetic behavior).

First, the theory used in the electromagnetic characterization of materials is discussed. Then, the various characterization methods currently used are examined, followed by an overview of the calibration and extraction algorithms developed for use with the free space characterization of materials. Next, the development of the proposed system is detailed, including the initial concept, design model iterations,

and final implementation. The testing used to prove out the system concept is then described. This included the successful characterization of four materials (FR4, 5880, 4350B, and Rohacell) at normal incidence, and successful measurement of the S-parameters with respect to incidence angle for both an isotropic material (FR4) and an anisotropic engineered material (a frequency selective surface). Finally, additional work is proposed to further inproved the system. The conceptualization, design, implementation, and proof of concept testing for this system was successfully completed in only six months, on a budget below $8,000.

Chapter 1

Introduction

1.1 Motivation

The widespread integration of wireless and radar applications into government and industry applications has created the need to develop new antennas and arrays that meet increasingly complex and difficult requirements. There is contantly a need for antennas that operate over wider bandwidths, at higher frequencies, with longer ranges, narrower beamwidths, and lower cross-polarizations, among other things. One of the key ways to improve antennas in order to meet these demands is to identify and design more effective dielectric and diamagnetic substrate materials. This has led to use of engineered composite materials in antenna substrates to achieve dielectric performances not found in naturally occuring materials. This thesis was part of a project that is attempting to develop a multiband radar system that utilizes an engineered substrate whose dielectric behavior changes significantly with respect to frequency.

The proper design of this substrate material will depend on an accurate understanding of how the material interacts with applied electromagnetic fields. This

behavior is quantified in two parameters: electric permittivity and magnetic permeability. These parameters are derived from the constitutive relations of electromagnetics, and are therefore commonly referred to as the electromagnetic constitutive parameters. Various methods have been developed to characterize the electromagnetic constitutive parameters of materials, each of which have different strengths and limitations. The particular characterization approach that is used will depend on the design requirements of the system for which the material is to be used. This thesis will examine these approaches to identify the one that best applies to the characterization of the aforementioned engineered material. A test system with then be designed and built that is capable of the characterization of such a material.

1.2 Literature Review

The characterization of electrical permittivity and magnetic permeability (constitutive parameters) is central to the development of components for a wide range of applications, and it has therefore been the subject of a great deal of research. As such, a wide variety of characterization methods have been developed. Each of these methods use the relationship between the constitutive parameters and some readily measurable electromagnetic property of materials. Based on which property is being measured (and how they are measured), these characterization methods can be divided into four broad categories: 1) Inductance/Capacitance Methods, 2) Resonance methods, 3) Transmission Line Transmission-Reflection metods, and 4) Free-Space Transmission-Reflection methods. Each method has its own strengths

and weaknesses, and the selections of a particular method depends largely on the requirements of the application for which a material is being characterized.

The Inductance/Capacitance method relies on the relationship between the constitutive parameters and the inductive and capacitive behaviors of a material. It is described in [1] and [2]. For this type of characterization, the material is placed in a circuit configuration, and the change it introduces to the inductance or capacitance of the circuit is measured. This method is widely used because it is straightforward to carry out and has low computational requirements. However, it is only viable for low frequencies below 1 GHz [2]. It also requires two different setups and two different sample configurations, one for inductance and one for capacitance. It is also requires significant machining of the sample being tested, making it difficult to use with non-uniform materials.

The Resonant method relies on measurement of the resonant frequency and quality factor to extract a materail's constitutive parameters. It is described in [1], [2], [3], and [4]. This method is the most accurate of the available techniques. However, it is only viable for measurements at the resonant frequency, limiting it usefulness for wideband applications or the characterization of dispersive materials. It is also has high computational requirements.

The Transmission Line Tansmission/Reflection method uses the transmission and reflection characteristics of materials in a transmission line to determine the constitutive parameters. This method is relatively simple to implement, and can be used over an extremely wide range of frequencies (only limited by the dimensions of the available transmission lines). It can also be used to characterize materials in

a wide range of states (solids, liquids, gases, powders), only requiring modification of the sample holder and calibration method. Due to this, it has become one of the most widely used characterization method, and is described in [5], [6], [7], [8], [9], [10], [11], and [12]. However, it is difficult to measure the constitutive parameters of a material at oblique angles of incidence using this approach.

The Free-Space Transmission-Reflection method uses the transmission and reflection characteristics of materials in free space to determine the constitutive parameters. It is straightforward to implement, and can be applied over an extremely wide range of frequencies, limited only by the available RF equipment. The test setup itself is also easily reconfigured, making the characterization of materials at oblique incidence angles possible. This method is described in [13], [14], [15], [16], [17], [18], [19], [20], [21], and [12]. However, this test setup is large, requires large samples, and is limited by the beam-width and far-field range of the antennas [22]. For this reason, Gaussian beams focused by dielectric lenses are often used to help reduces the size of the test setup and samples, as described in [17], [22], [23], [24], [25], and [26].

The development of engineered materials with designed electromagnetic properties not found in nature has opened up significant opportunities in the fields of radar and wireless communications. The design and behavior of such engineered materials is described in [27], [28], [29], [30], [31], [32], [33], [4], [34], [19], [35], and [36]. While these materials present great oppotunities, they are also challenging to characterize. Engineered materials typically exhibit both dispersive and anisotropic behavior, requiring characterization over a wide range of frequencies at multiple

incidence angles. These materials also frequently include periodic metallic inclusions, causing them to exhibit both dielectric and diamagnetic behaviors. While these engineered materials are composites, when they are used as substrate materials it is generally desirable to treat them as though they were simpler, homogenous materials with homogenized effective parameters. This can be accomplished using effective medium approximation, which is discussed in [15], [37], and [38]. Modelling of the effective constitutive parameters of such materials can be achieved with the Drude-Lorentz model, as described in [39] and [40], or Vector Fitting [41].

Due to the behaviors of engineered materials, the Free-Space Transmission-Reflection method is generally the most viable approach for characterization of such materials. The free-space characterization of engineered materials requires calibration of the system in order to mitigate noise ([42], [43], and [44]) and uncertainty ([45], [22], and [46]) in the measurement. Common free-space calibration approaches include the TR method described in [47] and [22], the TRL method described in [48], and the LNN and LRR methods described in [49]. Review of free-space calibrations can be found in [50] and [51]. Additionally, free-space characterization is typically done using a Vector Network Analyzer (VNA). Calibration of these systems is described in [52], [53], [54], [55], and [56]. The measurement errors in free-space characterization can be further reduced by applying time domain gating, as presented in [57] and [22].

Once a free-space characterization system has been calibrated, measurements have been made, and gating is applied, the constitutive parameters are extracted using and extraction algorithm. A variety of algorithms have been developed, which

either directly or iteratively compute the constitutive parameters of a material based on the transmission and reflection measurements. Good overviews of the more widely used extraction algorithms are provided in [58], [22], and [59].

Direct computation algorithms include the Nicolson-Ross-Weir (NRW) method, which was developed in [60] and [61] (and is succinctly explained in [62]), and the Smith algorithm proposed in [63]. Applications of these algorithms to the characterization of engineered materials at normal incidence are described in [64], [65], and [66]. These algorithms are widely used because they are simple and have low computational requirements. However, the parameters extracted using such algorithms are non-unique due to the branching of the computed complex logarithm. This branch ambiguity occurs when the sample thickness becomes large with respect to the wavelength of the transmitted signal travelling through it, and is explained in [58] and [27]. If the approximate values of the constitutive parameters are known, this ambiguity can be avoided by using thin samples. In order to overcome this ambiguity without prior knowledge of the sample properties, one of two approaches can be applied. The first of these is the Kramers-Kronig approach, which relies on the application of a truncated form of the well know Kramers-Kronig integral, as described in [67], [68], [69], [70], [71], and [72]. The other is the phase unwrapping approach described in [73] and [74].

Iterative algorithms recursively use a direct calculation method coupled with an optimization cost function to determine the values of the constitutive parameters. Such algorithms are described in [5], [75], [76], [77], [78], and [79], and have the

benefit of being unique. However, they are much more complex and computationally costly than the direct computation methods.

The simultaneous measurement of the free-space reflection and transmission characteristics of materials is non-trivial. As such currently available systems typically assume either constant permittivity or constant permeability. This allows the other parameter to be extracted using only transmission measurements (as in [80], [81], [82], [83], and [84]) or reflection measurements (as in [82], [85], [86], [87], and [88]). However, as explained above, this assumption cannot be reliably made with engineered materials. Due to this, significant work has been done to expand the free-space characterization extraction algorithms to the oblique incidence case using both transmission and relection measurements: [89], [90], [91], [92], [93], [94], [64], [95], and [96]. However, due to the lack of availability of a measurement system for the oblique incidence case, these algorithms have only been applied to simulated data.

1.3 Problem Statement

The desired behavior of the engineered material being designed will utimately require the non-destructive characterization of a flat sheet of material from 2-10 GHz. Due to the anisotropic nature of the artificial dielectric material being designed, it will be necessary to characterize the permittivity of the material at oblique incidence angles. These requirements make the free-space transmission-reflection approach the most viable characterization technique for this application. However, the metallic

inclusion used in the design to achieve the desired behavior will make it necessary to also characterize the permeability of the material at oblique angles of incidence. Existing free-space systems either assume that the material is non-magnitc, or else have high costs, testing times, and complexity due to the need for focussing lenses and/or multiple test configurations. As such, a novel approach to free-space characterization using three mobile polyrod antennas will be used for the design of this characterization system. This will allow for the full characterization of a material at oblique incidence angles using a single test setup without the need for focussing lenes.

1.4 Organization of the Thesis

This thesis is organized as follows. It begins with a review of the applicable electromagnetic concepts in Chapter 2. This begins with an examination of permittivity and permeability, followed by their relationship to the transmission and reflection characteristics of materials, discussions of dispersion and anisotropy in materials, and then concludes with an overview of metamaterials and effective medium approximation. Chapter 3 examines existing material characterization techniques. First, the commonly used mearurement approaches are examined, and the one that most effectively allows for the wideband characterization of anisotropic materials at oblique angles of incidence is identified. Then, the sources of error and uncertainty for the identified method are described, along with the design, calibration, and post-processing techniques that can be used to mitigate them. Finally, Chapter

3 examines the extraction algorithms that have been developed for use with the selected measurement approach. Chapter 4 focuses on the novel characterization system designed for this thesis. In this chapter, the problems with existing test apparatus is explained, the design approach is presented, and the design, assembly, and proof of concept testing of the system is described. This thesis then concludes with Chapter 5, which presents the current status of the project and the next steps that should be taken in the continued development/improvement of the novel system.

Chapter 2

Electromagnetic Properties of Materials

2.1 Introduction

As discussed above, this thesis examines various methods to characterize a material's response to applied electromagnetic fields, with a focus on those that apply to the characterization of anisotropic materials. Prior to beginning an examination of these techniques, it will be helpful to review some of the key concepts that are referenced throughout this thesis. In particular, the macroscopic material properties that are used to describe the way that materials interact with electromagnetic fields are described. The way in which these properties affect the reflection and transmission of energy by a material is also discussed. The material properties of dispersion and anisotropyare examined, with a particular focus on the complexities they add to the constitutive parameters Finally, an overview of metamaterials, their design/composition, and the particular challenges involved in characterizing them is provided.

2.2 Material Characteristics

The behavior of electric and magnetic fields in a material can be described by its permittivity and permeability, respectively. A material's electric permittivity

(denoted as ϵ) reflects the ability of charges within the material to polarize when an electric field is applied to it. It is the parameter that is used to relate an electric field applied to a material to the electric flux density produced by that field within the material. Equivalently, a material's magnetic permeability (denoted as μ) reflects the ability of magnetic dipoles within the material to align with the application of a magnetic field to the material. It is used to relate magnetic fields applied to the material with the magnetic flux density produced by those fields within the material. In electromagnetics, these two relationships are referred to as the constitutive relationships, and in their most basic form are written as:

$$D = \epsilon E \,, \tag{2.1}$$

$$H = \frac{B}{\mu} \,, \tag{2.2}$$

Due to their use in these constitutive relationships, permittivity and permeability are often referred to as the constitutive parameters of electromagnetics. These parameters and the associated relationships are described in detail in [97] and [34].

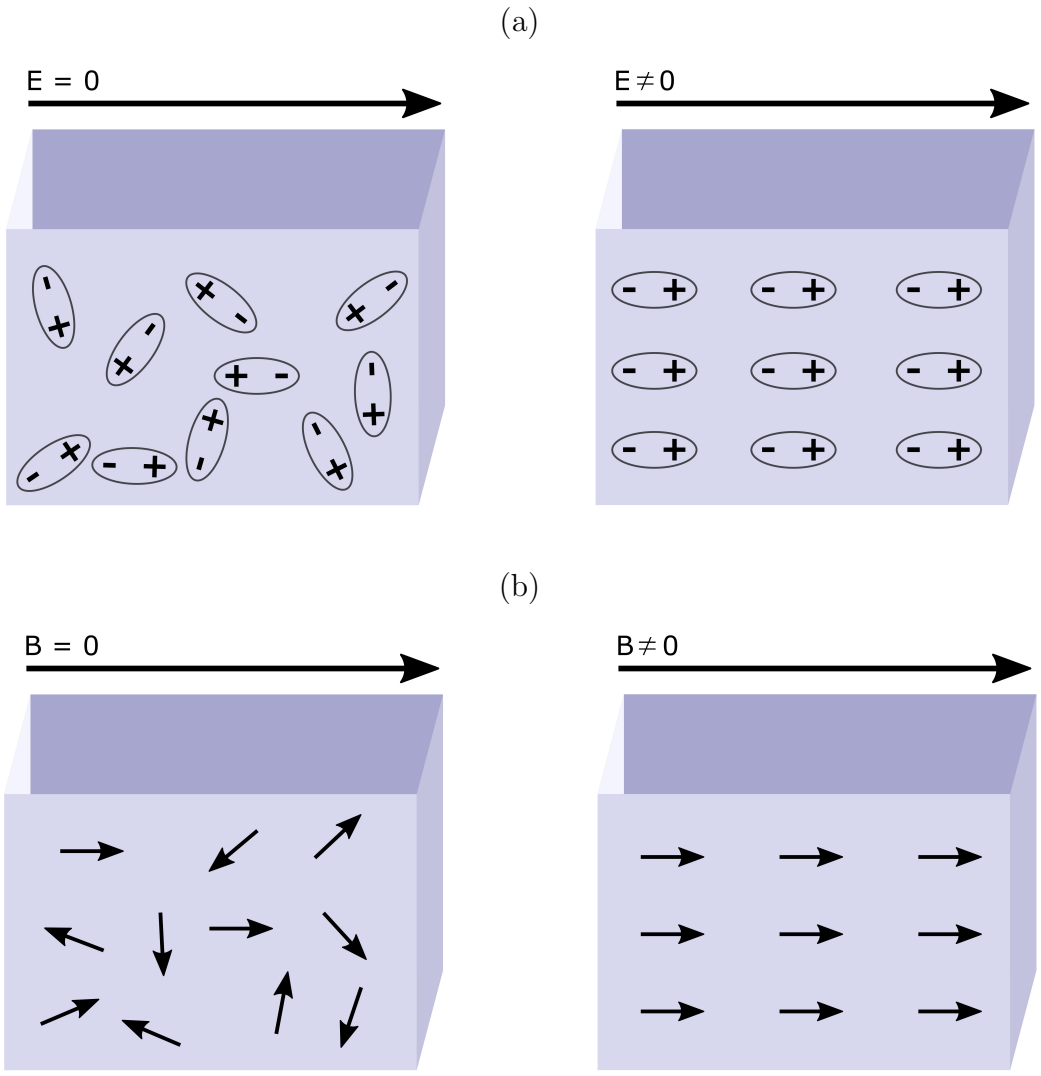

Figure 2.1: Charge/dipole alignment as a result of applied electric/magnetic field. a) Charge alignment with applied electric field. b) Dipole alignment with applied magnetic field.

Despite the apparent simplicity of the relationships in Equations 2.1 and 2.2, the values of permittivity and permeability are rarely simple real numbers in actual materials. To begin with, both permittivity and permeability have complex values

in many materials. The complex forms of the constitutive parameters are commonly written as:

$$\epsilon = \epsilon^{'} + j\epsilon^{''}\,, \tag{2.3}$$

$$\mu = \mu^{'} + j\mu^{''}\,. \tag{2.4}$$

In Equation 2.3, $\epsilon^{'}$ is the real part of the permittivity, which represents the material's ability to absorb electric fields. Conversely, the imaginary term in Equation 2.3 ($\epsilon^{''}$) represents the energy that is dissipated (or lost) by the material when an electric field is applied. Similarly, the real term in Equation 2.4 represents the material's ability to store applied magnetic fields, while the imaginary term corresponds to the energy dissipated when magnetic fields are applied. The ratio between the imaginary and real components of each the permittivity and permeability are known as the dielectric and magnetic loss tangents, respectively, and are denoted as:

$$tan\,(\delta_{\epsilon}) = \frac{\epsilon^{''}}{\epsilon^{'}}\,, \tag{2.5}$$

$$tan\,(\delta_{\mu}) = \frac{\mu^{''}}{\mu^{'}}\,. \tag{2.6}$$

Those materials that have extremely low dissipation terms are known as (electrically/magnetically) lossless media. Only in the case of lossless media can the constitutive parameters can be thought of as real valued.

As well as commonly being complex valued, both permittivity and permeability may be functions that may have one or more dependency based on the characteristics of the material. For the purposes of this thesis, there are two dependencies worth

mentioning: frequency and spatial [22]. These dependencies will be discussed later in this chapter.

As a final note on the constitutive parameters, it is important to understand that the more commonly reported/used values of permittivity and permeability are normalized with respect to the permittivity/permeability of free space [97]. These normalized values are called the relative permittivity/permeability, and are denoted:

$$\epsilon_r = \frac{\epsilon}{\epsilon_0}\,, \tag{2.7}$$

$$\mu_r = \frac{\mu}{\mu_0}\,. \tag{2.8}$$

These free space values of these parameters are denoted ϵ_0 and μ_0, and have values of 8.8541878210-12 (Farads/meter) and 1.2566370610-6 (Henries per meter), respectively. Free space is considered both an electrically and magnetically lossless medium.

Two additional material characteristics that are directly related to the constitutive parameters of a material are crucial to characterizing the electromagnetic behavior of a material. These two characteristics are the refractive index and the wave impedance of the material. A material's refractive index indicates the degree to which a propagating electromagnetic wave slows when travelling through that material. Specifically, it is the ratio of the speed of energy in free space to the speed of energy in the material. A material's wave impedance refers to the ratio of the

tangential electric and magnetic fields that arise within the material when an electromagnetic wave propagates through it ([97] and [34]). The refractive index and wave impedance of a material are related to its relative constitutive parameters by:

$$n = \sqrt{\epsilon_r \mu_r}\,, \tag{2.9}$$

$$\eta = \frac{\sqrt{\mu_r}}{\sqrt{\epsilon_r}}\,. \tag{2.10}$$

2.3 Reflection-Transmission Characteristics of Materials

As depicted in Figure 2.2 a), electromagnetic waves each travel in a particular direction, which can be represented by vectors in three-dimensional space. When travelling through free space (or some other homogenous medium), the direction of these waves will not change unless they are acted upon by some external field [97]. Figure 2.2 b) shows what happens when an EM wave interacts with the interface between two media with different electromagnetic characteristics. Here, the initial wave is assumed to be travelling perpendicular to the interface. As a wave propagating through the first medium encounters this interface, some portion of the energy passes through it and begins propagating through the second medium. This portion of the incident wave is known as the transmitted energy. The rest of the energy (assuming no losses) bounces off of the interface and continues propagating through

the first medium, but in the opposite direction. This portion of the incident wave is referred to as the reflected energy.

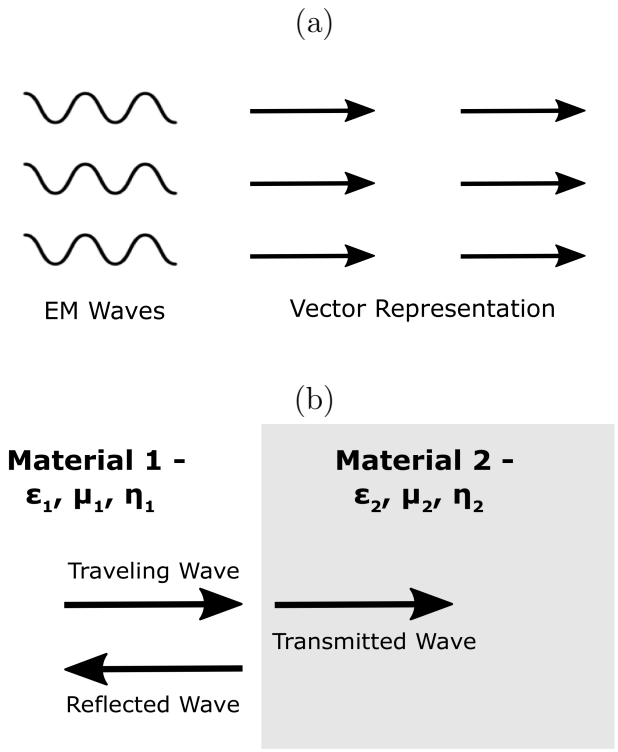

Figure 2.2: Electromagnetic wave propagation. a) Electromagnetic wave propagation through free space. b) Electromagnetic wave propagation at the interface between two media.

Understanding and being able to properly model the reflection and transmission of electromagnetic energy at the interface between two media is extremely important in most application of electromagnetics, and particularly so in radar systems. This is because they are two of the characteristics that primarily impact antenna patterns. They are quantified using parameters known as the reflection coefficient (Γ) and the

transmission coefficient (T). These coefficients are directly related to the mismatch in the wave impedance between the two materials at the interface:

$$\Gamma = \frac{\eta_2 - \eta_1}{\eta_2 + \eta_1}\,, \tag{2.11}$$

$$T = \frac{2\eta_2}{\eta_2 + \eta_1}\,. \tag{2.12}$$

where η_1 and η_2 are the wave impedances of the first and second materials (see Figure 2.2), respectively. Using equation 2.10 above, the reflection and transmission coefficients at an interface can be expressed as functions of the relative permittivities and permeabilities of each medium:

$$\Gamma = \frac{\sqrt{\mu_{r2}\epsilon_{r1}} - \sqrt{\mu_{r1}\epsilon_{r2}}}{\sqrt{\mu_{r2}\epsilon_{r1}} + \sqrt{\mu_{r1}\epsilon_{r2}}}\,, \tag{2.13}$$

$$T = \frac{2\sqrt{\mu_{r2}\epsilon_{r1}}}{\sqrt{\mu_{r2}\epsilon_{r1}} + \sqrt{\mu_{r1}\epsilon_{r2}}}\,. \tag{2.14}$$

Equations 2.11 – 2.14 are the simplest expressions for the reflection and transmission coefficients and are only valid for the case of a wave normally incident upon a single interface between two simple media. As with the constitutive parameters, reflection and transmission are typically also dependent on the frequency and angle of incidence of the exciting wave. Figure 2.3 a) illustrates what happens when an electromagnetic wave encounters an interface at an angle Θ_i. In this case, it can be seen that both the transmitted and reflected energy begin travelling along entirely new paths, defined by the angle of refraction (Θ_t) and the angle of reflection (Θ_r) at

the interface. These two angles can be calculated by Snell's laws of refraction and reflection:

$$n_1 sin(\Theta_i) = n_2 sin(\Theta_t)\,, \tag{2.15}$$

$$\Theta_i = \Theta_r\,. \tag{2.16}$$

Figure 2.3 b) shows what happens when the exciting wave encounters multiple interfaces. It is apparent that each interface between media results in its own reflection and transmission (and refraction in the case of oblique incidence). It should also be observed that the energy reflected by each interface after the first then encounters the interface though which it was previously transmitted, resulting in multiple reflections occurring within the interior mediums ([97] and [34]).

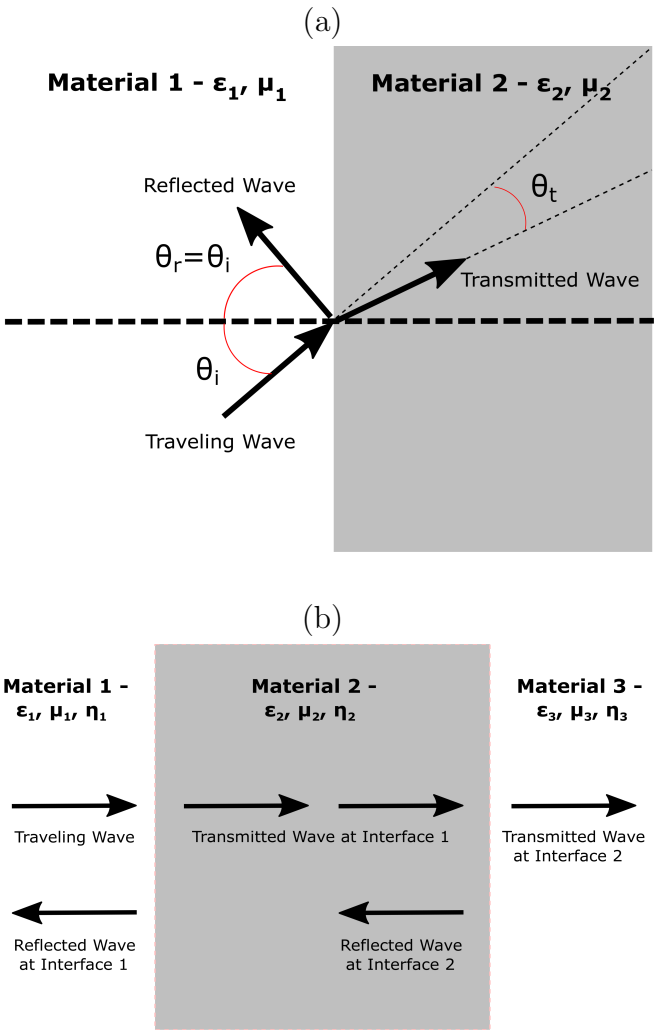

Figure 2.3: Electromagnetic wave propagation at oblique incidence. a) Electromagnetic waves obliquely incident upon the interface between regions. b) Electromagnetic wave propagation at multiple interfaces.

2.4 Dispersion

Earlier in this chapter, the electromagnetic constitutive parameters of materials were reviewed, along with their most basic mathematic forms. At that time it was also

mentioned that there are two key dependencies exhibited by the constitutive parameters of certain types of materials: frequency and spatial. Those dependencies will now be examined in more detail, leading to expanded mathematical representations of permittivity and permeability. The first of the aforementioned key dependencies to be examined here will be the frequency dependence.

As was discussed previously, the permittivity and permeability of a material refer to the polarization/alignment of electical charges and magnetic dipoles (respectively) within the material when a field is applied to it. The basic forms of these relationships provided in Equations 2.1 - 2.4 assume that the polarization/alignment of charges/dipoles occurs instantaneously. However, this assumption can not always be reliably made. Often is takes a non-negligible period of time for the charges/dipoles of a material to polarize/align when exposed to external fields. This results in different frequencies of energy traveling through such materials at different rates. This effect is known as dispersion, referring to the way in which different frequencies of energy will seperate, or disperse, from one another when travelling through such a medium (see Figure 2.4). This effect is described in detail in [34], and a good summary is provided in [22].

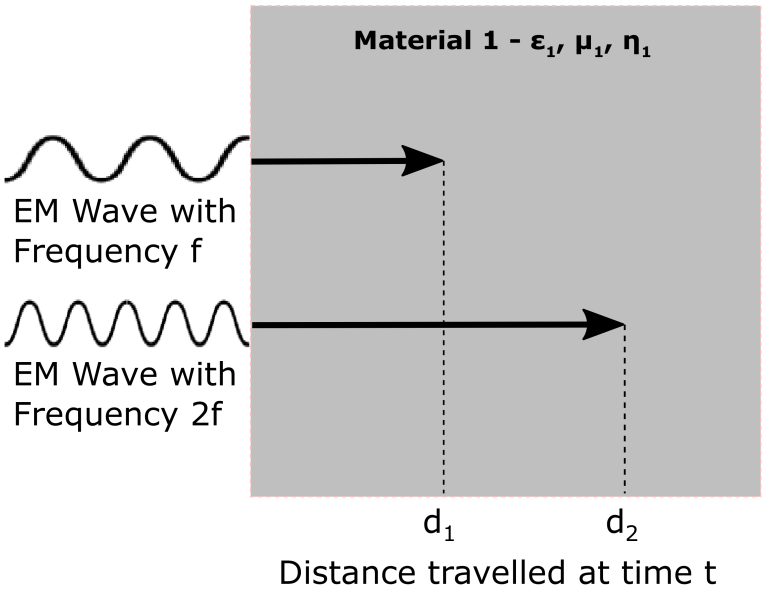

Figure 2.4: Electromagnetic waves in a dispersive medium.

The rate at which electromagnetic energy travels through a given medium is directly related to the refractive index of that medium by:

$$n = \frac{c}{v}\,, \tag{2.17}$$

where n is the refractive index of the medium, c is the speed of light, and v is the velocity of the electromagnetic energy travelling through the medium. Rearranging and using Equation 2.9, this becomes:

$$v = \frac{c}{\sqrt{\epsilon_r \mu_r}}\,. \tag{2.18}$$

From Equation 2.18 it can be seen that the dispersion of different frequencies of electromagnetic waves in a material necessarily reflects a change in the permittivity or permeability (or both) of that material depending on the frequency of the exciting

waves. For materials that display this sort of dispersive behavior, Equations 2.3 and 2.4 become:

$$\epsilon = \epsilon^{'}(\omega) + j\epsilon^{''}(\omega) \ , \tag{2.19}$$

$$\mu = \mu^{'}(\omega) + j\mu^{''}(\omega) \ , \tag{2.20}$$

Figure 2.5 depicts the kind of frequency dependance displayed by the constitutive parameters of dispersive materials.

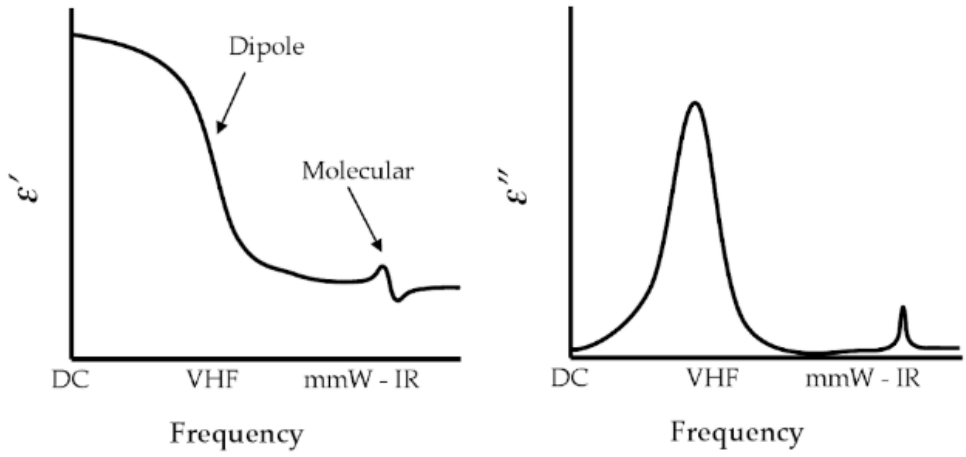

Figure 2.5: Real and imaginary permittivity of dispersive materials [22].

2.5 Anisotropy

As well as assuming the instantaneous polarization/alignment of electric charges/ magnetic dipoles, Equation 2.1 - 2.4 are based on another major assumption. These simplified expressions for the constitutive parameters hold true only if the polarization/orientation of charges/dipoles within a material occurs in the exactly the same direction as the exciting field applied to that matieral. However, as with the

previous assumption, this is frequently not the case. In many instances, some combination of a material's properties and composition make is easier for charges/dipoles to polarize/align in some directions than in others. As a result, such materials will react differently to energy fields and waves depending on the direction along which the field/wave interacts with them (see Figure 2.6). This type of nonuniform propogation of electric and magnetic energy is generally referred to as electromagnetic anisotropy. This effect is described in detail in [34], and a good summary is provided in [22].

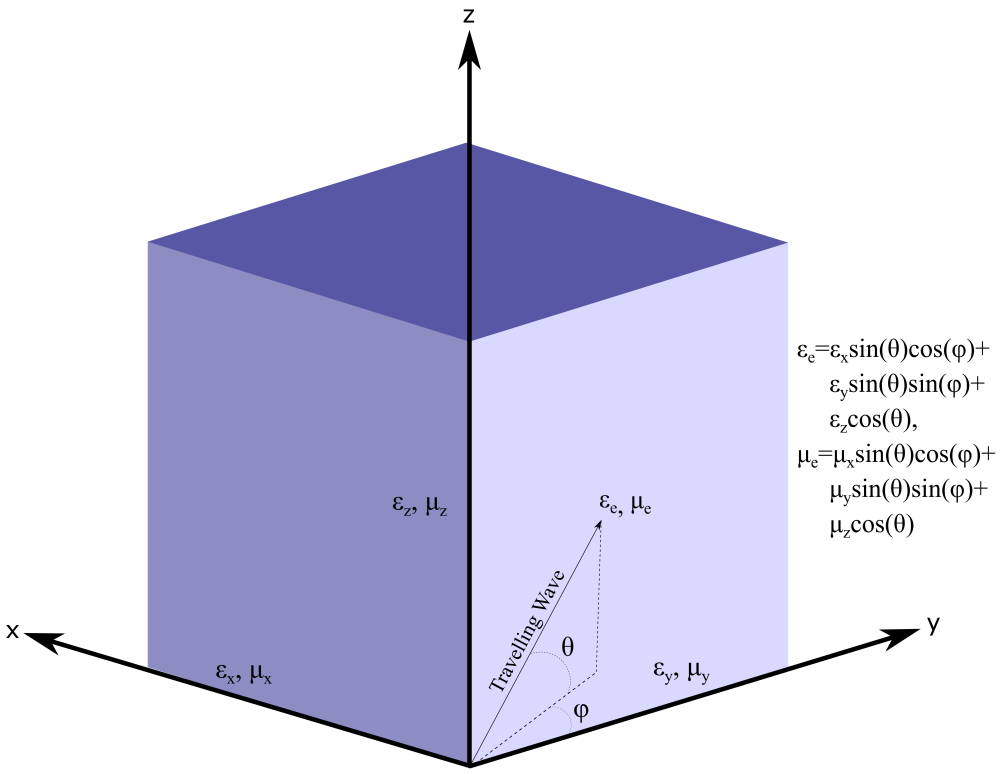

Figure 2.6: Angle dependence of electromagnetic characteristics.

While a number of factors may contribute to the electromagnetic anisotropy of a material, it can typically be attributed to two things. The first of these is at the

atomic level [34]. The particular arrangement of atoms within a material can make is significantly easier for electrons to move/orbit along certain axes than others. The result is that the charges and dipoles present in the material can be more easily polarized/aligned in those directions, allowing energy to be more easily propoated. This phenomenon is depicted in Figure 2.7.

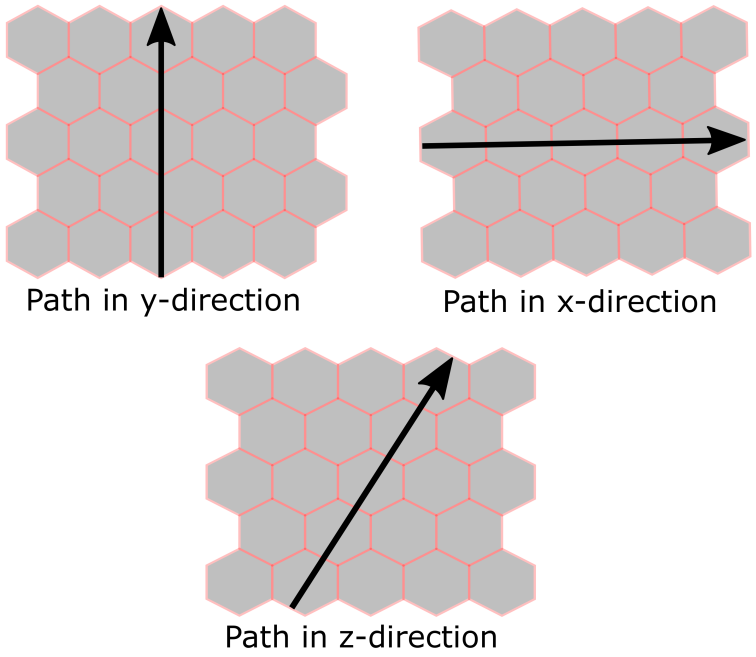

Figure 2.7: The impact of the atomic structure of materials on anisotropy.

The second primary cause of electromagnetic anisotropy in materials occurs at the macroscopic level, and is of particular interest to the field of antennas (and to this thesis in particular). It is the non-uniform composition of many materials [22]. In the continuing endeavors to improve antenna performance and taylor them to specific applications, designs now make regular use of composite materials. Such materials are made up of multiple other materials which can be distributed in layers, periodic structures, or even randomly. The component materials in composites typically

have different electromagnetic properties, meaning that the overall properties of the composite in a particular direction may vary significantly depending on the thickness of each component material that would be encountered by energy travelling through the material in that direction (see Figure 2.8).

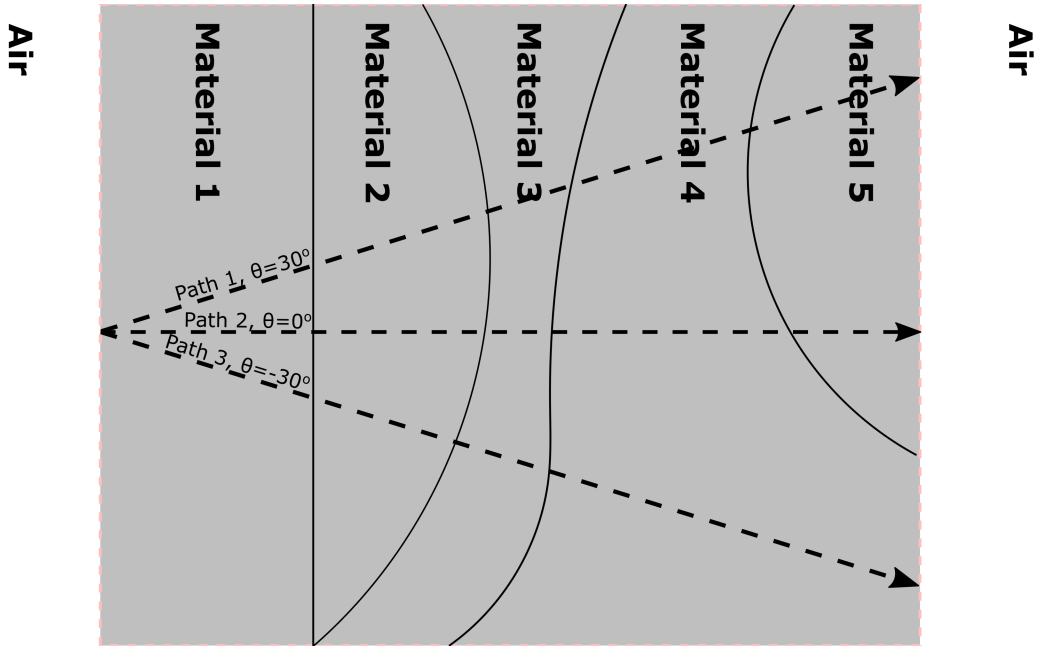

Figure 2.8: The impact of material composition on anisotropy.

Anisotropy in a material is reflected in a spatial (or angular) dependence of the constitutive parameters. In order to fully characterize the electromagnetic behavior of these anisotropic materials, one has to know the storage and dispersion characteristics along each direction for a given exciting wave normally or obliquely incident

upon the surface of the material. As such, rather than the integer values used in Equations 2.3 and 2.4, permittivity and permeability instead become tensors:

$$\epsilon = \begin{bmatrix} \epsilon_{xx} & \epsilon_{xy} & \epsilon_{xz} \\ \epsilon_{yx} & \epsilon_{yy} & \epsilon_{yz} \\ \epsilon_{zx} & \epsilon_{zy} & \epsilon_{zz} \end{bmatrix} \tag{2.21}$$

$$\mu = \begin{bmatrix} \mu_{xx} & \mu_{xy} & \mu_{xz} \\ \mu_{yx} & \mu_{yy} & \mu_{yz} \\ \mu_{zx} & \mu_{zy} & \mu_{zz} \end{bmatrix} \tag{2.22}$$

At this stage Equations 2.1 and 2.2 become:

$$\begin{bmatrix} D_x \\ D_y \\ D_z \end{bmatrix} = \begin{bmatrix} \epsilon_{xx} & \epsilon_{xy} & \epsilon_{xz} \\ \epsilon_{yx} & \epsilon_{yy} & \epsilon_{yz} \\ \epsilon_{zx} & \epsilon_{zy} & \epsilon_{zz} \end{bmatrix} \begin{bmatrix} E_x \\ E_y \\ E_z \end{bmatrix} \tag{2.23}$$

$$\begin{bmatrix} H_x \\ H_y \\ H_z \end{bmatrix} = \begin{bmatrix} \mu_{xx} & \mu_{xy} & \mu_{xz} \\ \mu_{yx} & \mu_{yy} & \mu_{yz} \\ \mu_{zx} & \mu_{zy} & \mu_{zz} \end{bmatrix} \begin{bmatrix} B_x \\ B_y \\ B_z \end{bmatrix} \tag{2.24}$$

Recalling that each entry in Equations 2.21 and 2.22 may be complex and/or functions with frequency dependencies, it is now possible to arrive at more complete expressions for permittivity and permeability:

$$\epsilon = \begin{bmatrix} \epsilon_{xx}^{'}(\omega) + \epsilon_{xx}^{''}(\omega) & \epsilon_{xy}^{'}(\omega) + \epsilon_{xy}^{''}(\omega) & \epsilon_{xz}^{'}(\omega) + \epsilon_{xz}^{''}(\omega) \\ \epsilon_{yx}^{'}(\omega) + \epsilon_{yx}^{''}(\omega) & \epsilon_{yy}^{'}(\omega) + \epsilon_{yy}^{''}(\omega) & \epsilon_{yz}^{'}(\omega) + \epsilon_{yz}^{''}(\omega) \\ \epsilon_{zx}^{'}(\omega) + \epsilon_{zx}^{''}(\omega) & \epsilon_{zy}^{'}(\omega) + \epsilon_{zy}^{''}(\omega) & \epsilon_{zz}^{'}(\omega) + \epsilon_{zz}^{''}(\omega) \end{bmatrix} \tag{2.25}$$

$$\mu = \begin{bmatrix} \mu_{xx}^{'}(\omega) + \mu_{xx}^{''}(\omega) & \mu_{xy}^{'}(\omega) + \mu_{xy}^{''}(\omega) & \mu_{xz}^{'}(\omega) + \mu_{xz}^{''}(\omega) \\ \mu_{yx}^{'}(\omega) + \mu_{yx}^{''}(\omega) & \mu_{yy}^{'}(\omega) + \mu_{yy}^{''}(\omega) & \mu_{yz}^{'}(\omega) + \mu_{yz}^{''}(\omega) \\ \mu_{zx}^{'}(\omega) + \mu_{zx}^{''}(\omega) & \mu_{zy}^{'}(\omega) + \mu_{zy}^{''}(\omega) & \mu_{zz}^{'}(\omega) + \mu_{zz}^{''}(\omega) \end{bmatrix} \tag{2.26}$$

2.6 Metamaterials

Over the past several decades, the field of electromagnetics has developed rapidly. Systems utilizing antennas, semiconductors, magnets, and similar devices that make use of the dielectric and magnetic properties of materials have become an integral part of everyday life around the globe. As a result, there has come to be a constant push in both private industry and government sectors to improve these technologies. In particular, the widespread use of antennas in the radar and telecommunications industry has generated substantial interest in increasing the range, operational frequency range, and data transmission and reception rates, as well as reducing the size of antennas. One of the key elements in making these improvements has

been the development of more effective dielectric layers, which requires the development/discovery of new materials with improved electromagnetic characteristics. It has now reached the point where some of the desired improvements require materials that have constitutive parameters that don't exist naturally.

This interest in improving antenna performance (as well as other electromagnetic systems) has generated considerable research into the development of artificial materials with characteristics specifically engineered for particular applications. Such materials are broadly referred to as metamaterials. The subject of metamaterials is broad, and so for the purposes of this thesis, the discussion of metamaterials will be limited to those used in one application: artificial dielectric layers (ADLs). The design and behavior of such engineered materials are described in [27], [28], [29], [30], [33], [4], and [34]. ADLs fall into a category of materials known as composites, and generally consist of two primary components: some dielectric substrate interwoven with metallic elements. Here, the dielectric substrate may consist entirely of one dielectric material or may be a composite of multiple layers of different dielectric materials. It provides the basis for the ADLs constitutive parameters. This substrate is then interwoven with metallic elements in some configuration that introduces capacitive elements, altering the overall dielectric characteristics of the composite, and/or inductive elements, altering the magnetic characteristics of the composite. Figure 2.9 ([98], [99], and [100]) illustrates several examples of metamaterials used in ADLs.

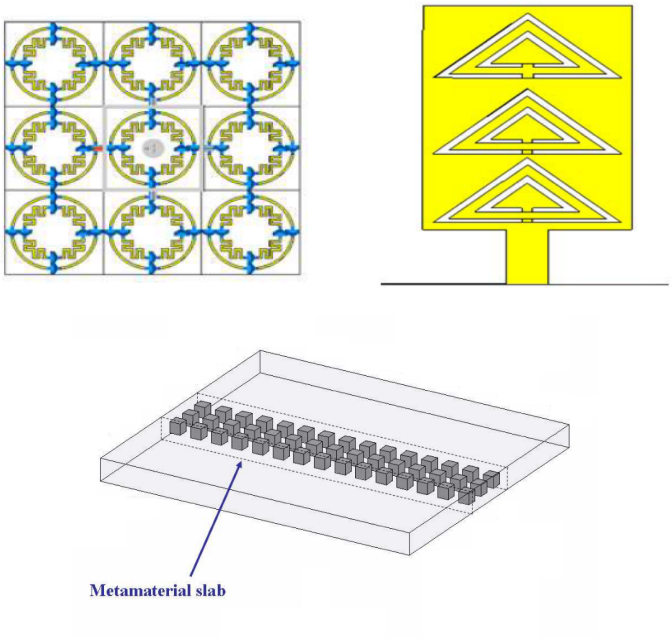

Figure 2.9: Examples of artificial dielectric layers (top left - [98], top right - [99], and bottom - [100]).

Due to the composite nature of metamaterials, they are inherently inhomogeneous. However, the performance of antennas and antenna arrays is reliant on predictable, consistent behavior throughout the various components of which they are comprised. So, in order for ADLs to be used as the dielectric substrate in antennas, it is necessary to be able to treat them as a single homogenous structure with uniform constitutive parameters. For composite materials in general, this is accomplished through the application of the effective medium theory (also known as effective medium approximation). This theory states that a composite material consisting of two or more materials with different electromagnetic characteristics can be equated to a single homogenous material whose constitutive parameters are an average of those of the individual materials in the composite (see Figure 2.10).

It has been demonstrated previously ([98], [4], [70], [93], and [101]) that this homogenization technique can be applied to metamaterials as long as they are periodic structures and as long as the thickness of the metamaterial is small with respect to the wavelength of incident electromagnetic waves.

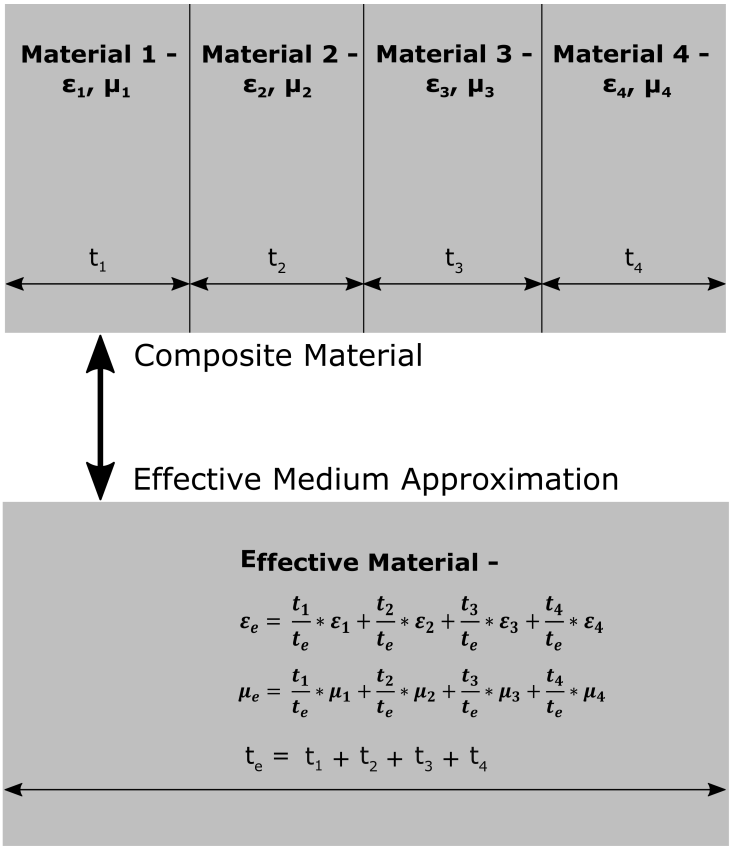

Figure 2.10: Illustration of the effective medium theory.

While the use of ADLs in antenna design presents significant opportunities for advancement in that field, these materials can be challenging to characterize. With respect to antenna performance, there are two key challenges to characterizing metamaterials. Firstly, ADLs frequently display dispersive behavior, requiring that their constitutive parameters be thoroughly characterized over the full frequency range in which they are to be used. Also, while the application of effective medium theory

allows these engineered composites to be treated like a single homogenized material, the inherent inhomogeneity of metamaterials results in anisotropic behavior in many ADLs. This requires the characterization of the constitutive electromagnetic parameters for these metamaterials at various angles of incidence and along multiple cuts in the plane of the ADL.

2.7 Summary

This chapter provided an overview of the basic electromagnetic principles that will be referrenced throughout this thesis. It began with a discussion of the constitutive parameters, including the physical definition of these parameters and the various forms they commonly take. The transmission and reflection of electromagnetic energy at material boundaries were then reviewed, with a focus on how they relate to the constitutive parameters. Next, the concepts of dispersion and anisotropy were examined. This included discussions on their physical meaning with respect to material properties and the dependencies they introduce to the constitutive parameters. The chapter concluded with a discussion of engineered materials known as metamaterials. The discussion focused on the typical composition of these engineered materials, their usefulness to antenna applications, and the particular challenges involved in characterizing them.

Chapter 3

Characterization of the Constitutive Parameters of Materials

3.1 Introduction

As discussed previously, the ability to understand and accurately model a material's response to electromagnetic waves is crucial to using that material in any sort of RF application. This in turn requires the proper characterization of the material's constitutive parameters (or effective constitutive parameters in the case of composites and metamaterials). However, these constitutive parameters are not easily measurable physical characteristics, but rather representations of a material's response to applied electric and magnetic fields. As such, these parameters must be extracted mathematically from directly measurable material responses. Numerous techniques have been developed over the years to achieve this, and each consists of some sort of calibration, a measurement procedure, and an extraction algorithm (digital post-processing). All of these techniques have strengths and limitations, and there is no ideal technique that works well for any application. Rather, one must develop an extraction technique by selecting each of the three component steps based on the requirements of their design.

Both the calibration and extraction algorithm are dependent on the type of measurement that is taken, and so the discussion here begins by examining the measurement techniques and selecting the one that works best for this project. The calibration and extraction algorithms that are used with the selected measurement technique are then examined. The commonly used measurement techniques can be divided into three four categories based on the particular material responses that are measured: 1) Resonance Techniques, 2) Impedance/Capacitance Techniques, 3) Transmission Line Transmission-Reflection Techniques, and 4) Free-Space Transmission-Reflection Techniques. Which of these categories is used in a particular material characterization technique depends on the following considerations: 1) material state of interest (i.e. solid sheet, powder, liquid, etc.), 2) frequency range of interest, 3) anisotropy, 4) unknown constitutive parameters (permittivity, permeability, or both), and 5) sample considerations (i.e. can the measurement be destructive, size and shape of the available sample, etc.). The available measurement techniques are reviewed, and the advantages and limitations of each examined. A technique is then selected that allows for the wideband characterization of anisotropic materials.

3.2 Conventional Measurement Methods

3.2.1 Inductance/Capacitance Techniques

Two of the most well-known electromagnetic properties are capacitance and inductance. They represent a material's resistance to changes in voltage and current,

respectively. These resistances to changing voltage and current are actually due to the storage of electric and magnetic fields within the material. This means that a material's capacitance and inductance are directly related to its relative constitutive parameters.

Inductive and capacitive materials and components are commonly used in many applications, particularly in electronic circuits. In the context of circuit design and analysis, capacitors most commonly take the form of two parallel conductive plates, whereas inductors most commonly consist of a looped conductive wire. Examples of these elements and their circuit representation can be found in Figure 3.1. Reliable measurements of the inductance and capacitance of individual circuit elements can be accomplished through straightforward and commonly used procedures similar to those described in [1]. Due to the relative ease of measuring these properties, coupled with their direct relationship to permeability and permittivity, the measurement of a material's capacitance and inductance provide one avenue for determining its constitutive parameters.

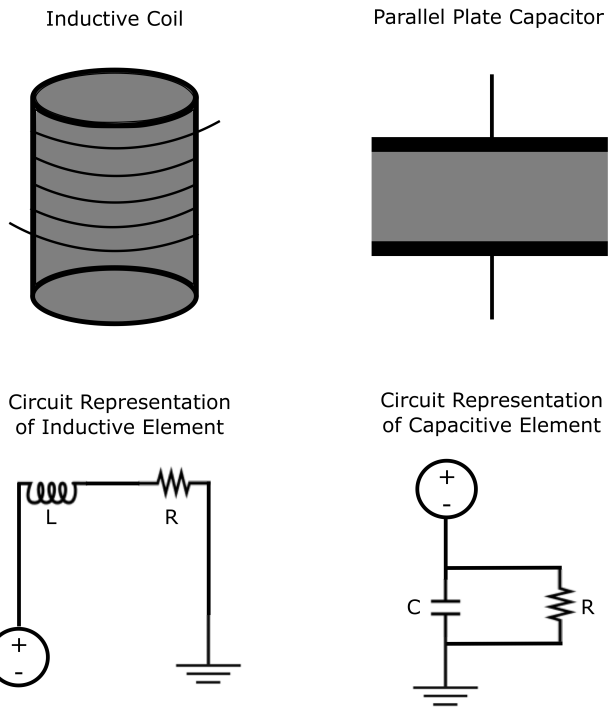

Figure 3.1: Inductors/capacitors and their circuit representations.

This particular approach to material characterization requires two separate test setups and sample configurations, one for each of the constitutive parameters. The process for measuring permittivity will be examined first. As discussed above, the capacitive behavior of a material is caused by the storing of electric fields within the material. This means that a material's permittivity can be mathematically extracted from its capacitance, which is obtained by measuring how much the material impacts the admittance of a simple circuit. In order to do this, a test setup similar to the one depicted in Figure 3.2 [1] is used.

Figure 3.2: Test setup for measuring the admittance of a material [1].

This setup consists of two parallel conductors, each with a flat surface of area A, connected to a power source. A flat sample of the material to be tested is prepared with known thickness t. Calibration measurements are then made to establish the baseline admittance of the system and compensate for noise. Next, the prepared sample is placed between the two electrodes, and the admittance of the test system is measured again. Once the baselined system admittance is removed from this measurement (effectively isolating the material admittance Y), the complex permittivity can be extracted through the following relationship [1]:

$$Y = j\omega \left(\frac{A\epsilon_0}{t}\right) \epsilon_r = j\omega \left(\frac{A\epsilon_0}{t}\right) \left(\frac{Ct}{\epsilon_0 A} - \frac{jG}{A\epsilon_0\omega}\right) , \tag{3.1}$$

In Equation 3.1, C is the capacitance of the sample, G is the conductance of the sample, and ω is the angular frequency of the excitation.

The second test setup required for this measurement technique is used to determine the permeability of the material of interest. As discussed above, the inductive behavior of a material is the result of that material storing magnetic fields, which allows the permeability to be extracted mathematically from the inductance. The material's inductive characteristics can be determined by measuring its contribution to the impedance of a simple circuit. Such a measurement is accomplished using a test setup similar to the one depicted in Figure 3.3 [1].

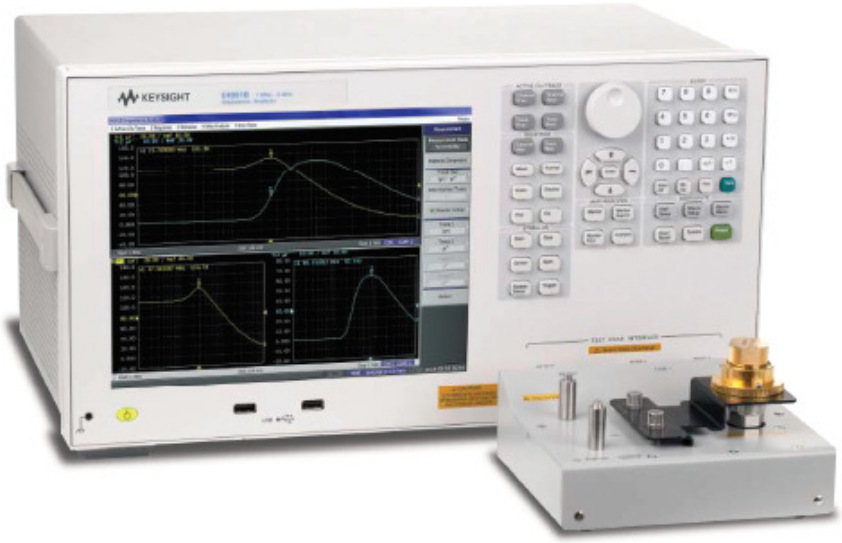

Figure 3.3: Test setup for measuring the impedance of a material [1].

The test setup depicted above consists of a test cell with a toroidal cavity in the center connected to an impedance analyzer. The test cell either contains or simulates a looped wire with some number of coils. The impedance of the test cell is first measured while it's empty. This provides a baseline system impedance and allows for calibration. A toroidal sample of the material of interest is then prepared and placed into the cavity of the test cell. The impedance of the system is then

measured again. The inductance of the sample can then be calculated from the two impedance measurements through the following equations:

$$Z = jL\omega\,, \tag{3.2}$$

$$L = L_T - L_0 = \frac{Z_T}{j\omega} - \frac{Z_0}{j\omega}\,. \tag{3.3}$$

Here, L and Z are the inductance and impedance of the sample, L_T and Z_T are the total inductance and impedance of the system when the sample is placed inside, and L_0 and Z_0 are the inductance and impedance of the system when the test cell is empty. Finally, the complex permeability of the material being characterized can be extracted using its relationship with the impedance of the sample [1]:

$$\mu = 1 + \frac{2\pi L}{\mu_0 H \ln \frac{C}{B}}\,. \tag{3.4}$$

In Equation 3.4 above, H refers to the height of the sample, C refers to the distance between the center of the test cell and the outer surface of the sample, and B refers to the distance between the center of the test cell and the inner surface of the sample.

The inductance/capacitance method of material characterization has become widely used due to both the relative ease of the measurements and the straightforward equations used to extract the parameters from those measurements. However, this technique is not a viable option for the wideband characterization of anisotropic metamaterials for RF applications. This is due primarily to two limitations, the first of which is the limited frequency range over which these measurement techniques

can be utilized. For each of the test setups, as the frequency rises above 1 GHz the unavoidable parasitic capacitances and inductances in each circuit become large enough that they create resonances in the signal [2]. These resonances prevent the accurate extraction of the constitutive parameters at frequencies above 1 GHz. The other key limitation is that the samples used in the capacitance/inductance technique must be uniformly excited and must therefore be both homogenous and entirely nonmetallic [2].

3.2.2 Resonance Techniques

In general, resonance refers to a particular occurrence in wave systems in which the waves of a system continuously interact constructively with the waves on an applied excitation, resulting in the growth of the system's wave amplitude. This growth is a result of oscillations within the system and occurs when the waves exciting the system are at a particular frequency, known as the resonant (or natural) frequency. The resonant frequency of any system is determined by its physical characteristics. Once a system has begun to resonate, it will continue to oscillate even after the excitation has been removed. However, some amount of energy will be lost after each oscillation, and eventually the system will eventually return to a relaxed state. The rate at which a system returns to a relaxed state after it resonates is referred to as the quality factor of the system.

As described in [102], the resonance of an electromagnetic system occurs when the energy stored in the system oscillates between electrical and magnetic states (i.e. the dissipation of electrical energy generates magnetic energy and vice-versa).

The frequency at which such an oscillation is directly determined by the capacitance and inductance of the system as a whole:

$$\omega_r = \frac{1}{\sqrt{LC}}\,. \tag{3.5}$$

In Equation 3.5, ω_r is the angular resonant frequency of the system, and L and C are the inductance and capacitance of the system, respectively. Furthermore, such a system's quality factor, Q, can also be related to its inductance and capacitance:

$$Q = \frac{\omega_r}{BW_r} = \frac{1}{BW_r\sqrt{LC}}\,. \tag{3.6}$$

Here, BW_r refers to the bandwidth of the resonance. Since a material's inductance and capacitance are directly related to its constitutive parameters (as described in Section 3.2.1), the relationships described in Equations 3.5 and 3.6 allow the constitutive parameters of a material to be extracted from its resonant frequency and quality factor.

In order to measure the resonant frequency and quality factor of a given material, a resonant test cell is used. These test cells can take many forms, but an example of one such device described in [3] is shown in Figure 3.4.

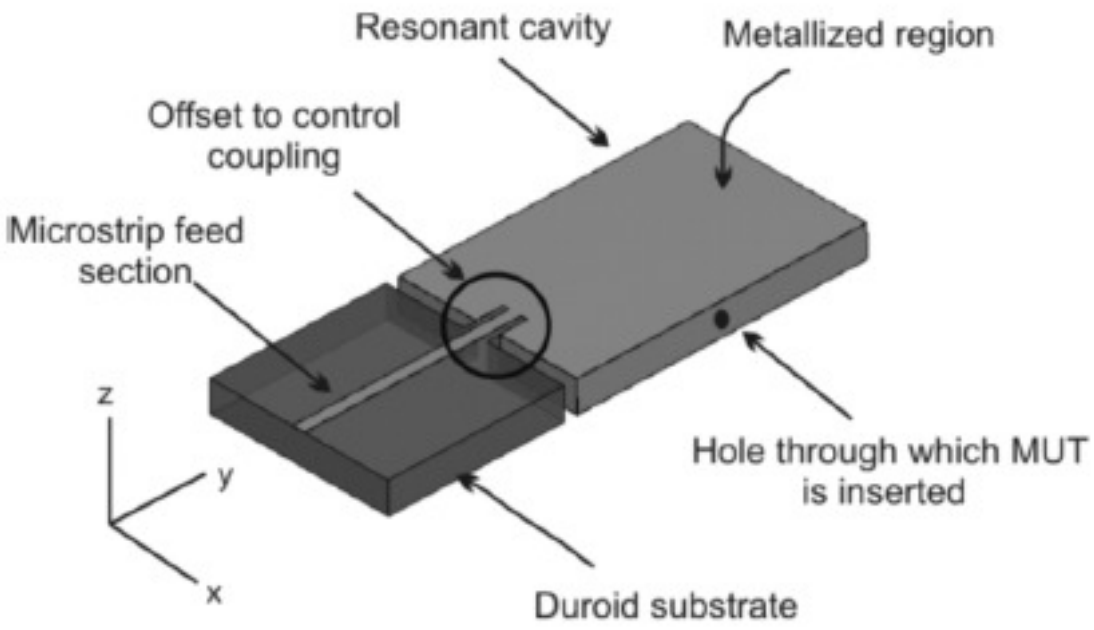

Figure 3.4: Test setup for measuring the resonant frequency and Q-factor of a material [3].

Here, a VNA is connected to an empty chamber and the resonant frequency and quality factor are measured. Next, a solid cylindrical sample of the material is placed into the resonance chamber and the resonant frequency and quality factor are measured again. After subtracting out the values of the empty test cell and isolating the material of interest's resonant properties, the constitutive parameters can be extracted. In particular, the measured resonant frequency is used to calculate the real part of the complex permittivity and permeability, and the measured quality factor is used to calculate the loss tangents. The equations used for these calculations are lengthy and require the evaluation of boundary conditions and Bessel functions for each exciting mode. A detailed description of these types of measurements, along

with the full set of equations used to extract each of the constitutive parameters can be found in [2].

Resonance techniques for the determination of a material's constitutive parameters are widely used due to the high level of accuracy they provide. The relative permittivities and permeabilities extracted from these measurements generally have errors of approximately 0.1%, much better than the errors present in the other commonly used techniques (at least 1%) [2]. However, this category of techniques can only be used to characterize the constitutive parameters of a material over an extremely narrow band of frequencies in the immediate vicinity of the material's resonant frequency. As such they are of limited usefulness when attempting to characterize dispersive materials. It is also not generally feasible to characterize materials in multiple orientations using resonant techniques, making them impractical when the material of interest is anisotropic. Finally, it should also be noted that the need to solve for boundary conditions and to evaluate Bessel functions when calculating the constitutive parameters from resonance measurements makes the extraction algorithms for this technique particularly costly, computationally speaking.

3.2.3 Transmission-Reflection Techniques

In Section 2.3 of this thesis, the direct relationships between the constitutive parameters of a material and its reflection-transmission characteristics were discussed. Based on these relationships it is possible to characterize the permittivity and permeability of a material based on its transmission and reflection coefficients. Fortunately, the increasingly widespread use of wireless and radar technologies has made

the measurement of the reflection and transmission of RF energy by devices and materials a common occurrence. These measurements can be made in a relatively straightforward fashion by utilizing transmission lines and a concept known as the scattering parameters of a system.

In simple transmission line systems, electromagnetic energy in the RF frequency range is guided down a specialized path, commonly consisting of either a coaxial cable or metallic waveguide. The behavior of electromagnetic energy in transmission lines is well documented and typically depends on two things: 1) the cross section of the transmission path and 2) the characteristic impedance of the line (which is in turn dependant on the length of the transmission line with respect to the wavelength of the energy being propagated through it). More specifically, the cross section of the transmission path determines the frequency range over which the transmission line can be used, while its characteristic impedance determines the reflection and transmission characteristics associated with the transmission line when it is connected to some load. Transmission line characteristics and behavior is described in detail in [34].

When the electromagnetic waves being propagated down a transmission line encounters the interface between the transmission line and a connected load, some portion of that energy is transmitted through into the load, and the rest is reflected back down the transmission line (if the transmission line itself is assumed to be lossless). The amount of energy reflected back down the transmission line versus the amount that is transmitted through the interface is determined by how well

the the impedance of the load is matched to the characteristic impedance of the transmission line:

$$\Gamma = \frac{Z_l - Z_0}{Z_l + Z_0}\,, \tag{3.7}$$

$$T = 1 + \frac{Z_l - Z_0}{Z_l + Z_0} = \frac{2Z_l}{Z_l + Z_0}\,. \tag{3.8}$$

In Equations 3.7 and 3.8, Γ is the reflection coefficient, T is the transmission coefficient, Z_l is the impedance of the load, and Z_0 is the characteristic impedance of the transmission line.

By connecting each end of a transmission line up to a seperate port that can each transmit and recieve RF signals as described in [5], the subsequent system becomes a simple two-port microwave network (as depicted in Figure 3.5).

(a)

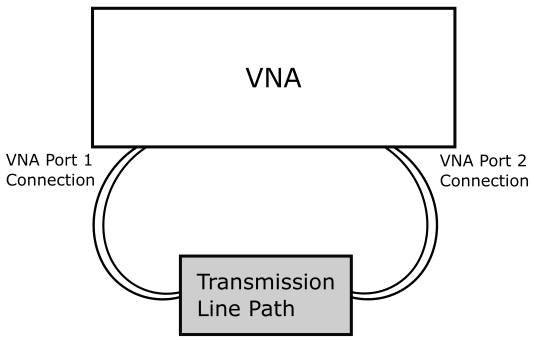

(b)

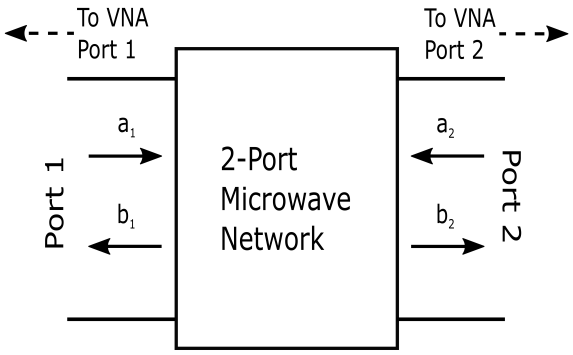

Figure 3.5: Transmission line transmission-reflection measurements through the use of 2-port microwave networks. a) Transmission line connected to a VNA. b) EM waves in a 2-port microwave network.

A good description of the behavior of waves in n-port networks is provided in [103]. In the two-port network depicted above in Figure 3.5 b), the variables a_1 and a_2 denote the transmitted waveforms from ports 1 and 2, respectively. Similarly, b_1 and b_2 denote the signals recieved by ports 1 and 2. At this stage, it will be assumed that the system behaves as an isolated, ideal two-port network (i.e. no external sources of loss or noise). If both both ports are simultaneously transmitting and receiving, then the recieved signal at port 1 (b_1) is equal to the portion of the signal

transmitted from port 1 (a_1) that is reflected back at the port by the system plus the portion of the signal transmitted by port 2 (a_2) that is transmitted through the system (as depicted in Figure 3.6). Equivalently, the recieved signal at port 2 (b_2) is equal to the sum of the portion of the signal transmitted from port 2 (a_2) that is reflected back at the port with the portion of the signal transmitted by port 1 (a_1) that is transmitted through the system. This can be represented by a set of linear equations:

$$b_1 = a_1 S_{11} + a_2 S_{12}\,, \tag{3.9}$$

$$b_2 = a_2 S_{22} + a_1 S_{21}\,. \tag{3.10}$$

These equations are usually presented in matrix form:

$$\begin{bmatrix} b_1 \\ b_2 \end{bmatrix} = \begin{bmatrix} S_{11} & S_{12} \\ S_{21} & S_{22} \end{bmatrix} \begin{bmatrix} a_1 \\ a_2 \end{bmatrix}\,. \tag{3.11}$$

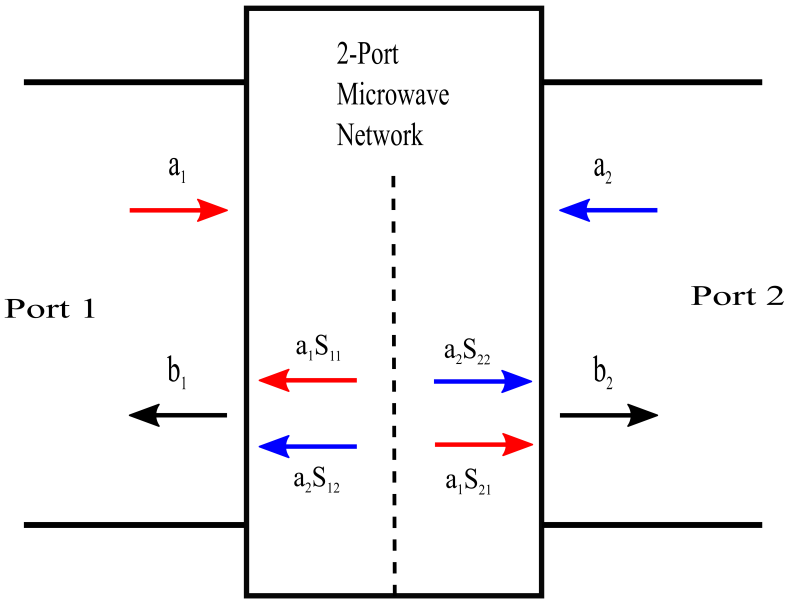

Figure 3.6: Signals travelling through two-port microwave networks.

The variables S_{ij} in Equations 3.9 through 3.11 are a commonly referred to as scattering parameters (or S-parameters) and the matrix containing a network's S-parameters is called that system's scattering matrix. S-parameters are widely used to represent the various impacts of linear networks on electromagnetic signals propagating though them (losses, noise, gains, reflection-transmission, etc.). Each S-parameter specifically represents the system impacts on a signal travelling from one specific port to another specific port. In the S-paramter notation, S_{ij}, the value of i indicates the port the signal arrives at, while j indicates the port from which it originated. For instance, S_{21} refers to the network's impact on a signal originating at port 1 and arriving at port 2 [103]. Keeping this in mind, it becomes clear that in a linear, two-port transmission line network the transmission of energy through the

system can be fully characterized by either S_{11} or S_{22}, and the reflection of energy within the system can be fully characterized by either S_{21} or S_{12}.

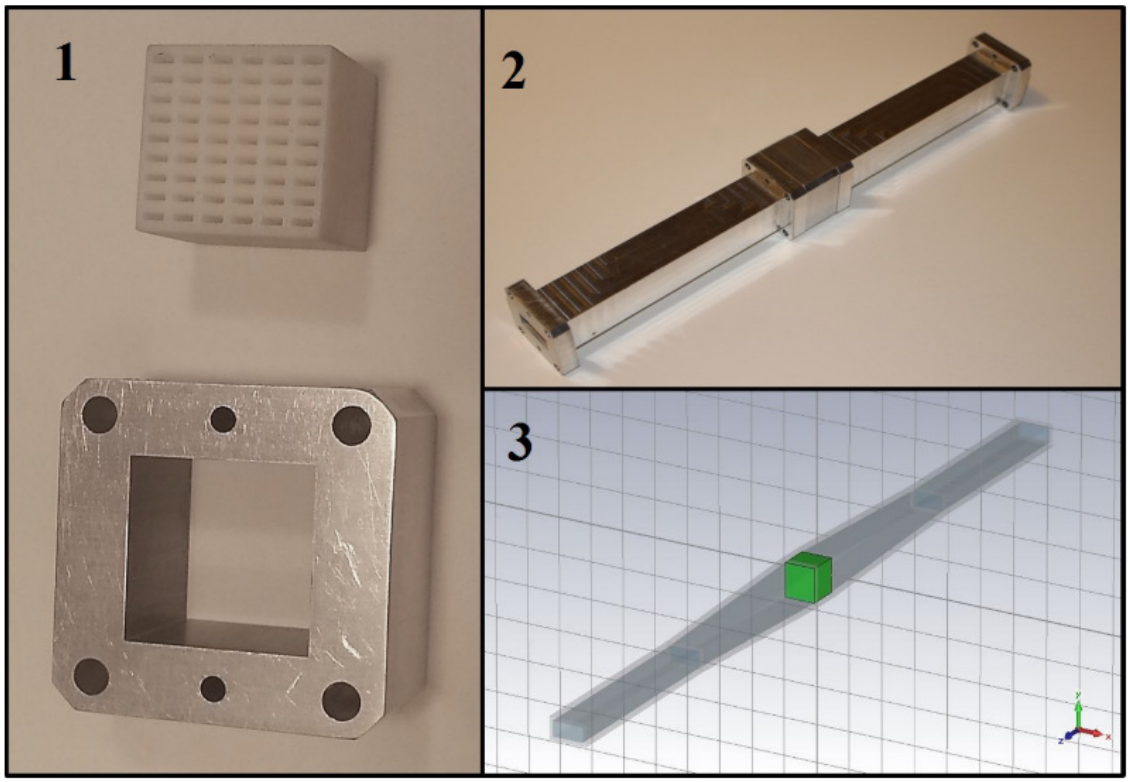

Figure 3.7: Material sample in a waveguide [104]. 1 - Sample under test and sample holder. 2 - Waveguide test setup. 3 - Simulation of waveguide test setup

Assuming that the interfaces between the two ports and the transmission line are perfectly matched (in terms of impedance), then no reflection occurs within the system itself. If this assumption can be accurately made, then the reflection and transmission characteristics of a material can be measured by placing a portion of that material in the transmission line, as shown in Figure 3.7 [104]. As long as the sample completely fills the cross section of the transmission line and is placed far enough away from any transmitting port that the signal approximates a plane wave and only the dominant mode is propagating [104], then a signal propagating

through the network will encounter the three distinct regions portrayed in Figure 3.8. The scattering matrix for each of these regions is:

$$S^I = \begin{bmatrix} \Gamma & 1-\Gamma \\ 1+\Gamma & -\Gamma \end{bmatrix}, \tag{3.12}$$

$$S^{II} = \begin{bmatrix} 0 & T \\ T & 0 \end{bmatrix}, \tag{3.13}$$

$$S^{III} = \begin{bmatrix} -\Gamma & 1+\Gamma \\ 1-\Gamma & \Gamma \end{bmatrix}. \tag{3.14}$$

Where Γ is the reflection coefficient of the material placed within the transmission line, and T is its transmission coefficient. The overall scattering parameters of the system are then [22]:

$$S^{Total} = S^I S^{II} S^{III} = \begin{bmatrix} \frac{\Gamma(1-T^2)}{1-\Gamma^2 T^2} & \frac{T(1-\Gamma^2)}{1-\Gamma^2 T^2} \\ \frac{T(1-\Gamma^2)}{1-\Gamma^2 T^2} & \frac{\Gamma(1-T^2)}{1-\Gamma^2 T^2} \end{bmatrix}, \tag{3.15}$$

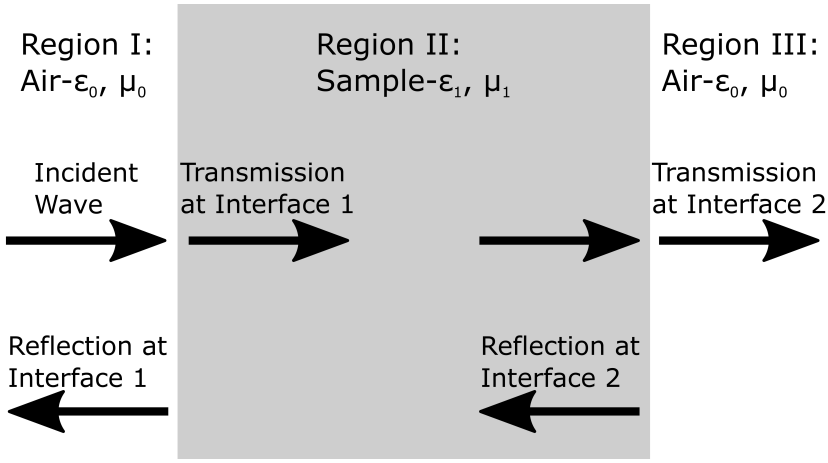

Figure 3.8: Plane wave propagating through a material sample.

It can now be seen that the S_{11} and S_{21} parameters of the setup described above constitute two equations with two unknowns. This allows both the transmission and reflection coefficients of the material sample to be calculated by measuring these S-parameters. Recalling from Chapter 2 that the reflection and transmission coefficients of a material are directly related to the constitutive parameters of the material by Equations 2.13 and 2.14, it then becomes possible to extract both the material's permittivity and permeability using only its measured S-parameters. A number of extraction algorithms have been developed based on this relationship, and they will be discussed in more detail later in this chapter.

In order to perform the S-parameter measurements needed for the transmission-reflection technique, a test setup similar to the one shown in Figure 3.9 [104] is used. Here, a two-port VNA is used, and each port is connected to a seperate section of waveguide (although other transmission lines can be used). The sections of waveguide must be of equal length. Initially, the system is calibrated by taking

measurements of the S_{11}, S_{22}, and S_{21} parameters. The system S_{11} and S_{22} measurements are typically taken by placing sheets of flat metal flush against the end of each waveguide and measuring the reflected signal at each VNA port. The S_{21} calibration typically includes two steps. First, the waveguides are secured together directly without the sample holder and measuring the transmitted signal. An empty sample holder is then placed between the two waveguides and the transmitted signal is measured again. These measurements allow the system's reflection-transmission and noise characteristics to be obtained.

Next, a sample of the material to be tested is prepared so that it will completely fill the cross-section of the waveguide, and so that both of the sides facing the waveguide antennas are flat and smooth. The preparation of the sample is very important, as any air gaps or non-planar surfaces in the sample (for solid materials) will significantly impact the measured S-parameters. The two waveguide sections are then fixed to one another with the sample secured exactly at the midpoint using the sample holder used during the calibration. The VNA is set up to transmit a signal sweep over the frequency range of interest, and the S_{11} and S_{21} parameters are recorded. The system data obtained during the calibration measurements is then removed, isolating the transmission and reflection data of the sample itself (the calibrated data may be automatically removed from the measurements by the VNA). The system configurations for each calibration step and material measurement for this type of setup is shown in Figure 3.9 [104].

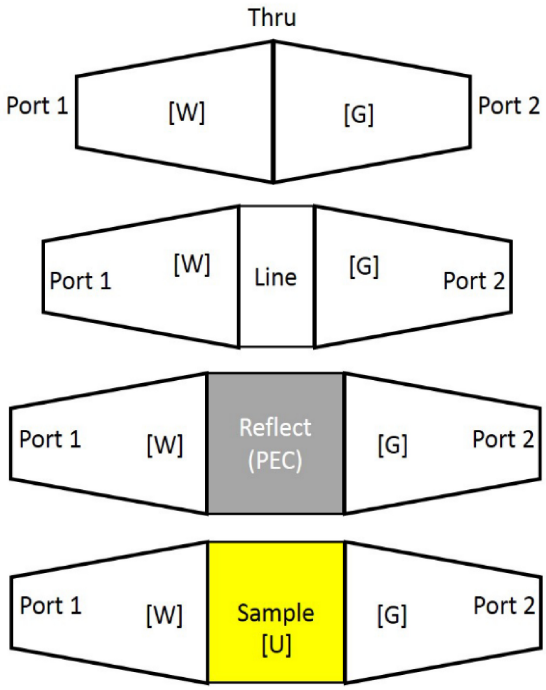

Figure 3.9: Typical test setup and calibration for the transmission line transmission-reflection measurement technique using a waveguide [104].

The use of the transmission-reflection technique to characterize the electromagnetic behavior of materials has seen widespread popularity for several reasons. The first being that it can be used over relatively large frequency ranges. The frequency band over which a particular transmission line can be used is dependent on the physical dimensions of the path along which the waves are propagated. By making use of multiple transmission lines in testing, a material could be characterized over a frequency range of interest that is only limited by the size and cost constraints of the test setup. This makes it an ideal setup for characterizing dispersive media. This measurement technique is ideally suited to characterizing materials at higher frequency ranges, easily covering the frequency range of interest in this thesis (2-10 GHz). In addition, it can be used for to characterize materials in almost any

state, including solids, powders, liquids, and gases (with proper adjustment of the test setup/transmission line). Also, thanks to the widespread use of waveguides and coaxial cables in RF applications, the test equipment is readily available and relatively inexpensive.

However, this technique does not easily allow for measurements to be taken when the transmitted signal is obliquely incident to the sample. To make such measurements, samples need to be prepared with the material structure in different orientations. This type of sample preparation is complicated and expensive, and does not reliably capture the angular components of the constitutive parameters in composite materials/structures.

3.2.4 Free-Space Techniques

The widespread use of antennas in modern technology has led to the extensive study of the propagation of electromagnetic energy in the RF range through free space environments. This has included examiniations of the reflection and transmission characteristics of different antennas, as well as the behavior of electromagnetic energy travlling through free space when it interacts with the surface of a new medium (described in Section 2.3). These principles can be used to characterize the constitutive parameters of a material using a type of measurement technique commonly referred to as free-space characterization techniques. This measurement approach is based on the reflection and transmission characteristics of the material being tested, just like the approach detailed in Section 3.2.3. The use of free-space material characterization systems has become widespread, and examples of these

systems are discussed in [13], [14], [16], [17], and [18]. Additionally, a good overview of the concepts and design of such a system can be found in [22].

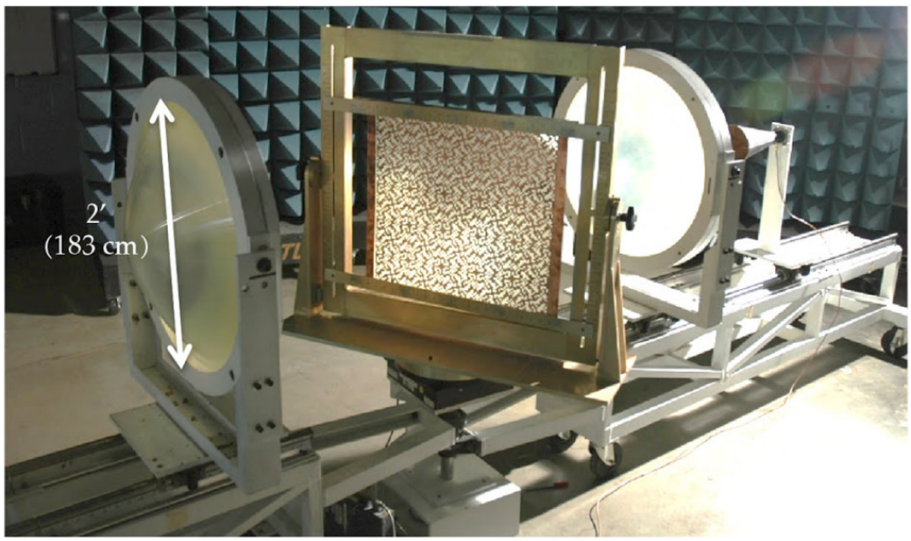

Figure 3.10: Test setup for the free-space characterization of EM material properties [22].

Utilizing a setup similar to the one depicted in Figure 3.10 it is possible to set up a free space system that behaves as a two-port microwave network, making it possible to measure the S-parameters at each port and use them to calculate the system's transmitted and reflected energy. It is apparent at this point that this measurement technique relies on the same concepts as those detailed in the previous section. In this setup, two identical antennas are connected to each port of a two-port VNA and are secured facing one another. The system is then calibrated, isolating any background or equipment noise and providing a baseline for the reflection and transmission characteristics of the system without any test sample in place.

Once the system has been calibrated, placing a sample of material at the mid-point between the two antennas and measuring the S_{11} and S_{21} parameters with the VNA allows the S-matrix in Equation 3.15 to be used to calculate the reflection

and transmission coefficients of the sample. Since this measurement method relies on the same electromagnetic principles as the transmission-reflection method in the previous section, the algorithms used to extract the constitutive parameters of the material under test are virtually identical (these will be discussed in more detail in Section 3.4).

Despite the obvious similarities between the free-space method with the previously discussed transmission-reflection method, the Free Space approach provides one significant advantage: it allows for relatively straightforward characterization of a material at oblique incidences. Because both the sample and the antennas are secured in a free-space environment, it is fairly simple to reposition any or all of them is such a way that the propagating waveform encounters the sample at a non-normal angle of incidence. [82] does a good job demonstrating this reconfigurability. Depending on the type of material to be tested and the parameters of interest, various types of configurations are commonly used for these measurments. These oblique incidence configurations typically fall into one of two categories; 1) transmission only (as in [80], [81], [83], [84]) or 2) reflection only (as in [85], [86], [87], [88]). Reflection only measurements are made by placing a ground plane (reflective metal sheet) immediately behind the sample under test and leaving it in a fixed position while the antennas are rotated around around it, as shown in Figure 3.11. Remembering Snell's Law of Reflection (Equation 2.16), the transmitting and recieving antennas are places at $+\theta$ and $-\theta$ [18], repectively (see Figure 3.13 a)). The S_{11} parameter can then be measured.

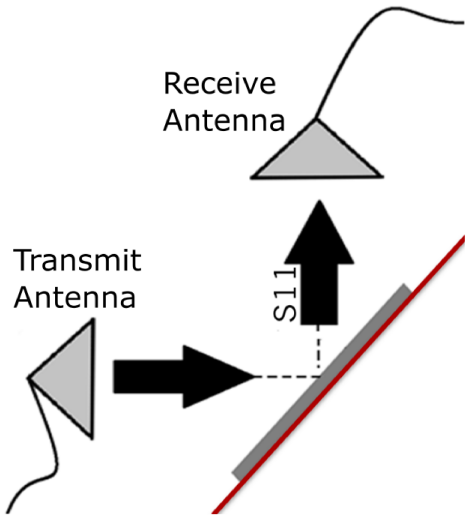

Figure 3.11: Reflection-only configuration of the free-space test setup.

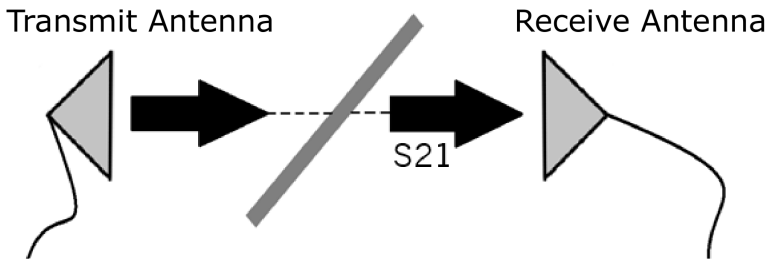

Figure 3.12: Transmission-only configuration of the free-space test setup.

Conversely, transmission only measurements are made by leaving the antennas in place, rotating the sample about its central axis, and measuring the S_{21} paramter. One might be tempted to wonder why the recieving antenna doesn't need to be rotated to adjust for refraction. From Snell's Law of Refraction (Equation 2.15), when the electromagnetic energy propagating through the system encounters the

interface between the air and the first face of the sample under test, the angle at which it is travelling change from Θ_i to Θ_t such that:

$$\Theta_t = sin^{-1}(\frac{n_1 sin(\Theta_i)}{n_2})\,. \tag{3.16}$$

However, it then encounters a second interface, going from the sample under test to air. This second interface is identical to the first, but in the opposite direction (i.e. n_2 becomes the refractive index in the left-hand term of Equation 2.15 and n_1 becomes the refractive index of the right-hand term). At this second interface, the angle in which the EM wave is travelling again changes direction. Using Θ_{final} as the new angle of refraction in Equation 2.15 and Θ_t as the new angle of incidence, the final angle of propagation can be found:

$$\Theta_{final} = sin^{-1}(\frac{n_2 sin(\Theta_t)}{n_1}) = sin^{-1}(\frac{n_2 sin(sin^{-1}(\frac{n_1 sin(\Theta_i)}{n_2}))}{n_1}) = \Theta_i\,. \tag{3.17}$$

Clearly, the final angle of incidence for the wave that is transmitted through the sample under test is the same as the initial angle of incidence [18], but the overall path of the wave is altered (see Figure 3.13 b)). This results in a phase shift that must be corrected in the S_{21} measurements.

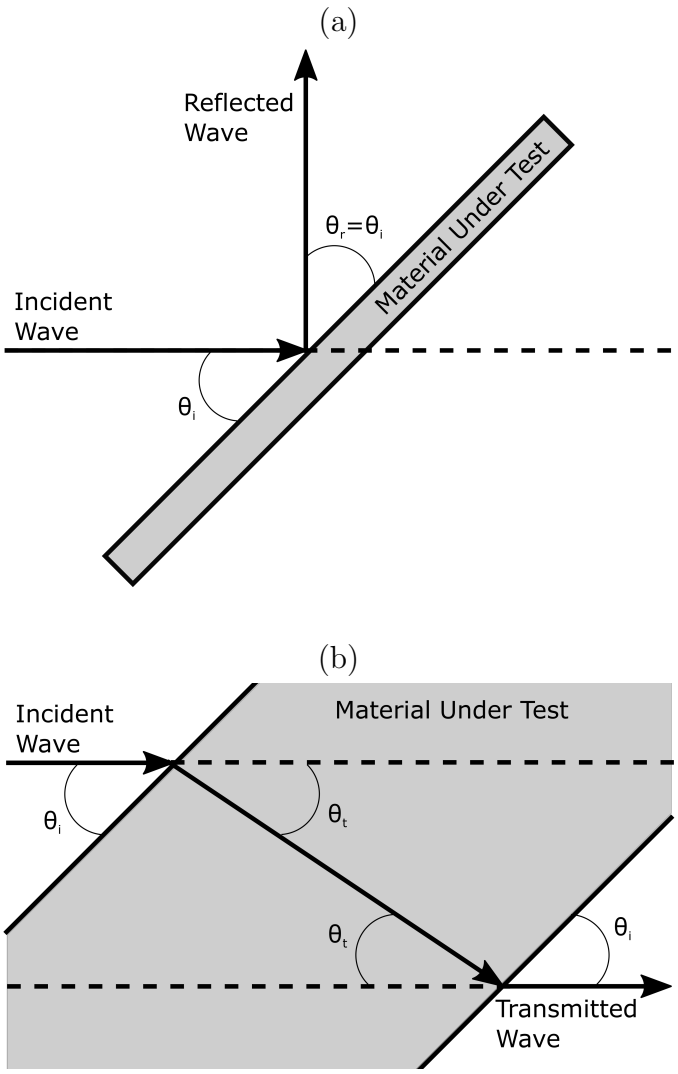

Figure 3.13: Reflection and transmission of plane waves obliquely incident upon a surface. a) Reflection of a wave obliquely incident upon an interface. b) Transmission of a wave obliquely incident upon an interface.

Since the transmission only and reflection only free space measurements each provide just one S-parameter, they can only be used to extract one of the constitutive parameters at oblique incidence. Typically, these approaches to free space measurement are used to characterize non-magnetic dielectric materials at oblique incidence, but can be used for any material whose permittivity or permeability is

both known and not a function of angle. With currently existing free space techniques, multiple test setups must be used in order to fully characterize the angle dependence of a material's constitutive parameters, each of which requires its own calibration. Unfortunately, this increases the complexity and the time required to make such measurements. It also increases the potential for errrors in the extracted parmeters.

While the free-space approach does provide the additional benefit of allowing material characterization at oblique angles of incidence, it also involves a more complex test setup and more potential sources of error than the transmission-reflection technique discussed earlier. As such the calibration and data processing required for this approach are more involved, and certain assumptions must be made in order for the measurements to be valid. The necessary assumptions will be discussed here, and the calibration and processing requirements will be discussed later in Sections 3.3 and 3.4.

In order for the free space test setup to be reliably used to extract the constitutive parameters of a material, two key requirements must be satisfied. The first of these is that the electromagnetic signal transmitted through the system must be propagating as a plane wave. This requires that the sample be place far enough awar from the two antennas that it is in their far-field region. If the signal is not propagating as a plane wave, then phase errors will be introduced to the measured S-parameters [22]. These errors are a result of different portions of the transmitted waveform reaching the test sample at different times (see Figure 3.14).

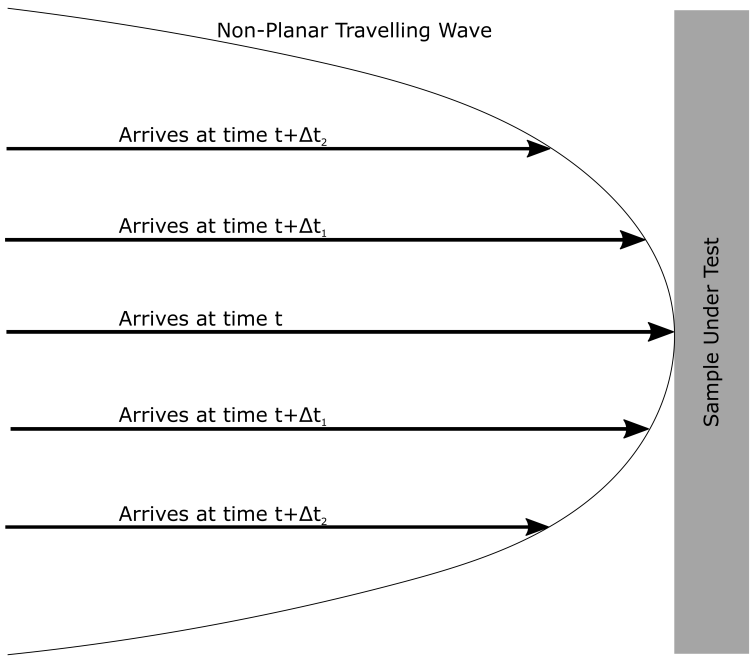

Figure 3.14: Phase error of a non-plane wave interacting with a material interface.

To ensure that the sample is in the far-field region of the test antennas, it is important to properly characterize those antennas. An antenna's far-field region varies depending on the type of antenna used, but is primarily dependent on both the physical dimensions of the antenna and the wavelength of energy that it is transmitting. In general, an antenna's far-field distance can be calculated using:

$$R = \frac{2D^2}{\lambda}\,, \tag{3.18}$$

In Equation 3.18, R refers to the far-field distance, D refers to the largest dimension of the antenna, and λ is the wavelength of the transmitted signal. At lower frequencies (such as S-band), considerations must be made when selecting the test antennas to balance antenna size and far-field distance.

The algorithms used for extracting the constitutive parameters from free space measurements assume that the test signal is a plane wave that only encounter the three regions shown in Figure 3.8. In the event that the area illuminated by the transmitted beam approaches or passes the edge of the sample, then direct transmission and edge diffraction effects begin to occur [22]. These can significantly impact the measured S-parameters, causing incorrect values for the constitutive parameters to be extracted. As such, the second requirement for the free space approach to be used is that the propagating wave is entirely transmitted through the sample without being impacted by edge effects. Ensuring that this is the case requires care to be taken with the arrangement of the test equipment, and additional considerations to be made when determining sample size and selecting test antennas.

For the arrangement of the test setup, it is important to ensure that the antennas are arranged directly facing one another, at the same height and distance from one another. The sample itself should be secured such that the transmitted beam is centered on the middle of the sample. It should also have x- and y-dimensions that are at least 1.5 times the diameter of the illuminating beam [22]. An electromagnetic beam transmitted by an antenna through free space will broaden the farther it gets from the end of the antenna (see Figure 3.15 a)). The area of the sample that gets illuminated by the transmitted beam is further increased for the case of oblique incidence due to projection (see Figure 3.15 b)). To mitigate this, and keep the size of the sample under test from becoming prohibitively large, the antennas used in free space characterization measurements should be selected to have as narrow a beamwidth as costs allow. Additionally, this provides increased incentive

to minimize the far-field range of the test antennas. Rather than using higher quality, more expensive antennas, some groups use dielectric lenses to focus a wider Gaussian beam, as in [22], [17], [14], and [16]. This reduces the beamwidth and allows it to approximate a plane wave at much shorter distances than it would normally take to achieve far field behavior.

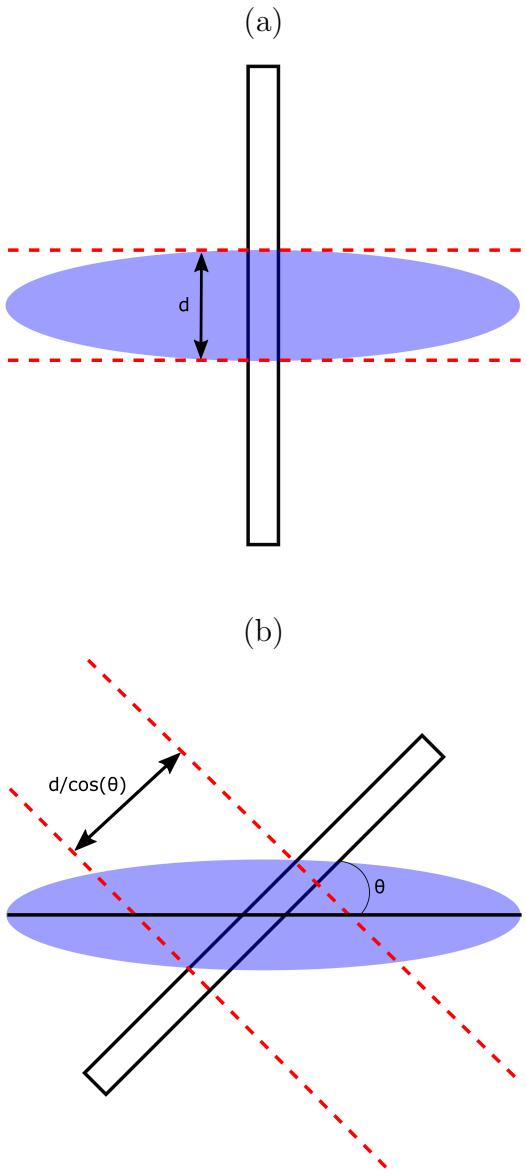

Figure 3.15: The effect of projection on the area illuminated by the transmitted beam of an antenna. a) Illumination area of a beam at normal incidence. b) Illumination area of a beam at oblique incidence.

As a final note, the free space technique for material characterization operates under the assumption that the transmitted waveform propagates through the sample in a uniform manner. Put another way, it assumes that the material being tested is homogenous. As was discussed in Chapter 2, many materials (including all artificial

dielectric layers), are non-homogenous. In fact, one of the primary interests in characterizing materials at oblique angles of incidence (as this technique is often used to do) is to characterize the anisotropic behavior of inhomogenous materials.

It may therefore seem as though the free space measurement technique is limited use in many modern applications. However, while the representations of permittivity and permeability found in Equations 2.21-2.26 provide more complete descriptions of these parameters, they are also difficult to fully extract and are computationally costly to use. Additionally, for many antenna applications only the behavior of a material along particular cuts in the ϕ plane are of interest, making the characterization of each ϵ_{ij} and μ_{ij} component unnecessary. It is therefore possible to characterize inhomogenous materials with the free space approach by applying the effective medium theory discussed in Section 2.6 and using the simpler expressions for the constitutive parameters [37] to characterize permittivity and permeability at different angles along the ϕ cuts of interest. This is illustrated in Figure 2.10.

The free space measurement approach provides the most promising path towards characterizing the constitutive parameters of dispersive, inhomogenous materials at different angles of incidence. It is the only approach currently available that meets all of the necessary criteria, and will be the focus of the remainder of this thesis. Measurements of both the transmission and reflection characteristics can be made, making it possible to extract both permittivity and permeability. It allows for the characterization of materials over wide ranges of frequencies, including the RF ranges that are commonly used in RF applications today. It also allows the

characterization of materials at various angles of incidence. It has the added benefits of a straightforward test procedure and sample preparation.

One of the main hurdles to using this method is the initial cost and setup. These test systems are frequently large and considerably more expensive than those used for the other measurement options. Also, the need to avoid the impact of edge diffraction on the measurements requires the use of larger samples in testing, further increasing the cost of testing. There are also a large number of potential sources of noise and error when using this approach. Due to the nature of the test setup, this method is also only viable for solid samples.

3.3 Error and Calibration

After determining which measurement method is preferred, based on the requirements of the project for which the charcterization is being performed, it then becomes necessary to understand the potential sources of error and noise associated with the selected measurement setup. Measurement errors and noise can have a huge impact on the collected data, potentially introducing large errors in the extracted constitutive parameters and invalidating the characterization of the material being tested. By correctly identifying these sources of error, it is possible to minimize (or eliminate entirely) their impact through a combination of experimental safeguards, digital post-processing of the collected data, and system calibration. In this context, experimental safeguards refer to inclusions in the measurement equipment designed to mitigate sources of error (like the use of RF absorbsers), data

post-processing refers to the removal of noise/error through purely digital means (such as digital filters), and calibration refers to the removal of noise/error through direct measurement and correction of said noise/error. This section will describe the more significant sources of error and noise, and then discuss the development of a calibration procedure. Since it was determined that the free space method for the electromagnetic characterization of materials is the best option for this project, this discussion will be limited to those noise/error sources and calibration concepts associated with this type of characterization method.

There are two broad categories of noise that can appear in a free space test setup: environmental and system. Here, environmental noise refers to a combination of ambient RF energy and external signal sources (other transmitting antennas, cell phones, wireless transmitters, etc.). System noise refers to noises internal to the VNA setup, and can include reflections caused by impedance mismatches in the cables and antennas. As well as noise, various measurement errors need to be accounted for. In the free space test setup these include misalignment, unwanted reflections, direct transmission of the signal between the test antennas, and edge diffraction effects. In this context, misalignment errors can occur when one or more pieces of test equiment are improperly positioned. This can be caused by the antennas or focusing lenses (when used) being slightly askew or offset, or by offsets in the samples position/angle. Unwanted reflections are caused by side lobe reflections and multiple reflections of the main beam (see Figure 3.16). Direct transmissions occur when energy from the main beam of the transmitting antenna reaches the receiving antenna without passing through the sample. Edge diffraction effects were

discussed earlier in Section 3.2.4. Free-space measurement error and noise sources are discussed in [22], [45], [105], [42], and [43].

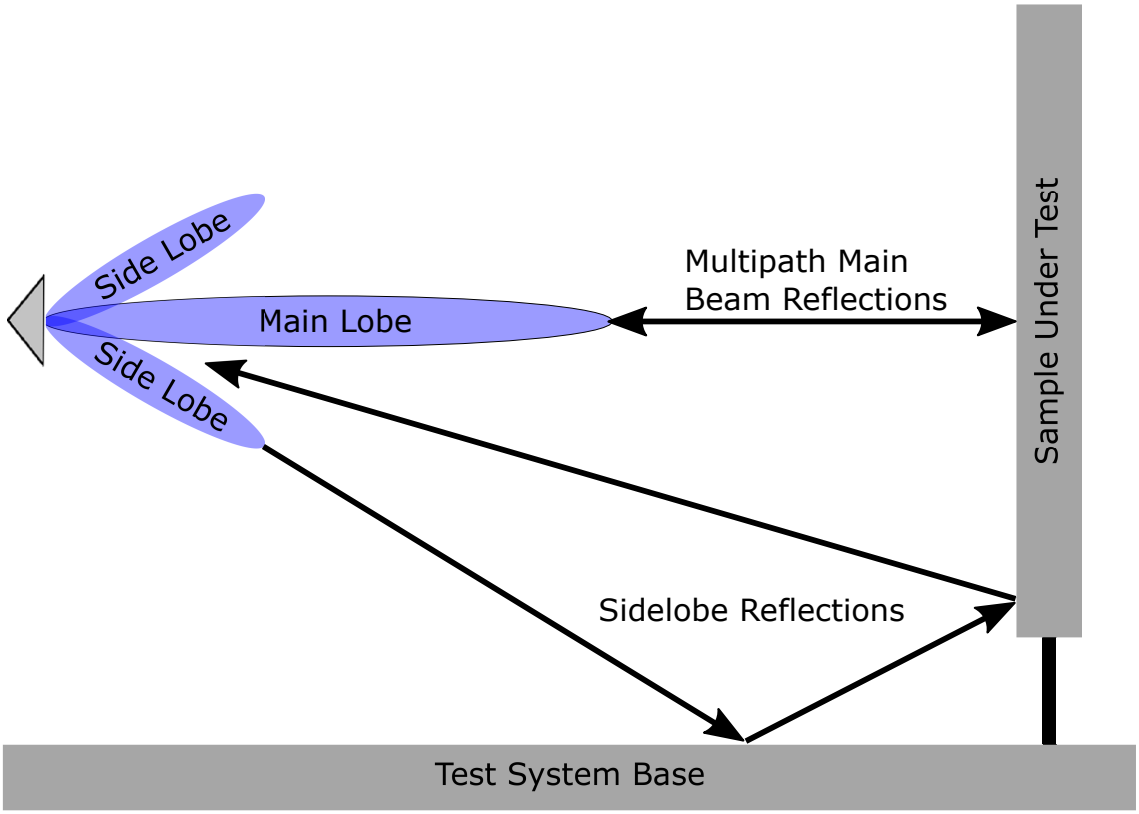

Figure 3.16: Unwanted Reflections in the Free Space Measurement Setup.

Much of the noise and measurement error involved in free space measurements can be reduced or eliminated through proper design and careful setup of the test equipment itself. Careful design and component selection can be used to mitigate misalignment errors and system noise caused by impedance mismatches. Isolation of the test setup (for instance by placing it in its own anechoic chamber) can reduce environmental noise. Direct transmission and edge effect errors can be eliminated through proper characterization of the test antennas and by using a sample with a large enough cross-sectional area (x- and y-dimensions at least 1.5 times that of the antenna beam width). Covering reflective suraces on or near the test setup with

anechoic foam can reduce unwanted reflections (although it can't entirely eliminate them). Any remaining noise/error will need to be dealt with through calibration or post-processing.

Calibration in the free space measurement technique provides a baseline of a system's transmission and reflection characteristics without the sample. This serves two primary purposes. First, it allows for the characterization and removal of environmental and system noise in the measurements. Second, it allows the reflection and transmission characteristics of the material to be de-embedded from measurements of the system as a whole. Ideally, to characterize a material using reflection and transmission characteristics, the test signal would be generated and measured directly at the surfaces of the sample under test, so that nothing else would have any impact on the measurements. This is not possible in practice, however, as the test antennas must be placed far enough away from the sample that it is in the far-field region (as discussed in Section 3.2.4). As such, there are both attenuations and phase shifts in the signal associated with the time that it travels through the air between the sample and the test antennas, which can impact the extracted material parameters. A proper free space calibration must capture these impacts as well as the system noise.

A number of ways exist to calibrate free-space transmission-reflection measurement systems. [50] and [51] provide good overviews of many of the more common ones. The simplest free-space calibration is the Thru Reflect (or TR) method, which is a two stage, four term calibration method [47]. The Thru stage is performed by measuring the S_{21} parameter of the system with the full test setup in place but

nothing in the sample holder, as shown in Figure 3.17 a). This provides a baseline measurement of the attenuation and phase shift for a signal that is perfectly transmitted through the system. The Reflect stage of the TR calibration is depicted in Figure 3.17 b). Here, a sheet of highly reflective metal is secured in the sample holder, and the S_{11} parameter is measured. Ideally, the thickness of the reflective sheet should exactly match the thickness of the sample to be tested. This allows the phase shift and attenuation of a signal that is perfectly reflected through the system to be baselined. After taking S_{11} and S_{21} measurements with the sample in place, the calibration is applied as follows [47]:

$$S_{11}^{cal} = \frac{S_{11}^{measured}}{R_{11}}\,, \tag{3.19}$$

$$S_{21}^{cal} = e^{-ik_0 t}\frac{S_{21}^{measured}}{R_{21}}\,, \tag{3.20}$$

where R_{11} and R_{21} are the reference S-parameter values measured during calibration, k_0 is the signal wavenumber in free space, and t is the thickness of the sample under test. The $e^{-ik_0 t}$ term in Equation 3.20 is a phase adjustment meant to correct for the space occupied by the sample [22]. Equation 3.19 assumes that the face of the reflective sheet is exactly the same distance from the antenna as the face of the sample to be tested. If that is not the case, then the right side of Equation 3.19 must also be multiplied by a phase correction term [22].

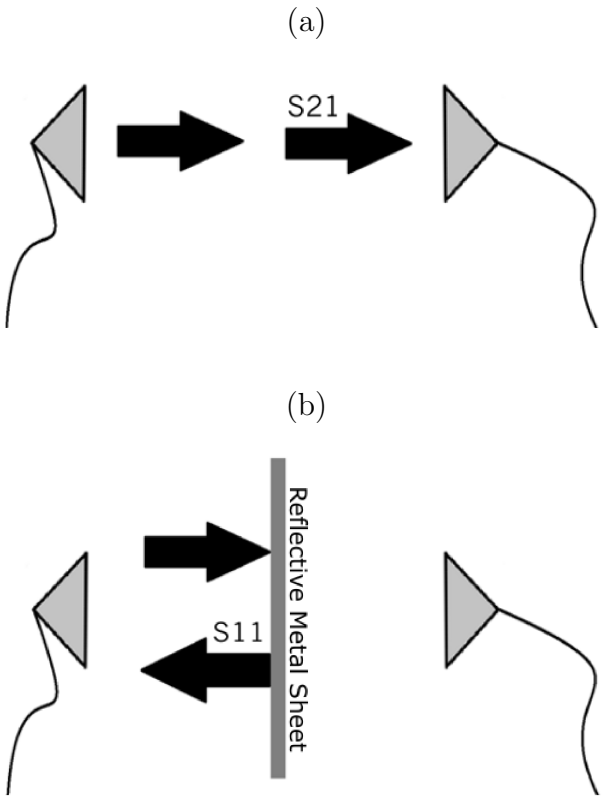

Figure 3.17: Setup for the four term free-space TR calibration. a) Setup for Thru measurement of the TR calibration. b) Setup for Reflect measurement of the TR calibration.

It is apparent that the standard TR calibration procedure described above is set up to be used with one way free space measurements (i.e. only one test antenna is used to tranmit) where both transmission and reflection measurements are made. However, the same principles apply to transmission-reflection only measurements and to two-way measurements. To calibrate transmission-reflection only measurements, only the associated step of the TR calibration is used (Thru for transmission only and Reflect for reflection only) [82]. For two-way free space measurements, the

TR calibration is applied identically in either direction, and the additional reference measurements are used to calibrate S_{22} and S_{12} [22]:

$$S_{22}^{cal} = \frac{S_{22}^{measured}}{R_{22}}\,, \tag{3.21}$$

$$S_{12}^{cal} = e^{-ik_0 t}\frac{S_{12}^{measured}}{R_{12}}\,. \tag{3.22}$$

In most free space characterization setups, the four term, one way TR calibration is sufficient. However, if high measurement accuracy is needed and misalignment error or system noise is a concern, the TR calibration method can be further expanded with the use of a well characterized isolation samples (opaque metal for transmission and absorbers for reflection). This is accomplished by running the steps of the two way TR method, and then measuring each of the four S-parameters again with the isolation standards in place. These additional measurements are referred to as isolation terms, and they are used in Equations 3.19 - 3.22 as follows [22]:

$$S_{ij}^{cal} = \frac{S_{ij}^{measured} - I_{ij}}{R_{ij} - I_{ij}}\,. \tag{3.23}$$

More complex free space calibrations have been proposed and used, including some that have been adapted from existing calibration methods commonly used in the transmission line transmission-reflection measurement setup. These include the variable transmission (LNN) [49], variable reflect (LRR) [49], and Thru-Line-Reflect (TRL) [48] methods. However, while these calibrations can provide higher measurement accuracy, they require multiple adjustments of the test setup during

calibration, increasing the run time, complexity, and the potential for introducing misalignment errors. As this project is focusing on devloping and testing a new free space test setup, the simple TR method will be sufficient when calibrating for oblique incidence measurements.

While most other sources of error and noise in the free space setup can be dealt with through a combination of careful system design work, proper sample preparation, and calibration, the issue of unwanted reflections persists. While the use of absorbing foam in the test setup can mitigate the issue of side lobe reflections from the test equipment and the surroundings, it does not help with the issue of multi-path reflections from the main beam. In order to deal with this, a post-processing technique known as time-domain gating is applied. Time domain gating is a process in which data is filtered by selecting and using only those portions of it that fall within a certain region of the time domain. It is described in [57] and [22].

In the free space test setup, the distance D between the test antennas and the sample is fixed and known for any given test being run. Since the velocity of electromagnetic waves travelling in free space is also a well known constant ($c = 2.99792458 \times 10^8$ m/s), the time t it takes the main beam of a signal transmitted by the test antennas to reach the sample, be reflected, and then travel back to the antenna can easily be determined:

$$t = \frac{2D}{c}\,. \tag{3.24}$$

Any multi-path reflections that reach the antenna will, of course, have travelled some integer multiple of the distance traveled by the initial reflection and therefore also take $n \times t$ (n = 2,3,4...) seconds to be detected by the antenna (see Figure 3.18). By limiting the range of data in the time domain that is used in extraction to those that fall near t, these multi-path reflections are removed.

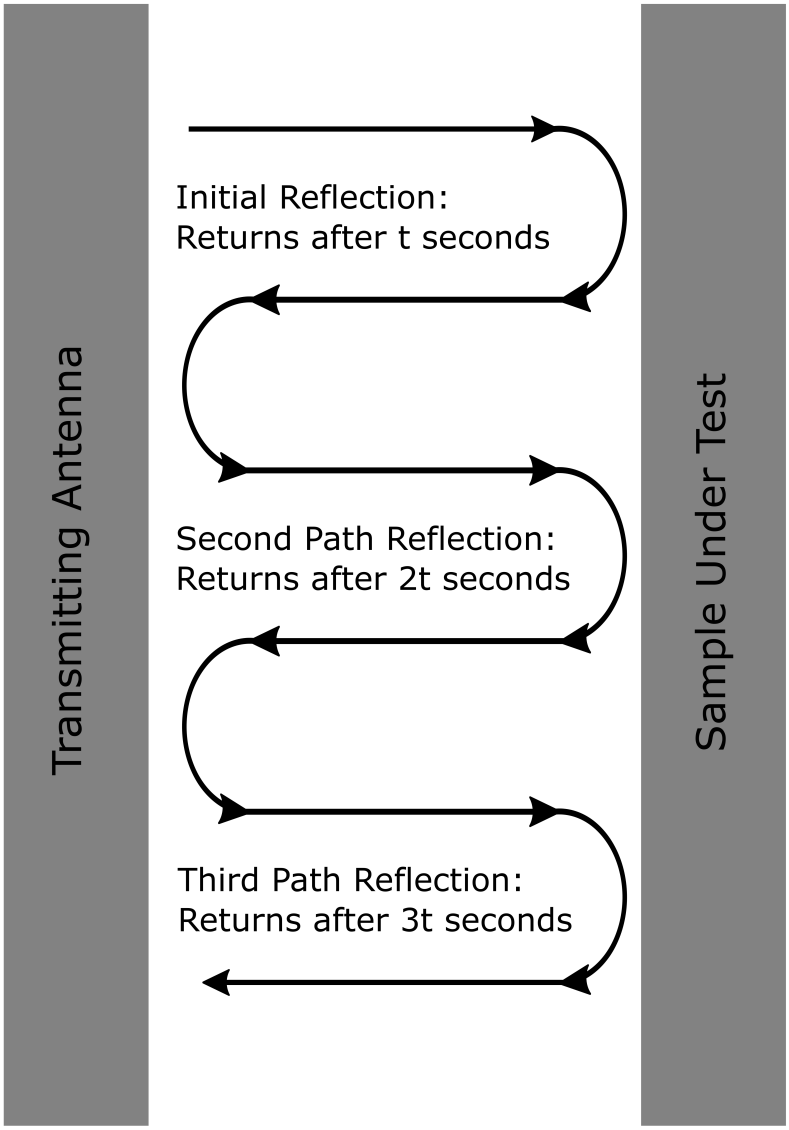

Figure 3.18: Multi-path reflections and time domain gating.

The VNA collects data at discrete frequency points that need to be converted to the time domain in order the time-domain gating to be applied. The inverse Discrete Fourier Transform is used to make the conversion:

$$x[n] = \frac{1}{N} \sum_{k=0}^{N-1} X[k] e^{jk\frac{2n\pi}{N}}, n = 0, 1, 2, ..., N-1 \tag{3.25}$$

where $x[n]$ is the signal in the time domain, X[k] is the signal in the frequency domain, and N is the total number of discrete data points. The number of samples taken by the VNA over the test bandwidth BW will determine the unambiguous range of system [22]:

$$R_{unambig} = \frac{c\frac{N-1}{BW}}{2}, \tag{3.26}$$

As such it is vital that a sufficient number of samples to be taken based on the test conditions (bandwidth and sample distance).

3.4 Extraction Algorithms

The last component that needs to be selected when designing a material characterization system is the extraction algorithm. Numerous algorithms have been developed to extract the constitutive parameters from the S-parameters measured in free space measurement setups. The most common of these algorithms will now be reviewed.

3.4.1 Nicholson-Ross-Weir Algorithm

The Nicholson-Ross-Weir, or NRW, algorithm is the most widely used algorithm for the free space characterization of materials. It was first developed by A. Nicholson and G. Ross in 1970 [60], and was later modified by W. Weir in 1974 [61]. [62] provides a good overview of the NRW algorithm, including its derivation and limitations. The widespread popularity of this algorithm is due to its relative simplicity and low computational requirements. This algorithm directly computes the constitutive parameters of a sample based on their relationship to the transmission and reflection coefficients at the interfaces between the material and air. First, the transmission and reflection coefficients are calculated from the measured S-parameters by defining the parameter χ:

$$\chi = \frac{S_{11}^2 - S_{21}^2 + 1}{2S_{11}}\,, \tag{3.27}$$

$$\Gamma = \chi \pm \sqrt{\chi^2 - 1}\,, \tag{3.28}$$

$$T = \frac{S_{11} + S_{21} - \Gamma}{1 - (S_{11} + S_{21}\Gamma)}\,. \tag{3.29}$$

Next, the parameter Λ is defined:

$$\frac{1}{\Lambda^2} = -[\frac{1}{2\pi l} ln(T)]^2\,, \tag{3.30}$$

where l is the thickness of the sample under test. Now the relative permittivity and permeability can be calculated using Equations 3.32 and 3.31

$$\mu_r = \frac{2\pi(1+\Gamma)}{\Lambda k_0(1-\Gamma)}\,, \tag{3.31}$$

$$\epsilon_r = \frac{4\pi^2}{\mu k_0^2 \Lambda^2}\,, \tag{3.32}$$

where k_0 is the wavenumber of the propagating signal in free space.

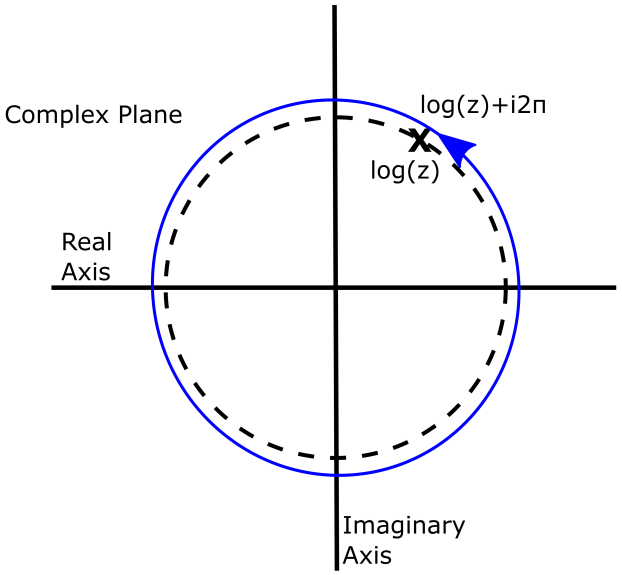

Figure 3.19: Ambiguous nature of the complex logarithm.

The NRW extraction algorithm suffers from one major flaw: the extracted parameters are ambiguous [62]. This ambiguity arises from the logarithm calculated in Equation 3.30. The transmission coefficient, T, in this equation is complex valued. Due to the periodic nature of the complex logarithmic function, this results in Equation 3.30 becoming:

$$\frac{1}{\Lambda^2} = -[\frac{1}{2\pi l} ln(T) + i2\pi n]^2\,, \tag{3.33}$$

where n can be any integer value. This is illustrated above in Figure 3.19.

Because there are an infinite number of possible solutions to Equation 3.33, there are similarly an infinite number of possible solutions to Equations 3.32 and 3.32, which can be vastly different. However, only one of these sets of solutions accurately reflects the values of ϵ_r and μ_r. Each potential solution to the complex logarithm is known as a different branch, and this issue is commonly known as the branching ambiguity. This ambiguity is well documented, and is discussed in [58] and [27].

When the thickness of the sample under test is low with respect to the wavelength of the transmitted waveform in the sample ($l << \lambda_r/2$), then the correct solution of Equation 3.33 occurs when $n = 0$ (referred to as the principle branch) [58]. However, as the thickness increases with respect to the propagating wavelength a phase wrapping will eventually occur, resulting in the solution switching to another branch. By keeping the thickness of the sample under test below $\lambda_r/4$, it is possible to avoid the branch ambiguity. However, since the wavelength of energy traveling through a material is dependent on its constitutive parameters, this would require some prior knowledge of the range in which those values fall. It also becomes increasing difficult at higher frequencies, limiting the range over which a material could be characterized. It is even more problematic with artificial dielectric layers, as the thickness of these metamaterial structures often can't be changed without significantly impacting their characteristics.

Other direct calculation algorithms have also been developed, such as the well known Smith algorithm presented in [63], but all suffer from some form of the branch ambiguity. Due to this, significant efforts have been made to overcome the

branch ambiguity, which will now be discussed. These will be discussed with repect to the NRW algorithm, but are directly applicable to the other direct calculation algorithms.

3.4.2 Additional Direct Calculation Algorithms

There are two primary methodologies used in direct calculation algorithms to overcome the issue of branch ambiguity. The first is commonly called the phase unwrapping or stepwise NRW method, and the second is called the Kramers-Kronig method. The phase unwrapping method, as presented in [73] and [74], tracks the phase of the transmission coefficient over the frequency range of interest in order to determine when a step change occurs.

Recalling that the branch ambiguity is a result of phase wrapping in the transmission coefficient, it is apparent that any branch change will be accompanied by a large phase jump (either from 359^o back to 0^o, or vice versa). By computing the change in phase ($\Delta\phi$) between each adjacent frequency point, it is possible to identify these phase jumps and adjust the branch accordingly. However, since the measured signals are sampled at discrete frequencies, it is unlikely that the full 360^o jump will be captured in every case. Instead, a threshold ($T_{\Delta\phi}$) is set such that whenever the phase jumps by $T_{\Delta\phi}$ or more from one sample to the next, it is assumed that the correct branch has changed. $T_{\Delta\phi}$ is typically set at 180^o.

This method is simple to implement, and does not significantly increase the computational requirements of the algorithm. However, it does have major limitations. First, it assumes that the banch at the lowest frequencies being measured is known.

Generally, it is assumed that this initial branch is the principal branch. Secondly, it requires that a very large number of frequcy points be measured in the range of interest in order to avoid missing phase jumps entirely. Finally, this method does not include any form of self-correction, so any incorrect or missed branch changes will corrupt the data for all subsequent frequency points in a given set of data.

The Kramers-Kronig method, presented in [67] and [70], makes use of the well known Kramers-Kronig relationships in order to correct for the phase ambiguity. This set of relationships allow for the direct calculation of either the real or imaginary component of a complex function from the other component. For the complex function:

$$x(\omega) = a(\omega) + ib(\omega), \tag{3.34}$$

these relationships take the form:

$$a(\omega) = \frac{1}{\pi} P \int_{-\infty}^{\infty} \frac{b(\omega')}{\omega' - \omega} d\omega', \tag{3.35}$$

$$b(\omega) = -\frac{1}{\pi} P \int_{-\infty}^{\infty} \frac{a(\omega')}{\omega' - \omega} d\omega', \tag{3.36}$$

where P is the Cauchy principal value. From Equation 3.33, it is apparent that the ambiguity of the complex logarithm lies entirely in its imaginary component. Since the real part of the complex logarithm can be computed unambiguously for the measured frequency range, it is possible to use a truncated version of the above Kramers-Kronig relationships to approximate the imaginary component unambiguously. Due to the necessary truncation of the indefinite integral, the Kramers-Kronig

approximation will not perfectly match any of the actual solution branches, but it will provide a close approximation to the ideal solution if applied over a wide frequency range. So, by computing multiple solution branches and comparing them to the Kramers-Kronig approximation, the solution branch closest to the approximation at each frequency point can be selected as the correct branch.

Several important considerations should be made when using the Kramers-Kronig method. Since this approach determines the correct solution branch for each frequency point independently, any branch misidentification at a particular frequency will not generally impact the rest of the data, meaning that this method has a sort of built in "self-correction" mechanism. However, this also results in a significant increase in both the complex and computational requirements of an extraction algorithm. The truncation of the indefinite integrals of the Kramers-Kronig relationships result in the computed approximation being more accurate the wider the measured frequency range, so it is best suited for wideband characterization. This truncation also significantly reduces the accuracy of the approximation near the upper and lower frequency bounds. Finally, in T/R and free-space measurements, the branches of the transmission coefficient converge as the thickness of the sample (l) approaches any integer multiple of one half of the wavelength of the energy propagating through the sample (see Figure 3.20). This makes it extremely difficult to accurately extract the material parameters at or near those frequencies where $\lambda = 2 \times n \times l$.

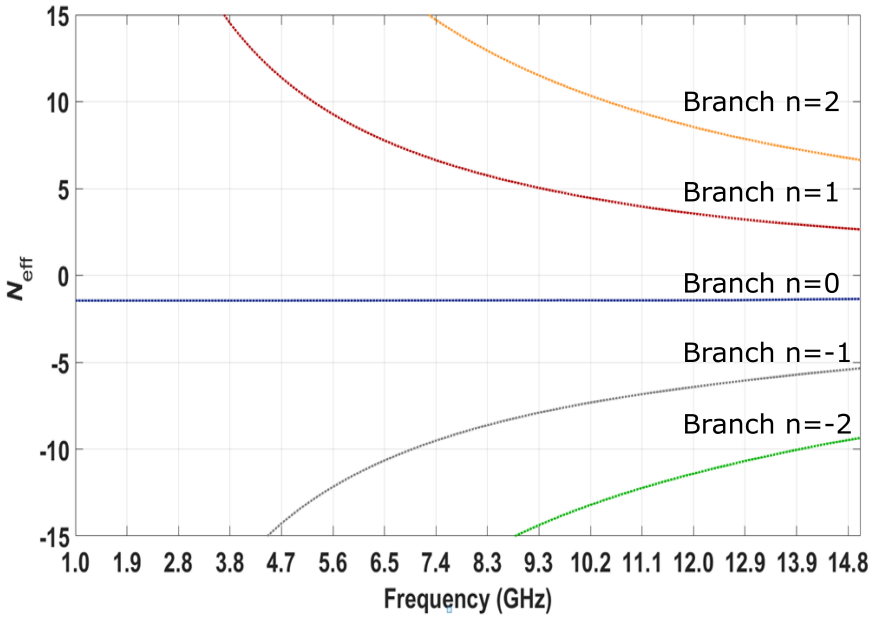

Figure 3.20: Branch convergence and the Kramers-Kronig approximation.

3.4.3 Iterative Algorithms

Additional algorithms to extract the constitutive parameters of materials have been developed that make use of iterative root-finding and minimization algorithms. The most famous of these is the NIST algorithm [5] that makes use of the Newton-Raphson root finding method, but various others have been developed that make use of a variety of techniques (such as the evolutionary algorithms used in [77] and [79]). These iterative algorithms follow the same general approach.

First, an initial estimation of the constitutive parameters is set. If the expected values are know, then these can be used. Otherwise, an initial estimate can be calculated using one of the direct computation algorithms (such as the NRW or Smith algorithms). These initial estimates are then used to compute approximations of the reflection and transmission coefficients. The Γ and T approximations are

compared to the values computed from the measured S-parameters. Next, a small change is applied to the constitutive parameter estimates based on the selected root finding/minimization technique, and the approximation of Γ and T are recomputed and recompared to the measured values. This process is repeated until the difference between the approximated and measured values of Γ and T is approximately zero.

Using iterative algorithms to extract the constitutive parameters has the key advantage that the obtained results are unambiguous. This makes these algorithms more reliable when characterizing materials over wide ranges of frequencies. However, since the parameters must be iteratively determined at each frequency point, these algorithms are computationally costly and have much longer runtimes than those that directly compute ϵ and μ. Also, both the accuracy of the extraction and the computational requirements of these algorithms are highly dependent on the quality of the initial estimates for ϵ and μ.

In general, the constitutive parameters of materials change slowly over frequency. This means that the values of ϵ and μ at adjacent frequency points will be very close, even for dispersive materials. By making use of this fact, the high computational requirements and runtimes of iterative algorithms can be reduced. If an accurate estimation of ϵ and μ can be obtained and used to find the constitutive parameters for the lowest frequency point of interest, then the obtained result can be reliably used as the initial estimate to compute the parameters for the next frequency point. Using the computed values of ϵ and μ at each frequency point as the estimates for the next frequency point, the number of iterations required is significantly reduced,

which in turn lowers the computational requirements and runtime of the utilized algorithm.

3.5 Summary

The primary goal of this thesis is to design a system to fully characterize the constitutive parameters (i.e. both real and imaginary parts of permittivity and permeability) of anisotropic materials over the S-, C-, and X- frequency bands. Based upon these constraints, the measurement technique must be able to measure the electromagnetic characteristics of solids over the minimum frequency range of 2-10 GHz. Additionally, the selected technique must allow for materials that are dispersive, inhomogeneous, and that contain metallic components. Due to the general structure of metamaterials, particularly those used in artificial dielectric layers, it is also preferable that the samples to be tested be solid sheets, meaning that the sample preparation should be nondestructive. As was mentioned previously in this chapter, the only measurement appraoch that meets all of these requirements is the Free-Space Transmission-Reflection method. As such, the designed test system will be a free-space system that allows for measurement at oblique angles of incidence.

At this stage of the project, testing will be limited to proof of concept testing. As such, calibration of the system for the normal incidence case will be done using the well known TRL calibration, and for the oblique incidence case will be done using the straightforward TR calibration. More elaborate calibration can be developed and implemented at a later stage to improve system performance. Post-processing of

the data will be limited to time-domain processing. Additionally, extraction will be done only for normal incidence using one of the simple direct calculation algorithms (either NRW or Smith). Due to the work presented in [89], [90], [91], [92], [93], [94], [64], [95], and [96], it will be sufficient for proof of concept to measure the S-parameters for the oblique case and compare against simulated data.

Chapter 4

Proposed Method for the Characterization of Anisotropic Materials

4.1 Introduction

This chapter will focus on the design and testing of a new free-space test setup to charaterize the constitutive parameters of anisotropic metamaterials. This discussion will begin with an examination of the necessary considerations that must be used for this type of characterization, as well as the issues that exist with current techniques. Then an overview of the proposed test method will be provided, focusing on its limitations and potential benefits. Following this will be a discussion of the designed measurement system, the iterations the design process went through, and the construction of the system. Next, the proof of concept testing performed on the system will be detailed, including descriptions of the methods used for calibration, measurement, and parameter extraction. This chapter will conclude with an analysis of the data collected during testing.

4.2 Considerations and Issues with Current Techniques

As was determined in Chapter 3 of this thesis, only the free-space method allows for the nondestructive, wideband characterization of materials at oblique angles of incidence. Historically, these free-space test setups have consisted of two antenna fixed so that they directly face one another, with the material to be tested secured equidistantly between them. Due to the plane wave requirements of this technique, most modern systems also have Gaussian focusing lenses attached to the ends of the antennas in order to reduce the width of the transmitted beam and the required distance between the antennas and the sample (which also reduces the minimum sample size). For the normal incidence case, this type of setup allows for relatively straightforward and reliable characterization of both of a material's constitutive parameters for various cuts in ϕ. It quickly becomes apparent, however, that such a test setup is severly limited for the case of oblique incidence.

In order to extract both the permittivity and permeability of a material using the free-space method, measurements must be made of both the S_{21} parameter (transmitted energy) and the S_{11} parameter (reflected energy). With regards to the measurement of the reflected beam in a free-space characterization setup, the "S_{11}" parameter doesn't actually refer to the energy returning to port 1 of the VNA, but rather to the specular reflection (for the normal incidence case these are the same thing). When the propagating beam is obliquely incident upon the surface of the material sample, the transmitted portion of the beam is refracted at the first

air/material interface, and then undergoes an equal but opposite refraction at the second interface, resulting in S_{21} experiencing a phase offset, but no net change in direction (see Figure 3.13). The specular reflection, on the other hand, ends up being redirected away from either antenna along an entirely new path (see Figure 4.1). As such, these specular reflections cannot be measured using the traditional free-space test setup.

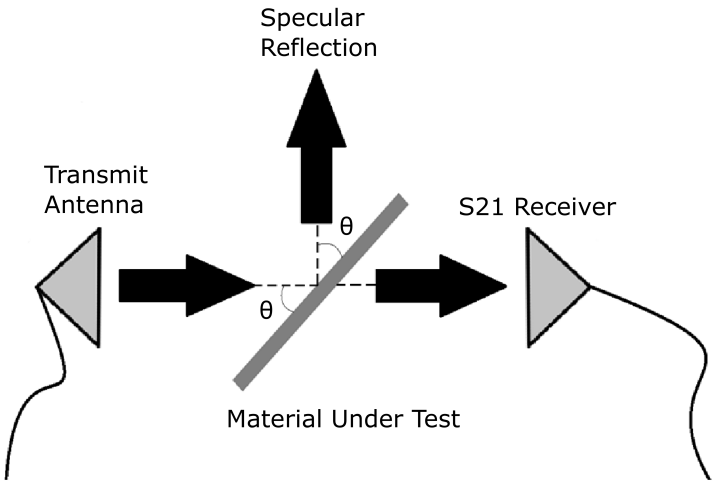

Figure 4.1: Specular reflection in the free-space test setup for the case of oblique incidence.

In order to overcome this limitation and characterize materials at oblique incidence, modern test facilities assume that the material being tested has constant permeability and use either the transmission-only or reflection-only methods depicted in Figures 3.11 and 3.12. However, the assumption of constant permeability frequently cannot be made for metamaterials, so a different approach is needed to characterize them. It is technically possible to use two seperate test setups to measure both the oblique incidence transmission and reflection characteristics seperately, but this significantly increases testing time and complexity, requires multiple

calibrations, and greatly increases the likelihood and impact of misalignment errors during testing.

4.3 Overview of Proposed Method

This thesis proposes a novel approach to the free-space characterization of anisotropic metamaterials. Rather than using the traditional two antenna approach, a third antenna will be added to the test setup. This third antenna will be mobile, allowing it to be easily adjusted in order to measure the spectular reflections for a wide range of incidence angles. This new measurement approach is depicted in Figure 4.2.

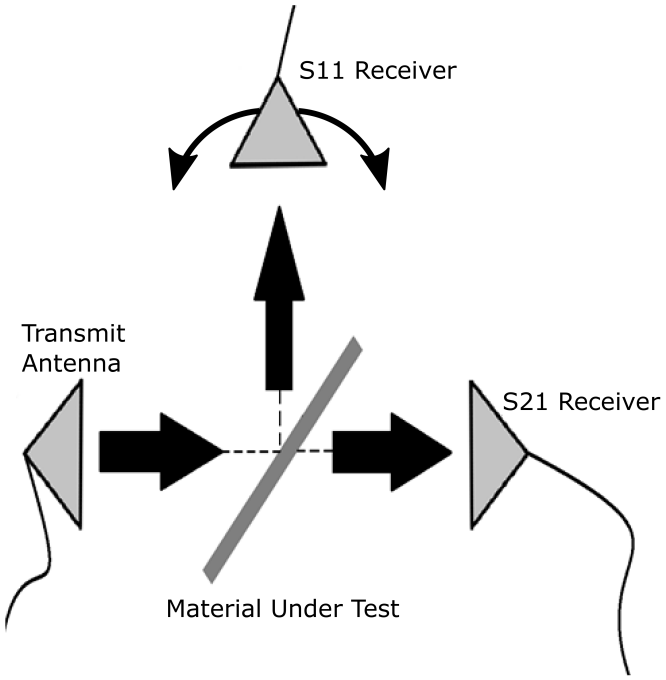

Figure 4.2: Proposed approach for the free-space characterization of anisotropic metamaterials.

A three antenna setup for free-space characterization with at least one mobile antenna would have far more versatility than the more traditional transmission-reflection-only systems. Such a system could be designed to allow for 2- or 4-parameter normal incidence, transmission-only, reflection-only, and 2-parameter oblique incidence measurements. All of which could be accomplished without alteration of the system. Also, in the case of 2-parameter oblique incidence measurements, the proposed measurement approach would allow all of the necessary measurements to be taken using a single test setup, and would only require a single calibration, making it faster, simpler, and more reliable than using multiple test setups.

While the three antenna approach would provide expanded functionality and versatility over other free-space measurement systems, it does introduce additional challenges as well. Adding a third antenna and the associated support structure increases the size and complexity of the test system. Additional alignment and calibration steps would be necessary to avoid introducing additional system and alignment errors. It also requires the ability to simultaneously connect three antennas to a VNA. This would require either using a VNA with more than two ports, which would significantly increase the overall system cost, or would require the use of a RF swith, which further increases the system complexity and would introduce additional losses. The addition of a third antenna and its associated support structure and connection components to the system would increase the overall system cost when compared with an equivalent two antenna system (although the cost would be less than building both the transmission-only and reflection-only systems).

Additionally, for use at lower RF bands, the use of Gaussian beam focusing lenses would not be practical with the three antenna measurement system proposed here. This due to the size of these lenses, which at S-band frequencies have diameters of several feet [22]. Such large lenses would be extremely difficult to manuever, and would significantly limit those angle of incidence for which a material could be characterized. As such, an alternative must be found in order to minimize the far field distance and overall illumination area of the propagating wave.

4.4 Measurement Apparatus Design

After examining the feasability of a three antenna free-space measurement system, along with it's potential benefits and limitations, it was determined that such a system could be developed and the concept drawing shown in 4.3 was created. In this initial concept, the system would consist of an elevated rotary table surrounded by three antenna mounts. A test sample would be fixed to the rotary table, which would allow the incidence angle to be easily adjusted. The antenna mounts would allow adjustment of both the height and the horizontal distance from the sample of each antenna. The initial design concept consisted of two fixed antenna mounts and one mobile one. The two fixed antennas would directly face one another and measure the S_{21} and normal incidence S_{11} parameters. The final antenna would be able to be rotated around the test sample in order to measure the specular reflection at oblique angles of incidence.

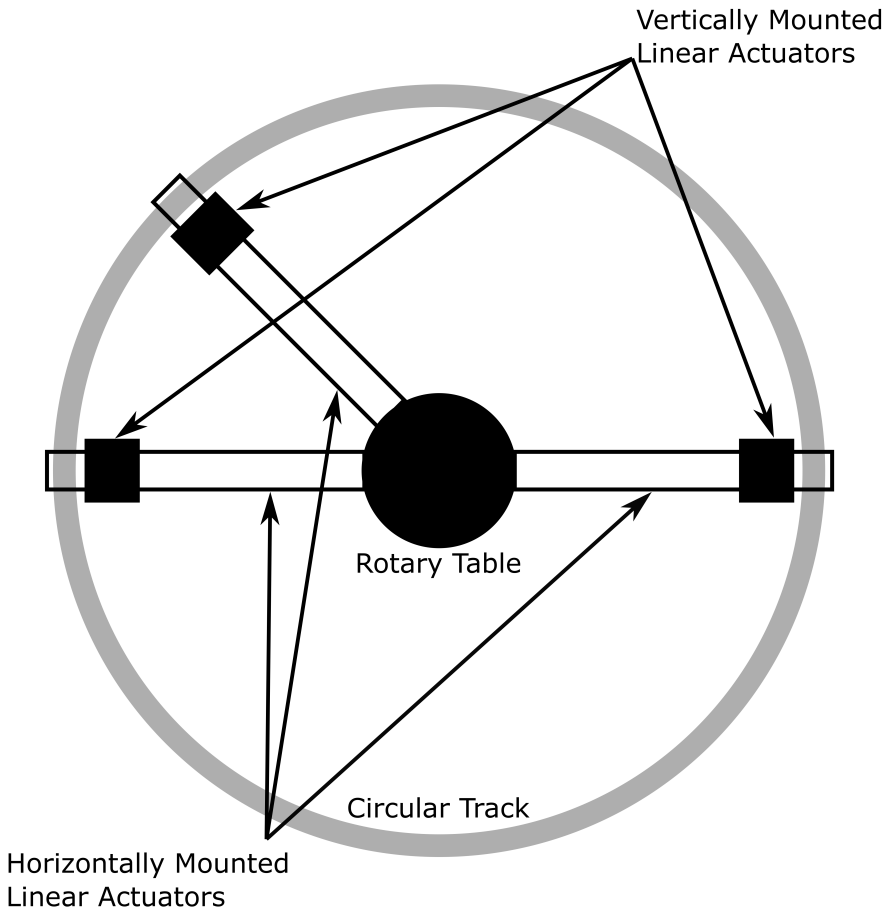

Figure 4.3: Initial design concept.

After the initial concept drawing was made and reveiwed by the team, a $10,000 budget was allotted for the system. Additionally, a rotary table and VNA already owned by the team were provided. Two weeks were then spent refining the design, sourcing potential parts, and creating a model of the system. During this time, it was decided that all three antenna mounts would be made mobile in order to allow for more test flexibility and easy modfication/expansion of the system in the future. The initial design model of the proposed system was developed in Solidworks, and is depicted in Figure 4.4.

At this stage, the design could be divided into three subsystems: 1) the base and central mount assembly (see Figure 4.5), 2) the antenna mount assemblies (see Figure 4.6), and 3) the track and cart assembly (see Figure 4.7). The base and central mount assembly depicted here consists of a base plate, two elevating platforms, and a rotary table. The base plate is a 52" $\times$ 52" $\times$ 0.5" square sheet of metal that serves as a support structure/mount for the rest of the system. The larger track and both elevating platforms would be mounted directly to the base plate. The first of the two elevating platforms has a radius of 7.67" and a height of 0.79". It serves to elevate the smaller track (which is mounted to this platform) to the same height as the larger one. The second elevating platform would have a radius of 4.9" and a height of 3.9". It would be fixed on top of the first elevating platform, and would serve as the fixture for the rotary table. A sample being tested would be fixed to the rotary table, which allows the sample to be rotated for characterization of the material at oblique incidences.

The antenna mount assembly consists of two 19.69" long stepper motor driven linear actuators with attached gantry plate carts and a 9.84" long C-Beam linear rail. One of the linear actuator and cart pairs is fixed in the horizontal plane and is used to control the distance from the antenna to the test sample. The second actuator/cart pair is mounted verically to the gantry plate cart of the first. Doing this allows both the height and horizontal distance of the antenna to be simultaneously and indepently controlled. Finally, the linear rail is fixed to the gantry plate cart of the vertical actuator and serves as the actual support for the antenna. These components were all sourced from Openbuilds.

The track and cart assembly consists of two circular metal tracks and six carts (three for each track) designed to travel smoothly around the tracks. Such track and cart systems are commercially available, and the ones used in this design model are from HepcoMotion. The larger track has an inner radius of 23.6", an outer radius of 26.4", and a height of 0.79". The smaller track has an inner radius of 6.3", an outer radius of 7.5", and a height of 0.39". Each of the three antenna mount assemblies is fixed to one pair of carts (one on the larger track and one on the smaller track). This allows the antennas to be rotated around the sample under test while maintining a constant distance from it.

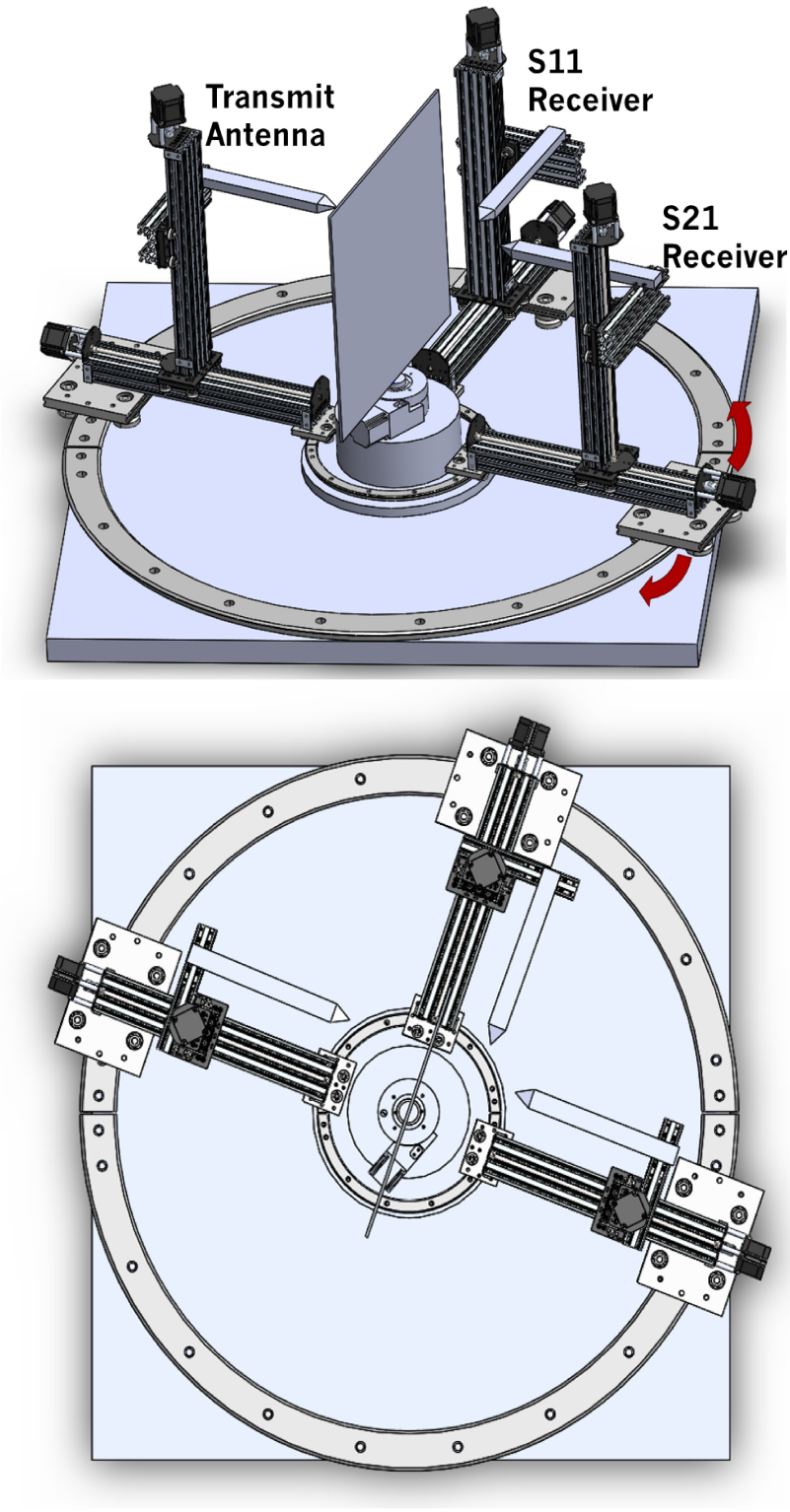

Figure 4.4: Initial Solidworks design model.

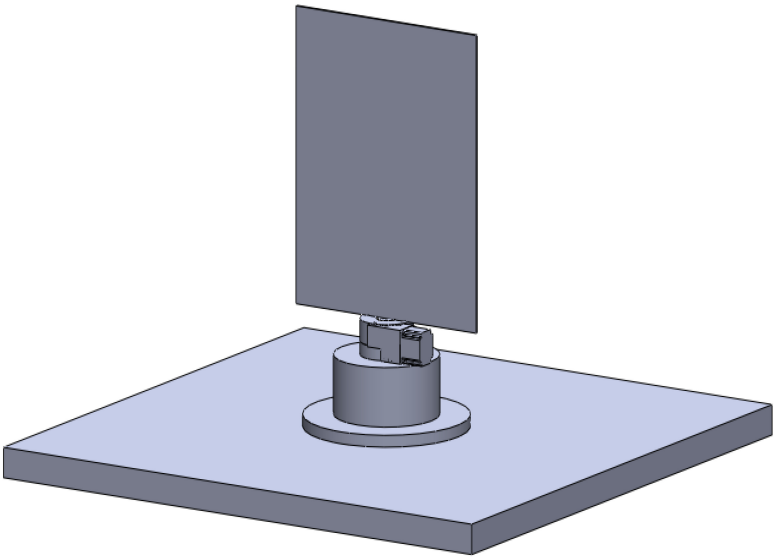

Figure 4.5: Initial Solidworks design model of subsystem 1: base and central mount assembly.

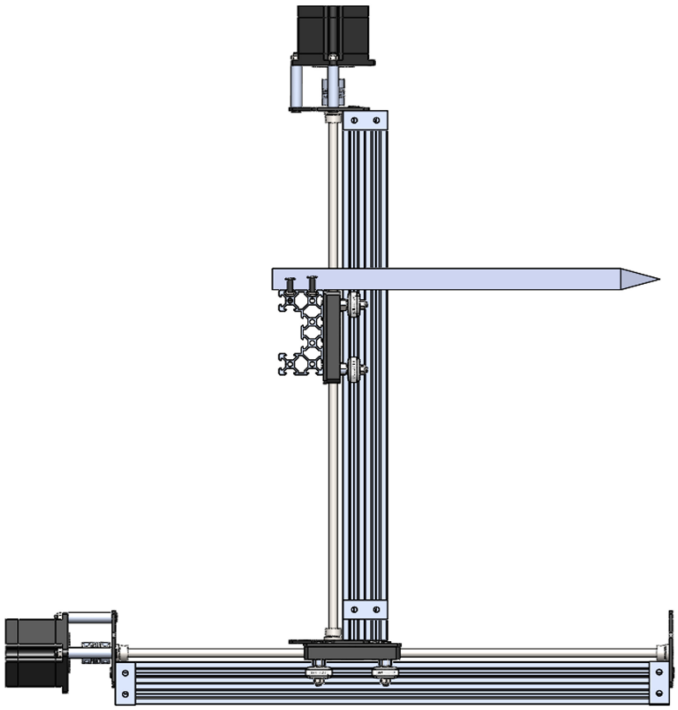

Figure 4.6: Initial Solidworks design model of subsystem 2: antenna mount assembly.

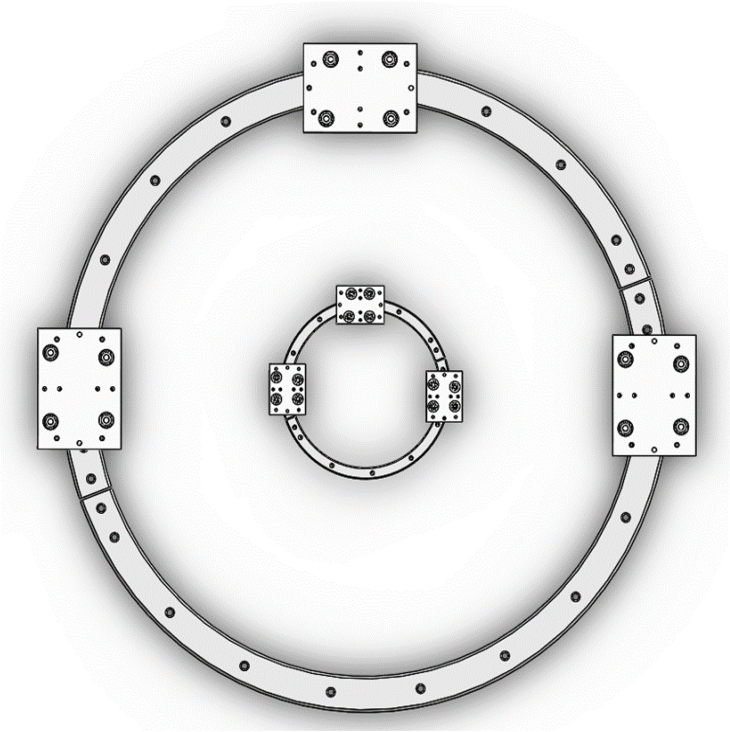

Figure 4.7: Initial Solidworks design model of subsystem 3: track and cart assembly.

Once an initial design model was completed, a design review was held. During this review, it was determined that the cost of the track and cart system needed to be replaced with something else. This was due in part to high cost, and in part to the excessive tolerance requirements of having the antenna mount assemblies connected between two concentric circular tracks. This required significant redesign work to be made, resulting in a second iteration of the design models. The second iteration of the model of the overall system is shown in Figure 4.8. The track and cart subassembly was removed entirely. Instead, the antenna mount assemblies are mounted on omnidirectional rollers and connected to the central mount via ball bearings. The revised system design consists of two subsystems: 1) the base and

central mount assembly (see Figure 4.9) and 2) the antenna mount assembly (see Figure 4.10).

The revised base and central mount assembly consists of a base plate, a mounting structure, and a rotary table. Without the tracks defining the minimum size of the base plate, the overall size could be reduced. It now consists of a tight tolerance 48" $\times$ 48" $\times$ 0.5" square aluminum sheet. This sheet serves as the support structure for the overall system, and the central mounting structure is mounted directly to it. It was important that the base plate be tight tolerance in order to make sure that the surface the antenna mounts roll across is perfectly flat. The central mounting sturcture consists of an 8.5" long solid aluminum pipe with 1" diameter, two high-pressure pipe flanges, and three flange-mounted ball bearings. The pipe flanges are secured to either end of the pipe, with one fixing the pipe to the base plate and the other fixing the rotary table to the pipe. This both secures the rotary table at the exact center of the test setup and elevates it so that the sample is well above the aluminum base plate. The flange-mounted ball bearing are secured around the pipe, and the flanged ends are each connected to one of the antenna mount assemblies. This allows the antennas to be rotated around the sample without impacting the distance between the antennas and the sample. All of the components for the central mounting structure were sourced from McMaster-Carr.

The revised antenna mount assemblies are largely the same as the in the previous design iteration, but with two additions. In order to make the antennas mobile without the track and cart assembly, each antenna mount assembly is now also fixed atop a 39.37" long V-Slot linear rail that gets connected to the central mounting

structure and an omnidirectional ball transfer. The use of ball transfers allows for free movement of each antenna mount subassembly over the surface of the base plate. The addition of the longer linear rail connected to the central mount ensures that this motion is limited to being purely rotational.

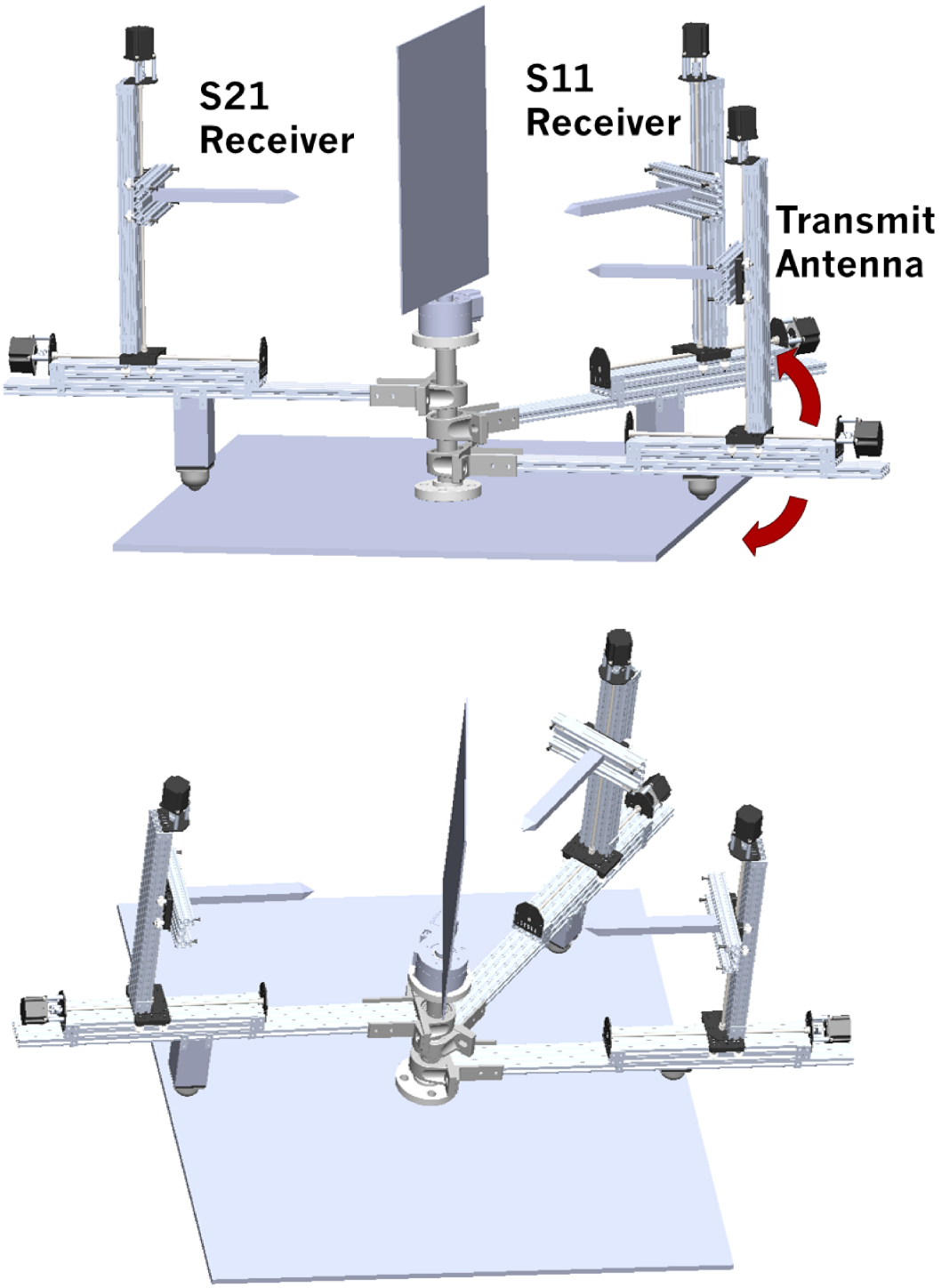

Figure 4.8: Final Solidworks design model.

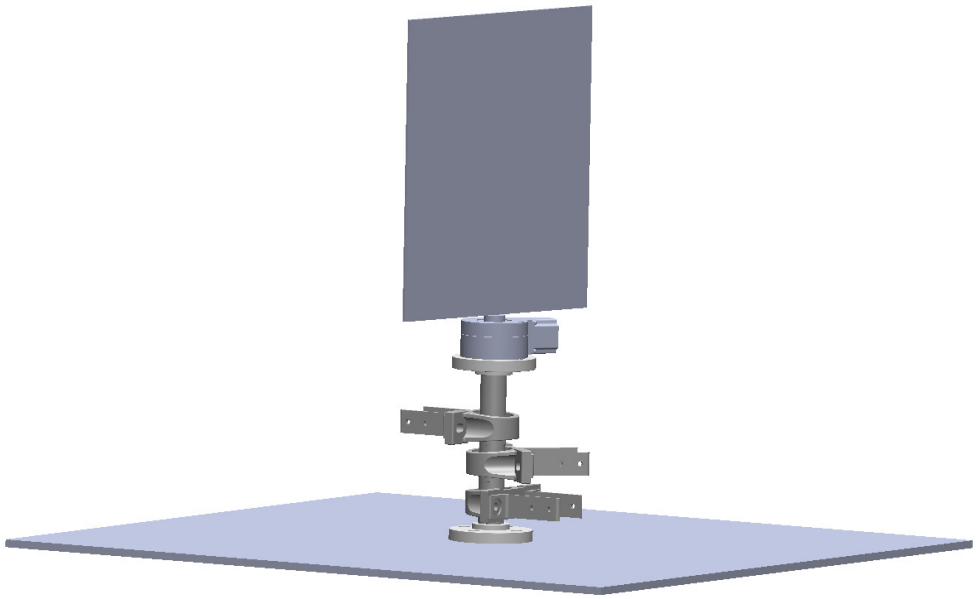

Figure 4.9: Final Solidworks design model of subsystem 1: base and central mount assembly.

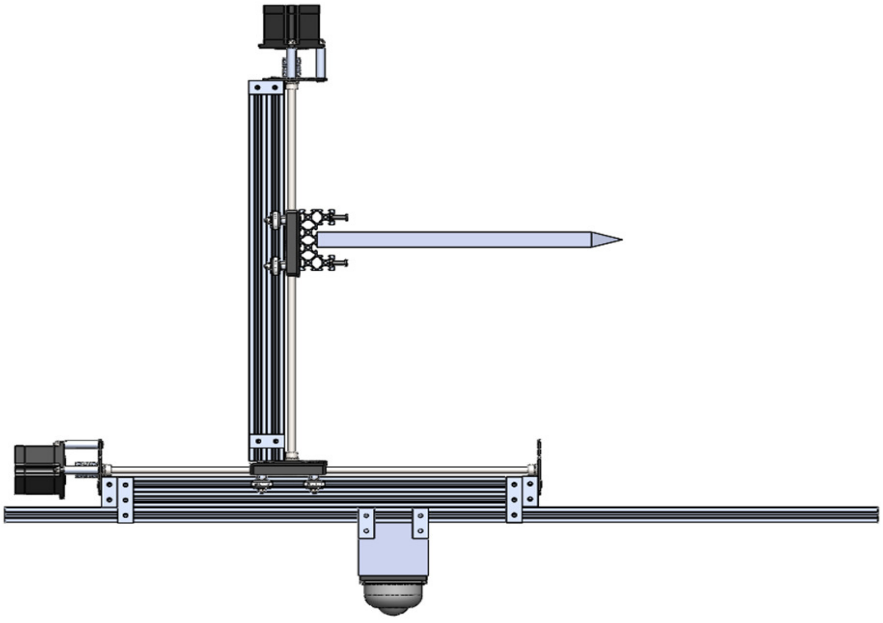

Figure 4.10: Final Solidworks design model of subsystem 2: antenna mount assembly.

After revision of the design model was completed, a second design review was held. In this review, it was recommended that each antenna mount assembly have two sets of two omnidirectional ball transfers, spaced far enough apart that they could stand upright when not connected to the central mount. Doing so would help the overall stability of the system, and help to minimize offset errors in measurement. It was also determined that a small precision machined aluminum transfer plate should be placed between the rotary table and the central mount. This would allow for easy replacement of the rotary table (when needed), and help minimize offset errors in testing. Aside from those two minor adjustments, the design was approved as presented, and parts were ordered.

All parts used in the design of the system were commercially available at relatively low-cost. The linear actuators, stepper motors, and gantry cart assemblies were purchased through OpenBuilds, and the rest of the rest of the antenna mount subassemblies and central mounting structure were purchased through McMaster-Carr. The linear actuator assemblies selected for automation of the system were the V-Slot NEMA 23 lead screw linear actuators with NEMA 23 stepper motors available from OpenBuilds. These actuator/motor assemblies provide high torque at low speeds, and are accurate to within 0.091mm (see the OpenBuilds website for the NEMA-23 linear actuator and DQ542MA stepper motor documentation). The aluminum sheets were ordered from through the ARRC engineering team. The rotary table, VNA, and rf cables/components were provided by OU's PAARD team.

The provided rotary table was the Velmex 4800 Series with attached VXM stepping motor controller. The VNA was the Copper Mountain Technologies PLANAR 804/1. This VNA operates over the frequency range from 100 kHz to 8 GHz.

In addition to the test setup itself, a control and power subsystem was designed for the linear actuators. This subsystem consisted of one 24V Meanwell power supply (available from OpenBuilds), six DQ542MA stepper motor drivers (available from OpenBuilds), and one TinyG CNC controller board v8 (avalable from Adafruit). The DQ542MA stepper motor driver is a 2-phase hybrid stepper motor driver that is ideal for bidirectional control of the NEMA 23 stepper motor. The DQ542MA stepper motor driver manual can be found online at the OpenBuilds website. The TinyG CNC controller board v8 is a microcontroller designed for use as a motor control board. It has four motor outputs (two one-directional and two bidirectional), has a simple USB interface, and comes preloaded with control firmware that allows axis mapping of the motor outputs and motor control through G-code commands.

The final components needed to complete the system were the antennas. The antennas selected were polyrod antennas designed by Allessio Mancinni (similar to those described in [106], [107], and [108]). These antennas were desirable for several reasons. They have narrow beamwidths and extremely short far-field ranges, which help to minimize the minimum sample size needed for testing. This also removed the need to use focussing lenses , reducing the overall size and complexity of the test system. These antennas could also be 3-D printed at the OU ARRC facility, substantially reducing lead time and cost. For this thesis project, testing was limited to the H-band, so the printed antennas were designed to operate from 7-10 GHz, and

are shown in Figure 4.11. These antennas have a far-field range of two inches. After being printed in the labs, each antenna's return loss was measured and was found to be ¡10dB for the center frequency of interest (see Figure 4.12). The beam pattern for each antenna was also measured using the ARRC's far field chamber, as shown in Figure 4.13. The patterns were found to be extremely consistent between the printed antennas, as shown in Figure4.14, with a 3 dB beamwidth of approximately 10^o.

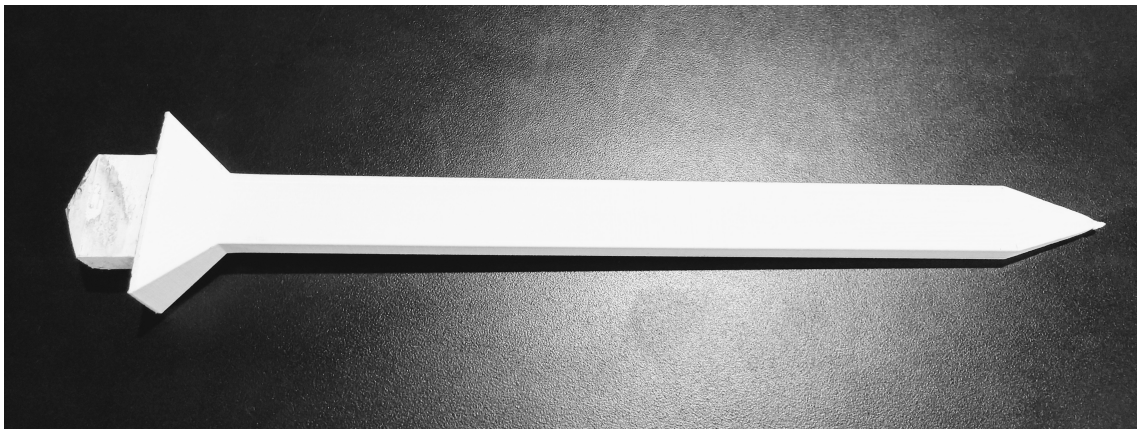

Figure 4.11: Final design: polyrod antenna.

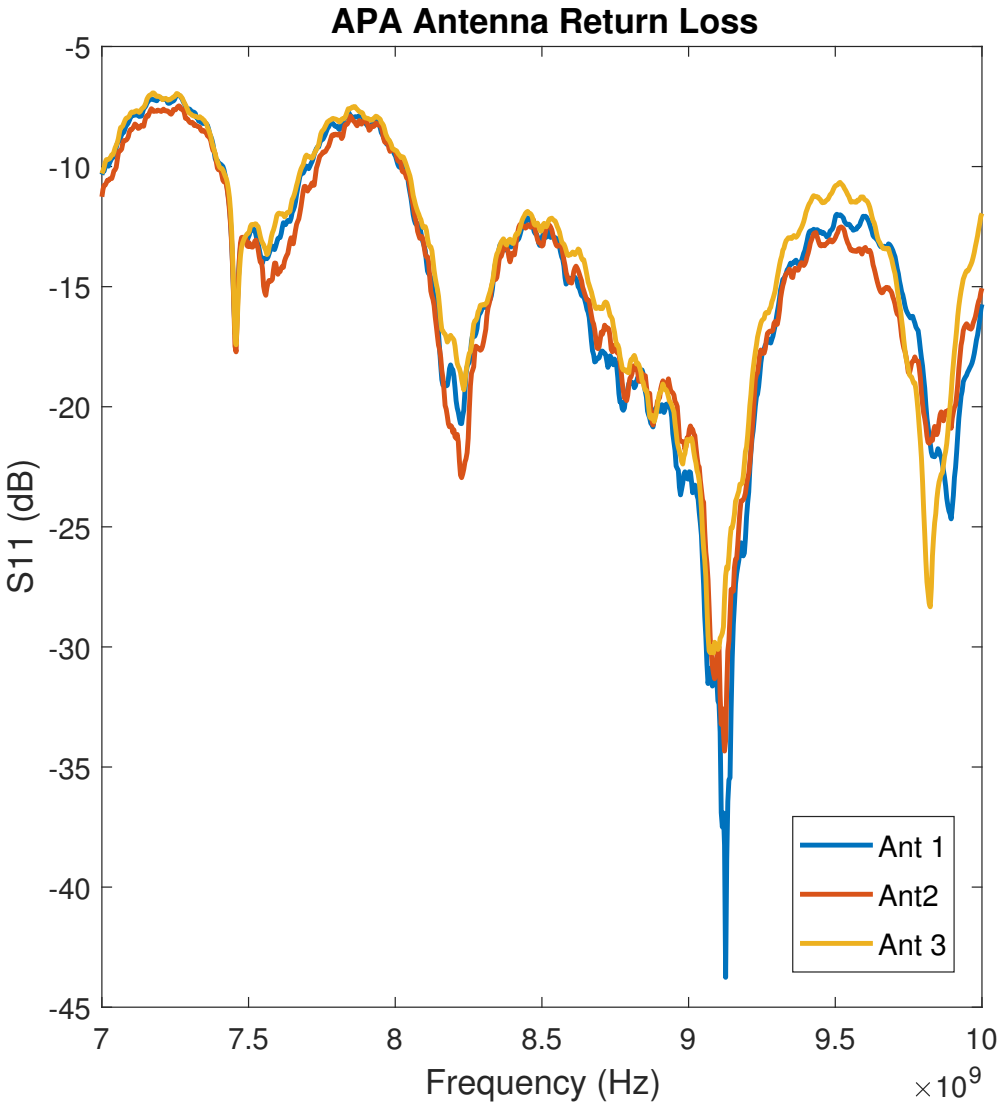

Figure 4.12: Final design: antenna return losses.

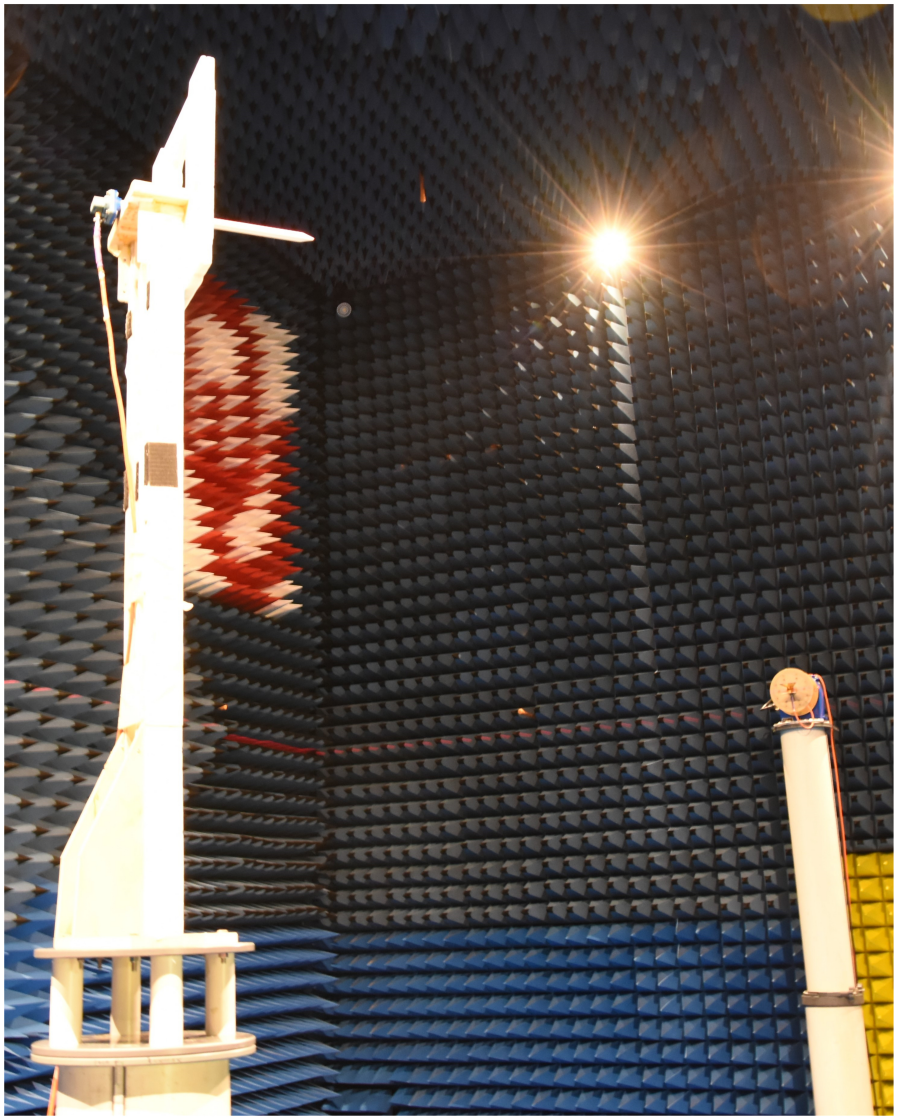

Figure 4.13: Final design: antenna beam pattern measurement setup.

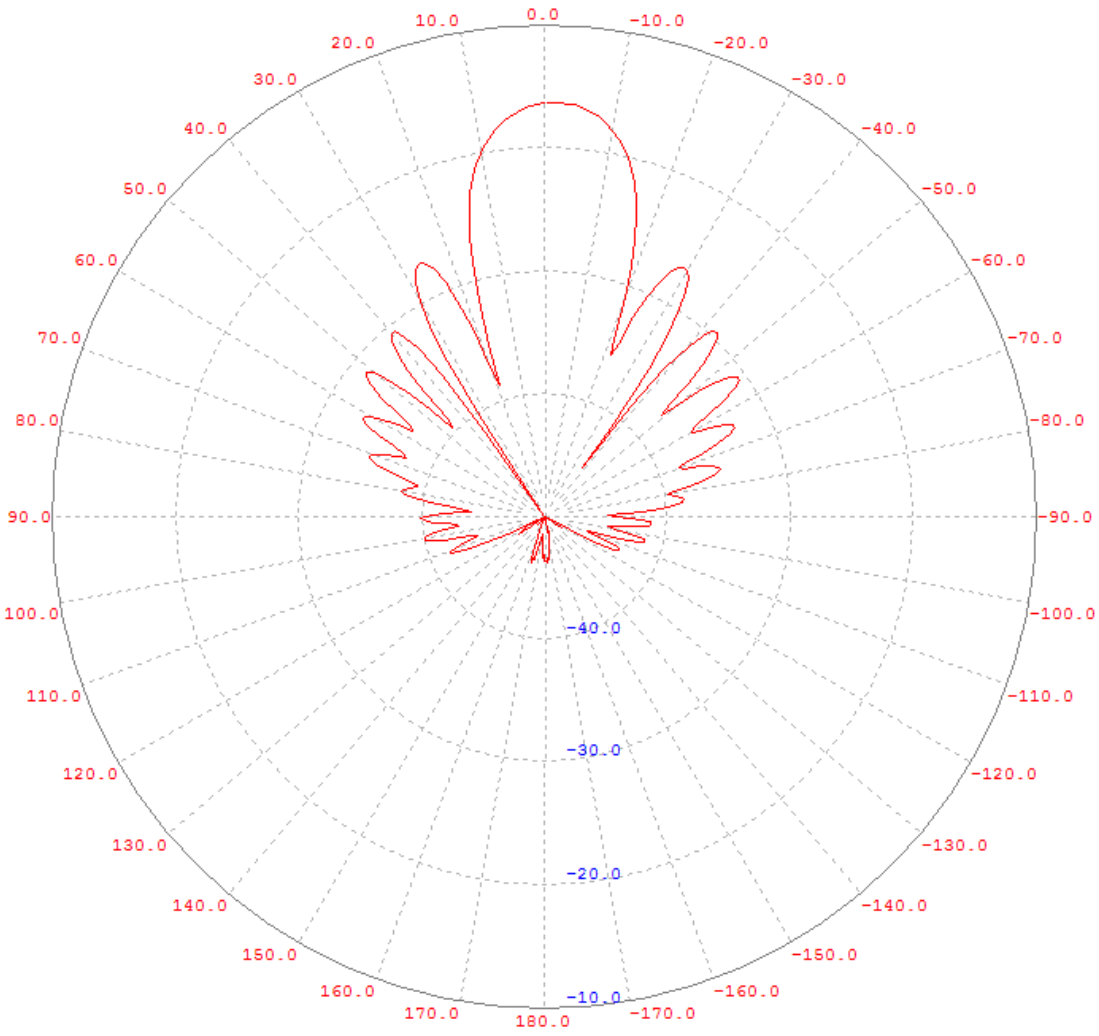

Figure 4.14: Final design: antenna beam patterns.

Finally, the system was assembled in the OU ARRC facility. The fully assembled system is shown below in Figure 4.15. Figures 4.16 and 4.17 show the fully assembled antenna mount and central mount, respectively.

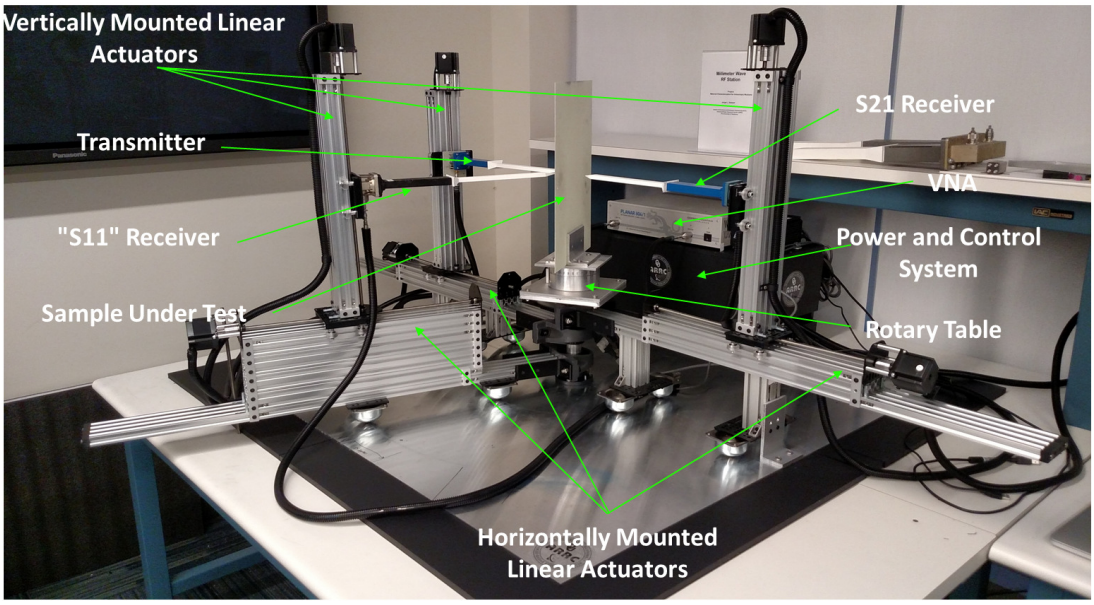

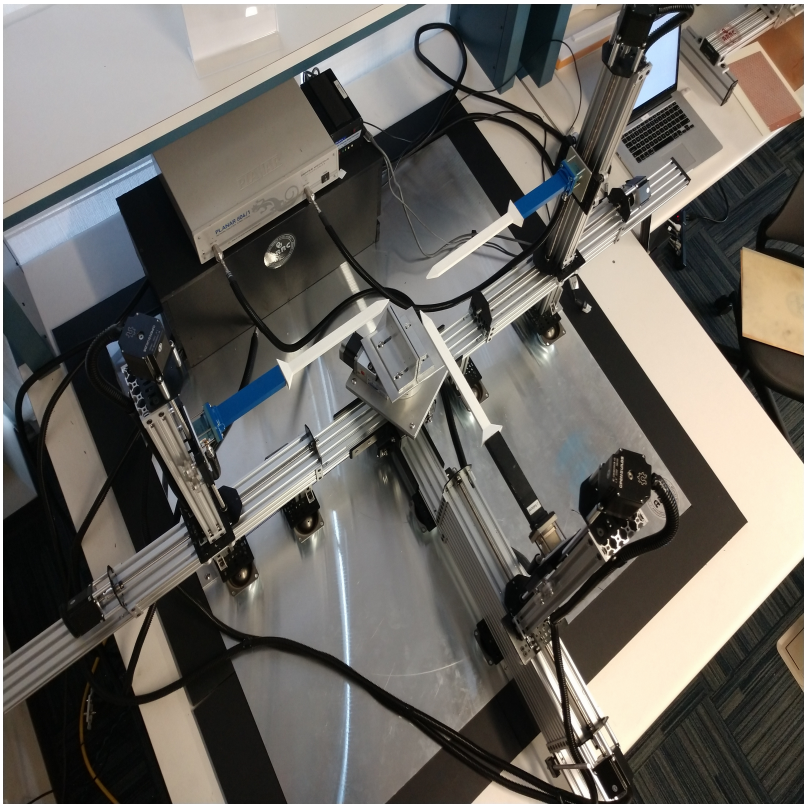

Figure 4.15: Final design: fully assembled system. Top: side view. Bottom: top-down view

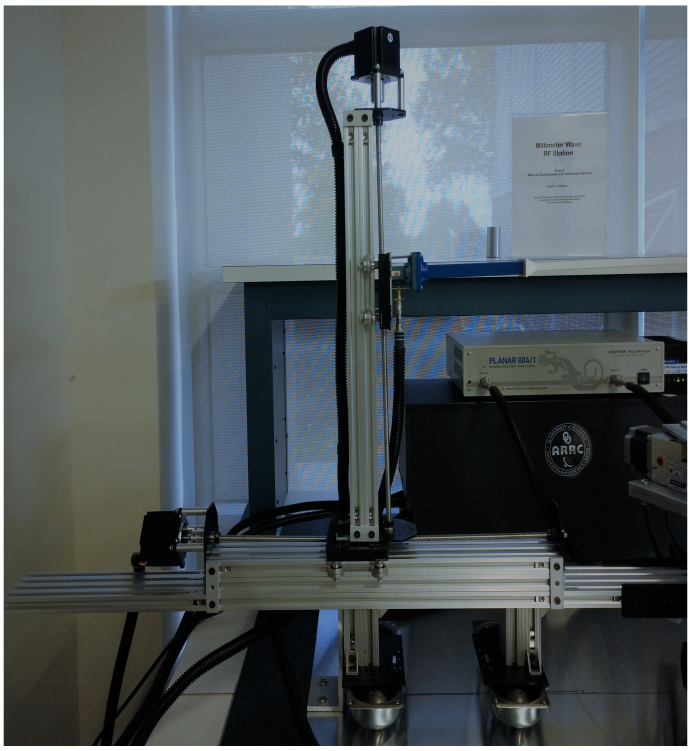

Figure 4.16: Final design: antenna mount assembly.

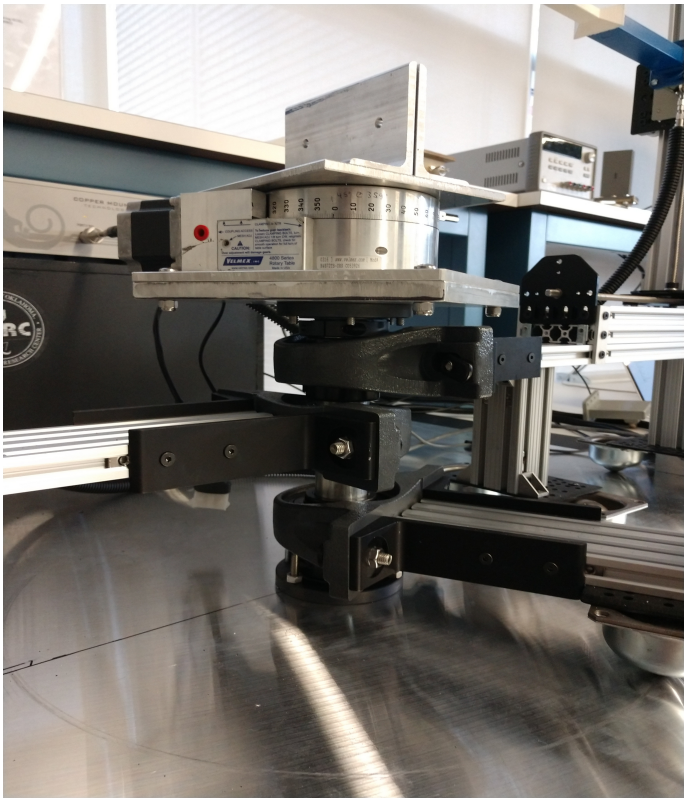

Figure 4.17: Final design: central mount assembly.

4.5 Materials Used in Testing

The ultimate goal for this system is to allow for the full characterization of anisotropic materials over a wide range of incidence angles. However, since this is a newly designed and built system, the majority of the proof of concept testing performed for this thesis project was limited to simple isotropic dielectrics. The characteristics of these materials are well documented, allowing the evaluation of system itself, as opposed to the material samples. At this stage of the development process, it also made it more clear what improvements may need to be made to the system, calibration process, or extraction algorithm. Normal incidence testing was performed on four isotropic samples: 1) 1.57 mm thick FR4, 2) 1.01 mm thick 5880, 3) 1.52 mm thick 4350B, and 4) 1.52 mm Rohacell. The thickness of the samples was kept well below $\lambda/[4\sqrt{(\epsilon_r\mu_r)}]$ in order to avoid the Smith algorithm's branch ambiguity. Due to the existence of various oblique incidence extraction algorithms whose performances have been proven using simulated data (as in [89], [90], [91], [92], [93], and [94]), when proving the system's ability to characterize materials at oblique angles of incidence it was sufficient to demonstrate that the measured S-parameters with respect to incidence angle closely match the simulated values. Oblique incidence testing was performed on the isotropic medium FR4 and an anisotropic frequency selective surface designed and provided by Dr. Qamar Zeeshan.

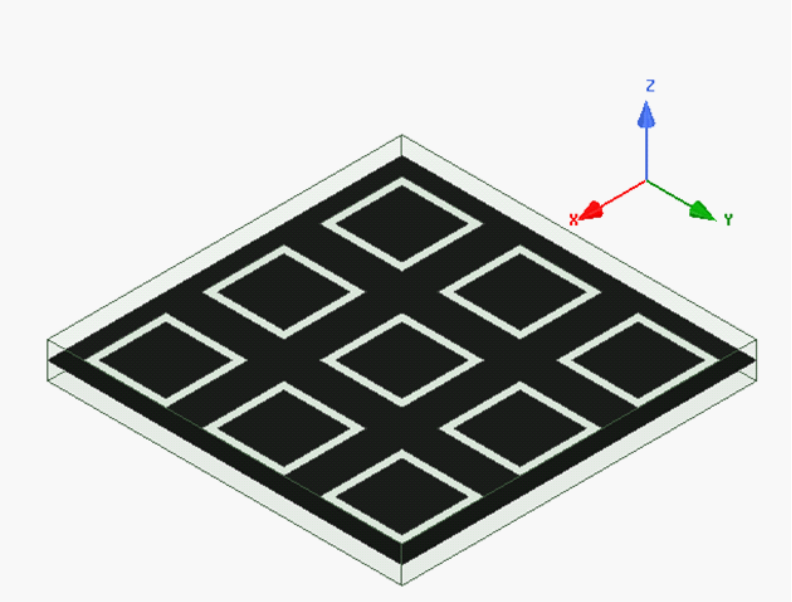

Figure 4.18: Frequency selective surface used in oblique incidence testing.

The provided frequency selective surface (depicted in Figure 4.18) was designed to behave as a spatial bandpass electromagnetic filter with the passband centered at 7.5 GHz. This engineered material consisted of a single layer of copper patch elements between two layers of Rogers 4350B. The layer of copper patch elements is used to introduce capacitive and/or inductive behaviors that set the filter characteristics of the material. Capacitive behavior is achieved through the use of square copper patches, as shown in Figure 4.19 a), while inductive behavior is achieved through the use of a copper wire mesh, as shown in Figure 4.19 b).

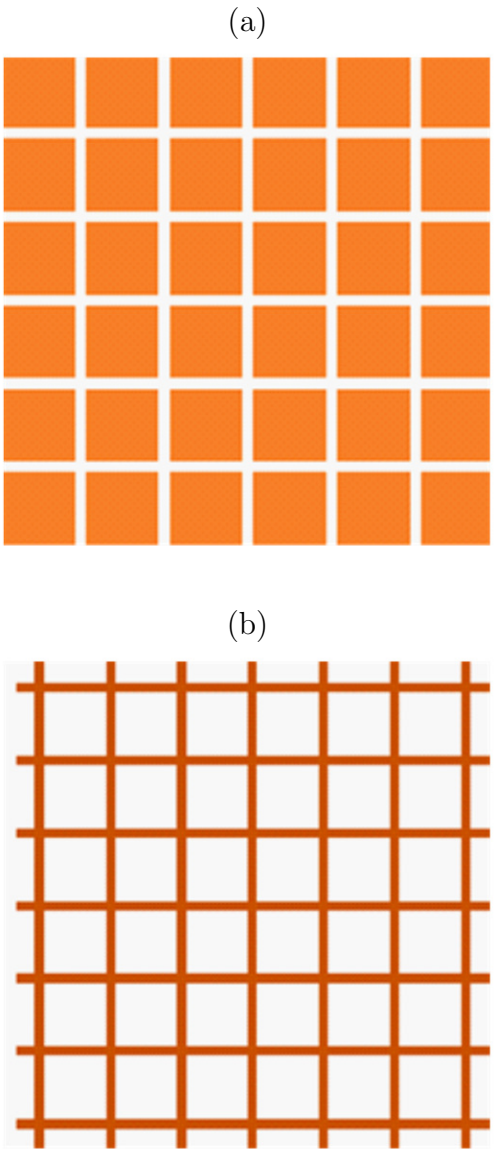

Figure 4.19: Frequency selective surface (FSS) capacitive and inductive meshes. a) FSS capacitive mesh. b) FSS inductive mesh.

The provided frequency selective surface achieves the desired bandpass filter behavior through the use of a copper layer consisting of a combination of capacitive square patches and an inductive wire mesh. This copper layer is depicted in Figure 4.20, where $L_o = 7\text{mm}$, $L_i = 5.6\text{mm}$, $W = 1.5\text{mm}$, and $P = 10\text{mm}$.

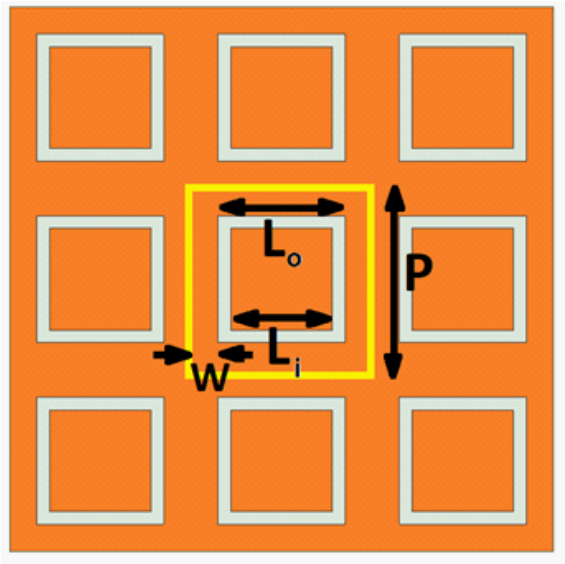

Figure 4.20: Copper layer of frequency selective surface used in oblique incidence testing.

4.6 Calibration and Measurement

Once the system was assembled, proof of concept testing was conducted. This consisted of two distinct sets of measurements. First, four materials were characterized at normal incidence. Then, the transmission and specular reflection of two materials (one isotropic and one anisotropic) were measured with respect to incidence angle. All measured data was then compared with ideal values simulated in HFSS. Both sets of measurements were made over the frequency range 7-8 GHz.

First, the alignment of the system was set. This was accomplished in several stages. A metal sheet was secured to the rotary table at the center of the test setup, and the three horizontal linear actuators were manually adjusted so that the tip of each antennas was just flush with the surface of the metal sheet. The rotational position of two of the antenna mount assemblies were then adjusted using a two

axis laser level and 90^o angle ruler until they were both exactly perpendicular to the surface of the metal sheet. These two antenna mount assemblies were secured in these positions using L-brackes fixed to the base plate. Next, the metal sheet was removed and the three vertical linear actuators were manually adjusted until the antennas were at the same height. This was verified using digital levels. Finally, the two axis laser level was again used to verify that the two previously fixed antenna mount assemblies were aligned with respect to one another.

At this stage, the system was powered on, and all subsequent adjustments of the linear actuator positions was handled programmatically. This was done by sending gcode commands via USB connection to the TinyG CNC controller board v8 using a free terminal software called CoolTerm, as shown in Figure 4.21. Calibration, time-domain gating, and data collection were all done using the Copper Mountain Technologies S2VNA VNA control software. A custom calibration kit was defined and used for all testing in this project. This calibration kit was created according to the procedure found in Chapter 5 of the S2VNA Operating Manual available from the Copper Mountain Technologies website, and is shown in Figure 4.22.

(a)

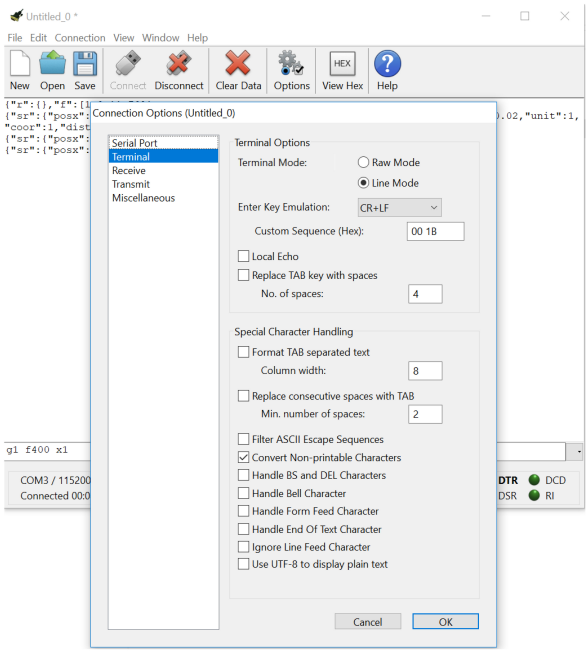

(b)

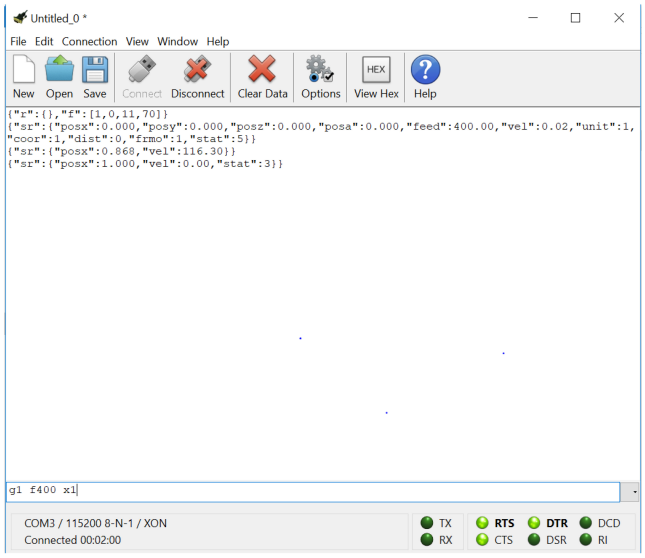

Figure 4.21: Testing: automated linear actuator control using CoolTerm. a) CoolTerm connection options setup screen. b) CoolTerm command window.

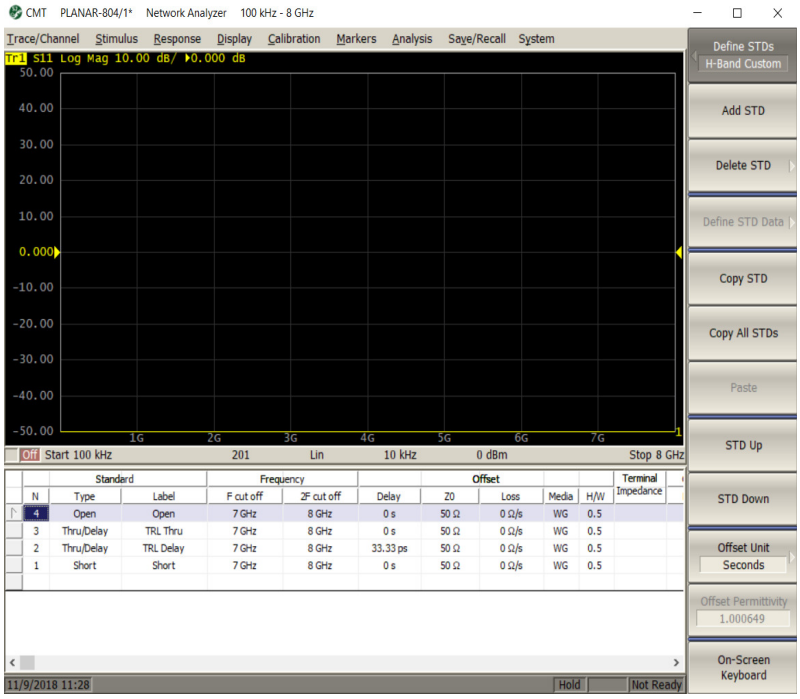

Figure 4.22: Testing: S2VNA calibration kit.

4.6.1 Normal Incidence

When extracting the parameters at normal incidence, the system was calibrated using the S2VNA's 2-port TRL calibration. This calibration is shown in Figure 4.23. The horizontal position of the antennas was adjusted so that the tip of each antenna was two inches from the surface of the test sample. A copper plated sample with the same thickness as the sample to be tested was then placed in the sample holder fixed to the rotary table, and measurements of S_{11} and S_{22} were taken for the case of perfect reflection. Then the copper plated sheet was removed and S_{21} was measured for the case of direct transmission. Next, the seperation between the antennas was increased by $\lambda/4$ of the center frequency, which for this testing was 10 millimeters, and the direct S_{21} was measured for this longer path. Finally, the

antennas were returned to their previous positions, and the calibration was applied in S2VNA.

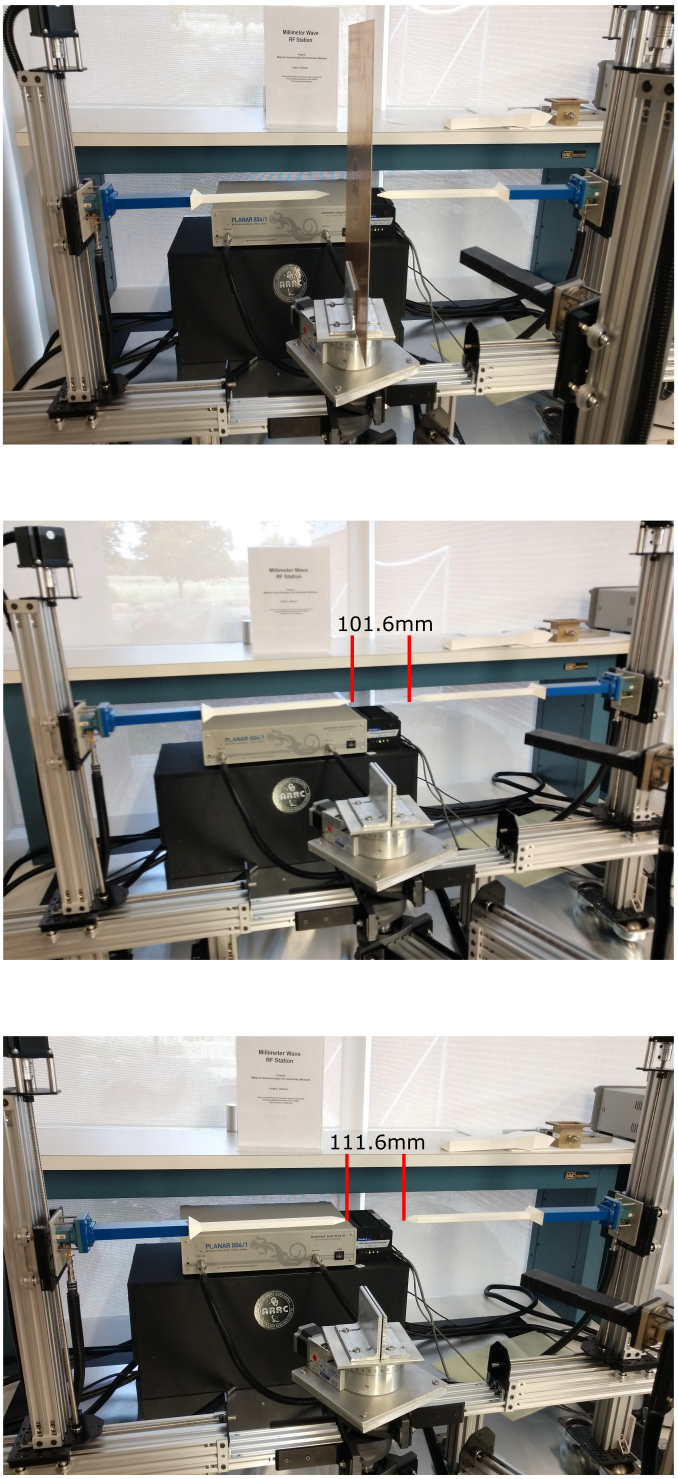

Figure 4.23: TRL calibration used in normal incidence testing. Top: reflect measurement. Middle: thru measurement. Bottom: line measurement.

After the system was calibrated, the sample under test was placed in the sample holder as shown in Figure 4.24, and measurements were taken of S_{11} and S_{21}. In order to minizize the effects of unwanted reflections, time-domain gating was applied to the data. This was done in S2VNA according to the procedure found on pages 228-230 of the S2VNA Operating Manual. For this testing, the gating settings were as follows: 1) type - bandpass, 2) window shape - normal, 3) Span - 10 ps, 4) Center - 0 ps. A phase correction of e^{-ik_0t} was applied to S_{21} in post-processing to correct for the difference in calibration path length between S_{21} and S_{11} that occurs in free-space TR or TRL calibration (as described in [22]). Finally, permittivity and permeability were extracted from the measured S-parameter data using the Smith algorithm described in [63], and these extracted parameters were compared with ideal values extracted using simulated data.

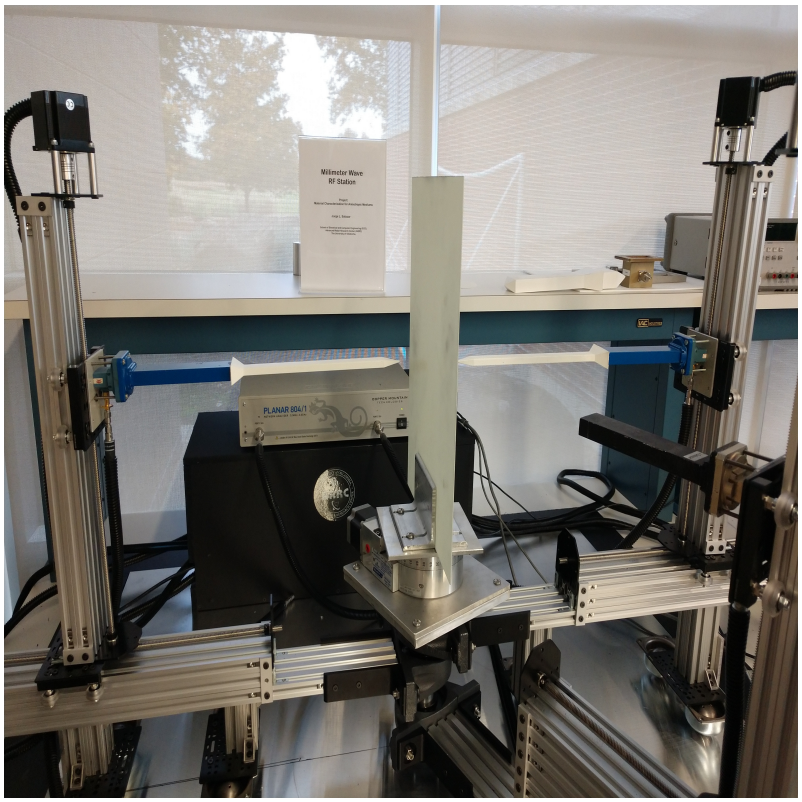

Figure 4.24: Testing: normal incidence measurement.

4.6.2 Obliquel Incidence

When extracting the parameters at oblique incidence, the system was calibrated using the TR calibration method. With the Planar-804/1 VNA and S2VNA software this required two independent Response (Thru) calibrations. These calibrations could be easily stored and recalled using the Store/Recall State features of the S2VNA software, as detailed in Chapter 7 of the S2VNA Operating Manual. As with the normal incidence measurements, the horizontal position of the antennas was first adjusted so that the tip of each antenna was two inches from the surface of the test sample. Next, the rotary table was rotated to the desired angle of incidence using the VXM stepping motor controller. The third antenna mount assembly

was then rotated so that its incidence angle was equal but opposite to that of the transmit antenna. This angle was verified using the two axis laser level. A copper plated sample with the same thickness as the sample to be tested was then placed in the sample holder (as shown in Figure 4.25), and the specular reflection S_{31} was measured for the case of perfect reflection. This calibration was applied, and the state was saved as State 1. Then the copper plated sheet was removed and S_{21} was measured for the case of direct transmission, (as shown in Figure 4.25). This second calibration was applied and the state was saved as State 2.

Figure 4.25: Testing: free-space Thru-Reflect (TR) calibration. Top: thru measurement. Bottom: reflect measurement.

After the system was calibrated, the sample under test was placed in the sample holder, and measurements were taken of the specular reflection (S_{31}) using the State 1 calibration and transmission (S_{21}) using the State 2 calibration. In order to minizize the effects of unwanted reflections, time-domain gating was applied to the data. This was done in S2VNA according to the procedure found on pages 228-230 of the S2VNA Operating Manual. As with the normal incidence testing, the gating settings were as follows: 1) type - bandpass, 2) window shape - normal, 3) Span - 10 ps, 4) Center - 0 ps. The measured S-parameters then were compare with simulated values with respect to incidence angle.

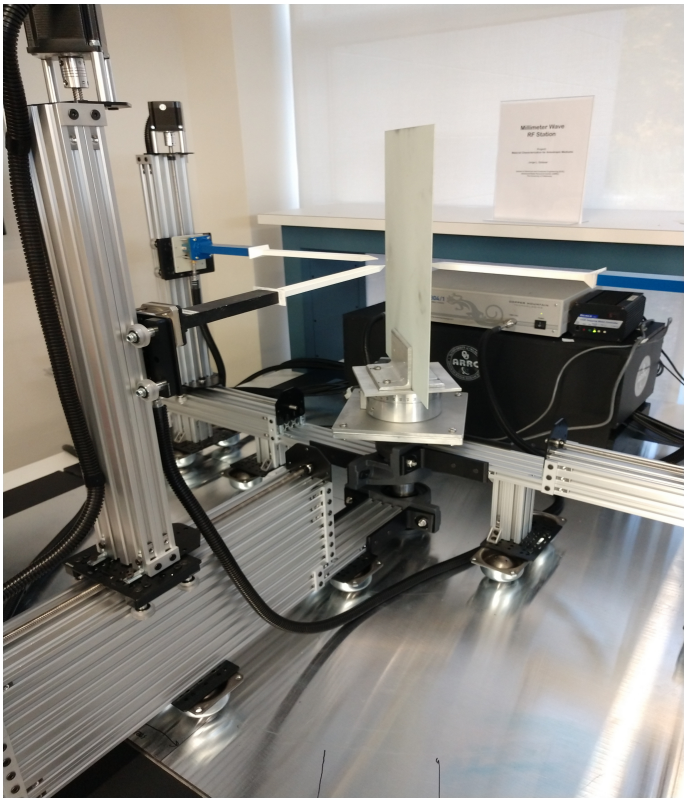

Figure 4.26: Testing: oblique incidence measurement.

4.7 Results

The results of normal incidence testing are presented below in Figures 4.27-4.38. From Figures 4.27, 4.30, 4.33, and 4.36, it can be seen that the measured values of S_{21} match perfectly with the simulated values for all four test samples. There is also close agreement between the measured and simulated values of S_{11}. With S_{11}, however, there is a non-negligible difference between the measured values and the simulated ones that varies with respect to frequency. This is strongly indicative of a phase error present in the measurement of S_{11}. This is further demonstrated in Figures 4.28-4.29, 4.31-4.32, 4.34-4.35, and 4.37-4.38. Here it can be seen that there is excellent agreement in all cases between between the measured and simulated $\epsilon^{'}$ (with errors at or below 2.2%), which is primarily dependent on S_{21}. For $\epsilon^{''}$ and μ, which are more dependent on S_{11}, the error is much higher (frequently more than 10%). Also, the difference between the measured and simulated values of $\epsilon^{''}$ and μ become less as the permittivity of the material gets closer to 1. This is because more energy is transmitted through the material rather than reflected, reducing the overall impact of the S_{11} phase error.

The observed S_{11} phase error is common in new free-space test setups, and is almost certainly due to some combination of two factors. First, the reflection standard used for calibration for each sample consisted of a sample of equal thickness that was copper plated. This results in a difference between the calibrated path and the test path equal to the thickness of the copper. This potential source of error can be mitigated during the next phase of the project by determining the

thickness of the copper and applying a phase offset in post-processing similar to the one that was applied to S_{21}. The second likely cause of the phase error in S_{11} is small offset/alignment errors in the test setup. If the samples were slightly offset from the center of the test setup, or the rotary table was slightly rotated (resulting in a very small angle of incidence), a non-negligible phase error would be introduced. This potential source of error should be investigated further in the next phase of system development. It's impacts could be mitigated through the use of 4-parameter calibration and extraction techniques or by adding isolation standards to the calibration process. The characterization and removal of this S_{11} phase error will take some time, but will otherwise be trivial and does not reflect a major limitation of the system itself. These results are very promising, and demonstrate the ability of the system to properly characterize both permittivity and permeability at normal incidence.

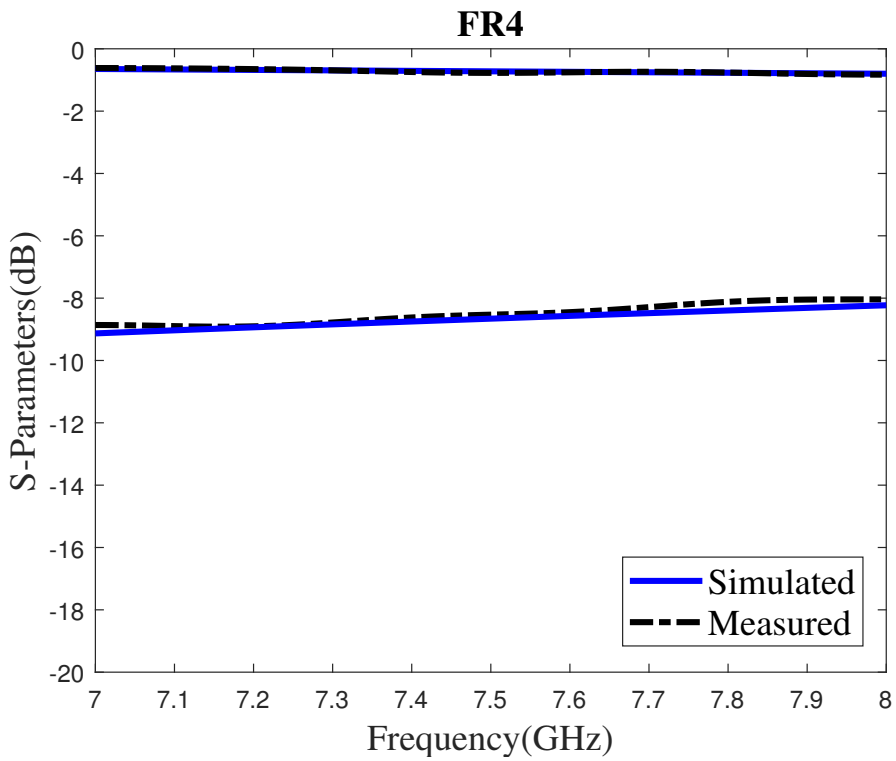

Figure 4.27: FR4 seasured and simulated S-parameters at normal incidence.

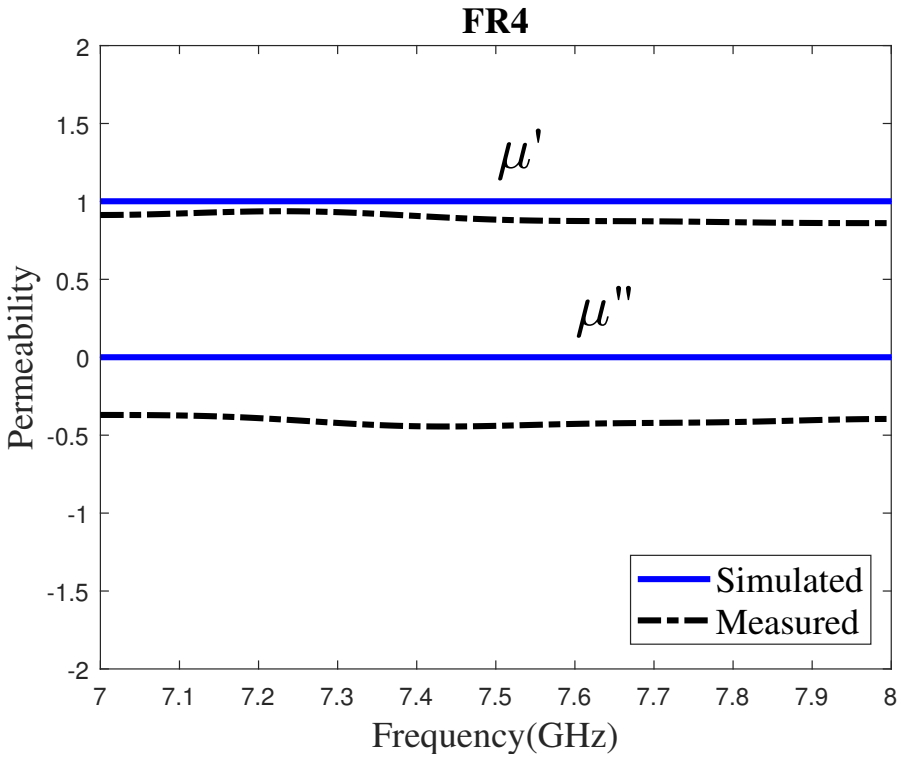

Figure 4.28: FR4 measured and simulated permeability at normal incidence.

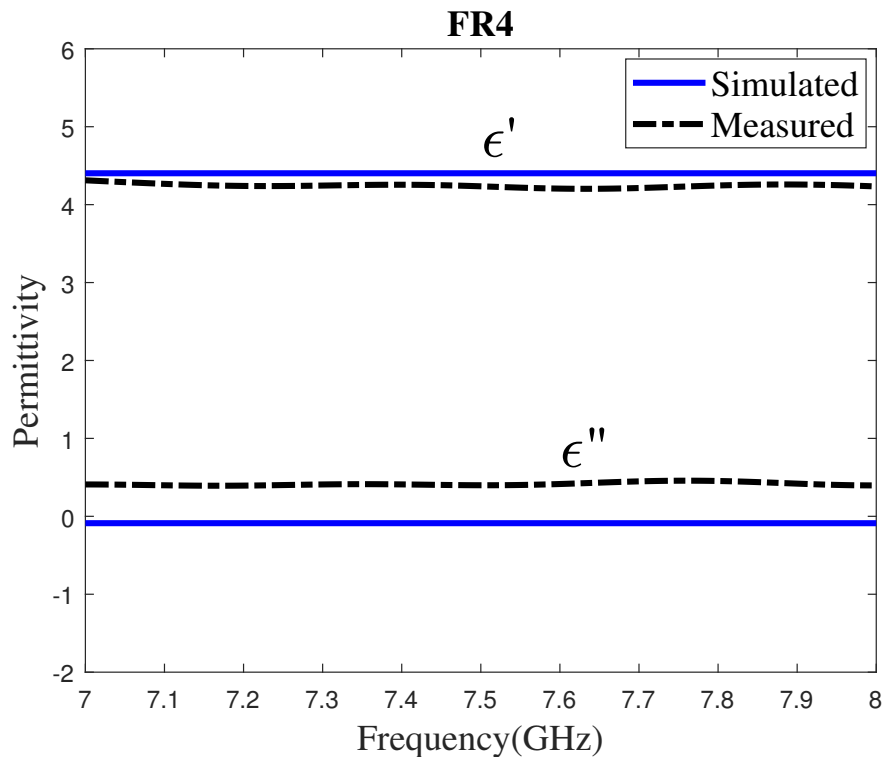

Figure 4.29: FR4 measured and simulated permittivity at normal incidence.

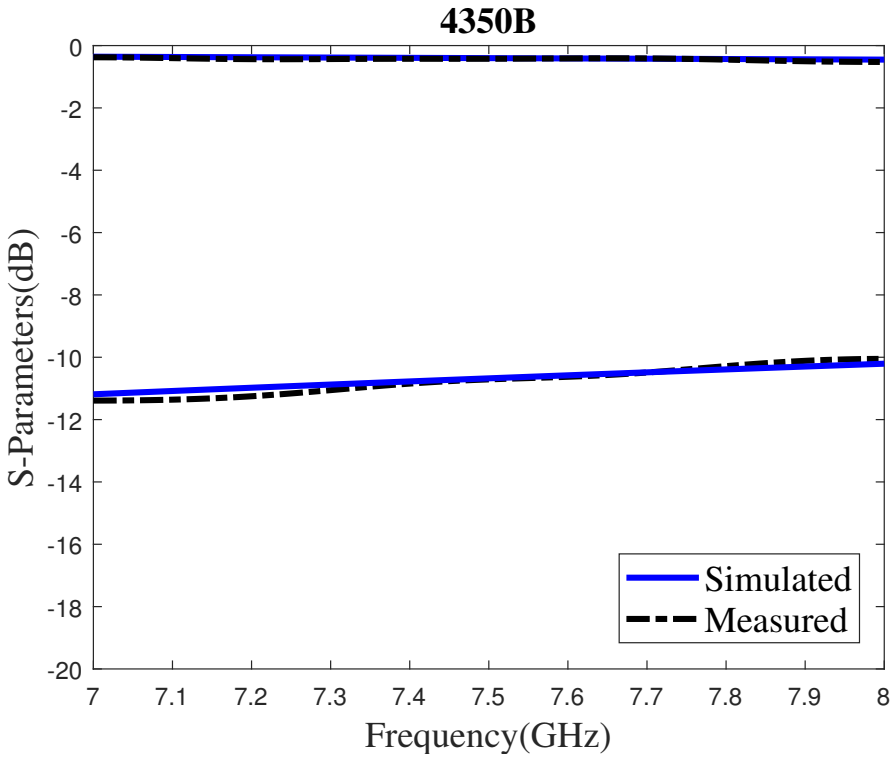

Figure 4.30: 4350B measured and simulated S-parameters at normal incidence.

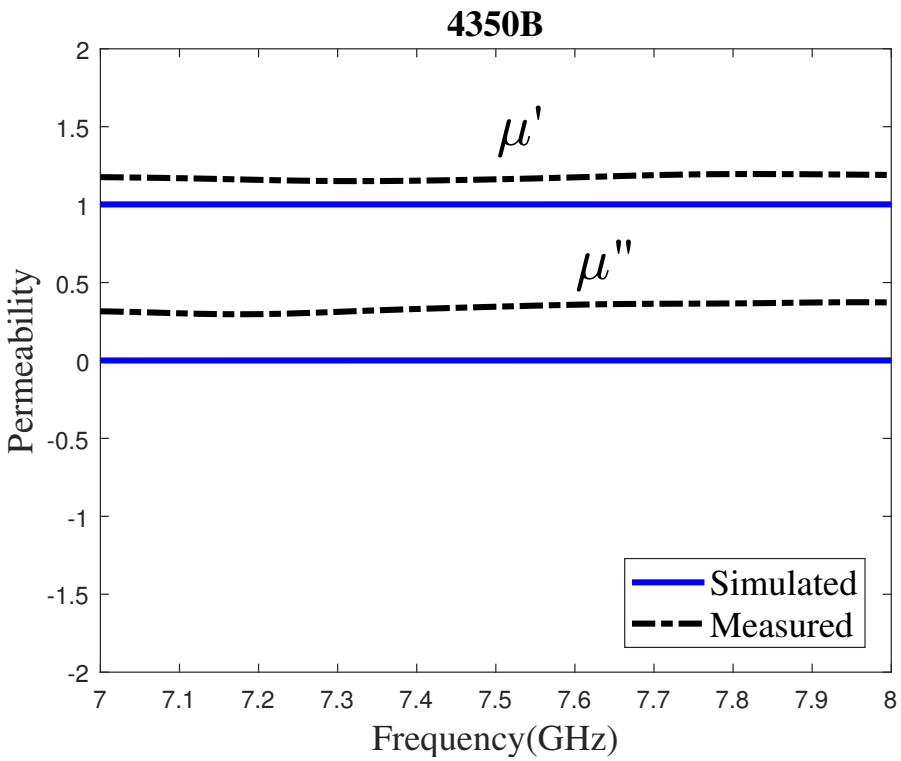

Figure 4.31: 4350B measured and simulated permeability at normal incidence.

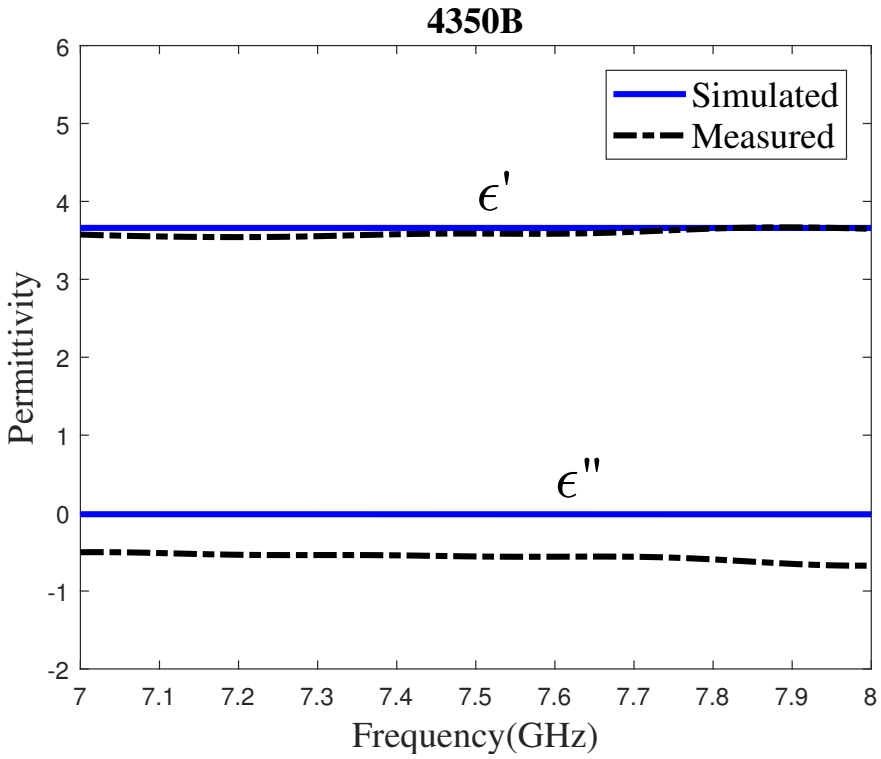

Figure 4.32: 4350B measured and simulated permittivity at normal incidence.

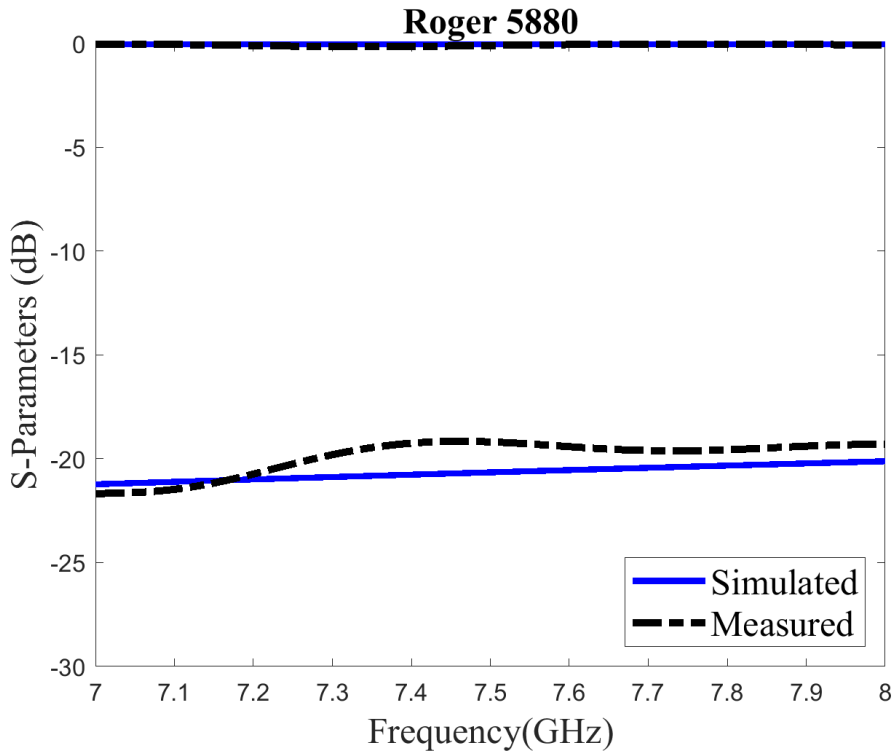

Figure 4.33: 5880 measured and simulated S-parameters at normal incidence.

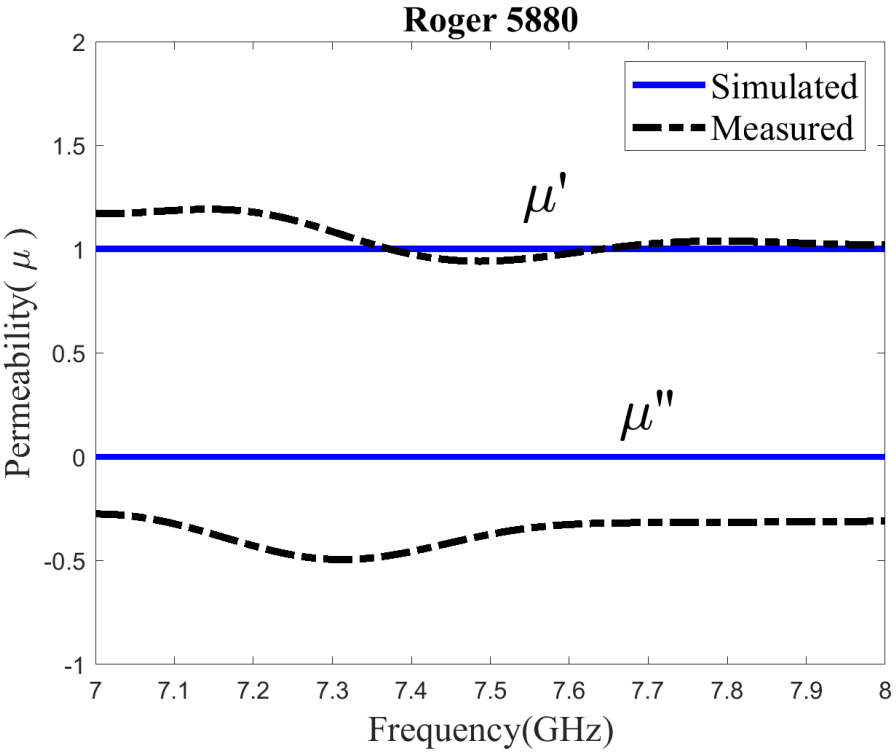

Figure 4.34: 5880 measured and simulated permeability at normal incidence.

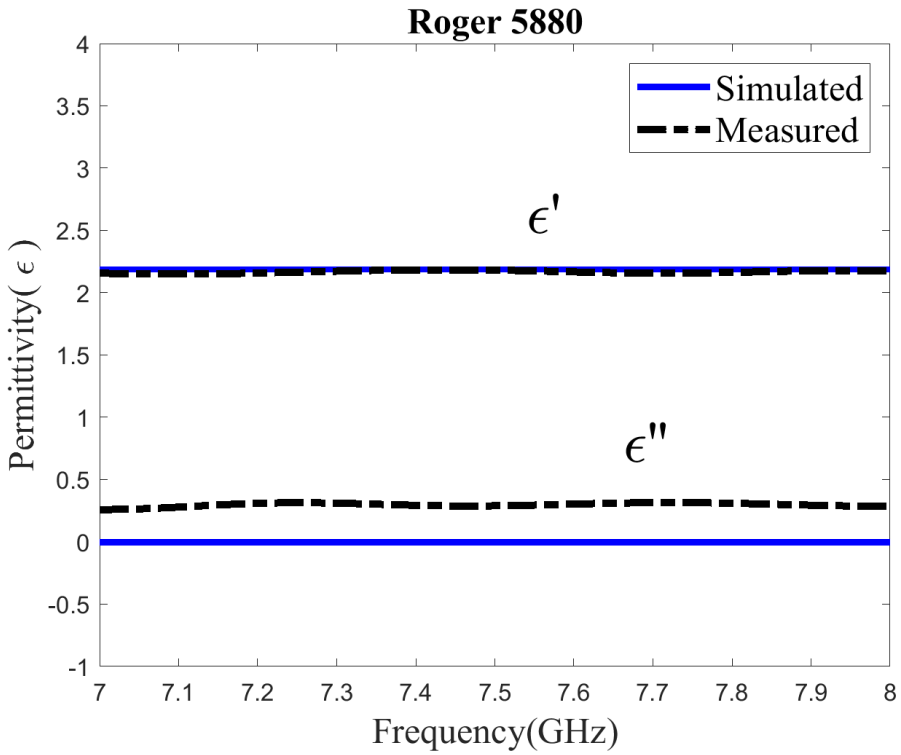

Figure 4.35: 5880 measured and simulated permittivity at normal incidence.

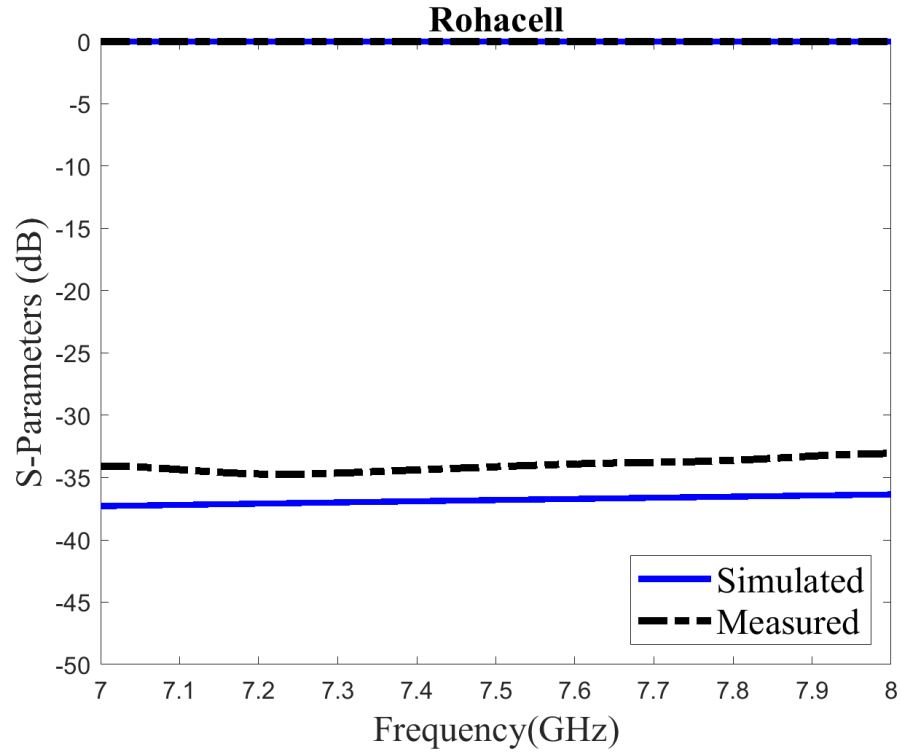

Figure 4.36: Rohacell measured and simulated S-parameters at normal incidence.

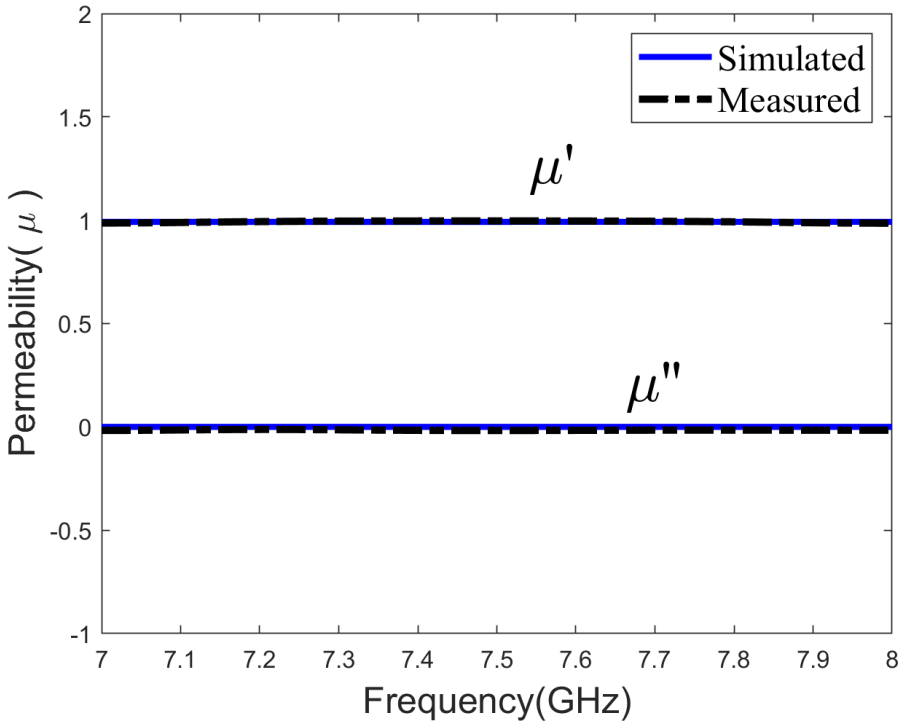

Figure 4.37: Rohacell measured and simulated permeability at normal incidence.

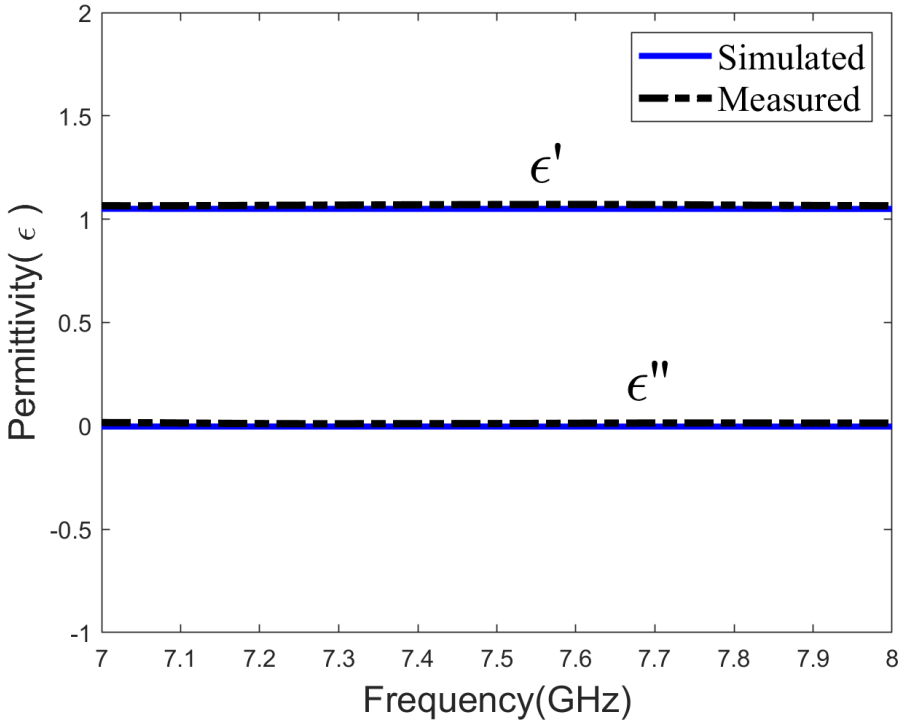

Figure 4.38: Rohacell measured and simulated permittivity at normal incidence.

The results of the oblique incidence testing for FR4 are presented below in Figures 4.39 and 4.39. In particular, Figure 4.39 shows the measured and simulated S-parameters of FR4 at 7.5 GHz with respect to incidence angle. These measurements were made at 0^o, 30^o, 45^o, and 60^o.

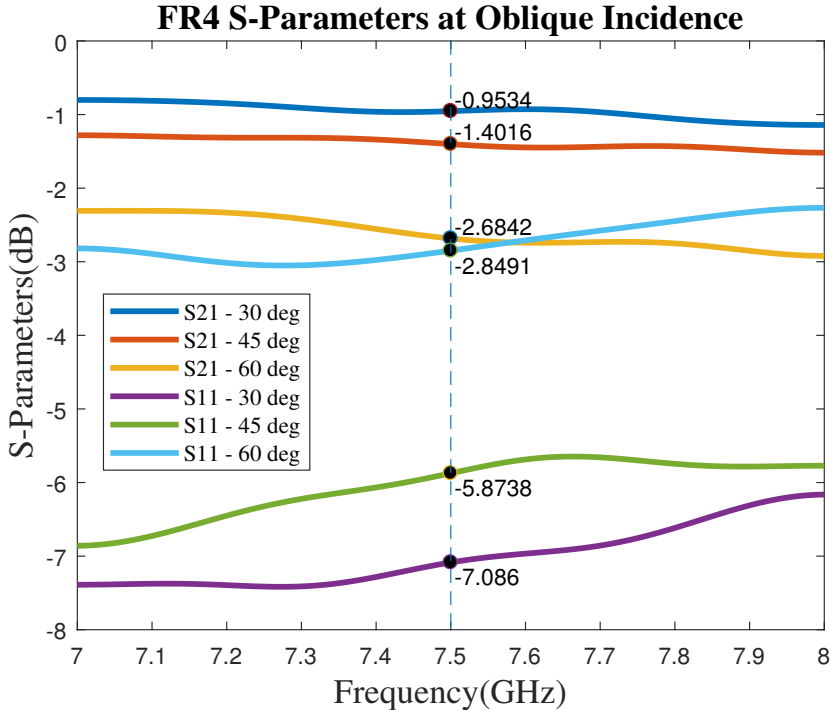

Figure 4.39: Measured S-parameters with respect to incidence angle.

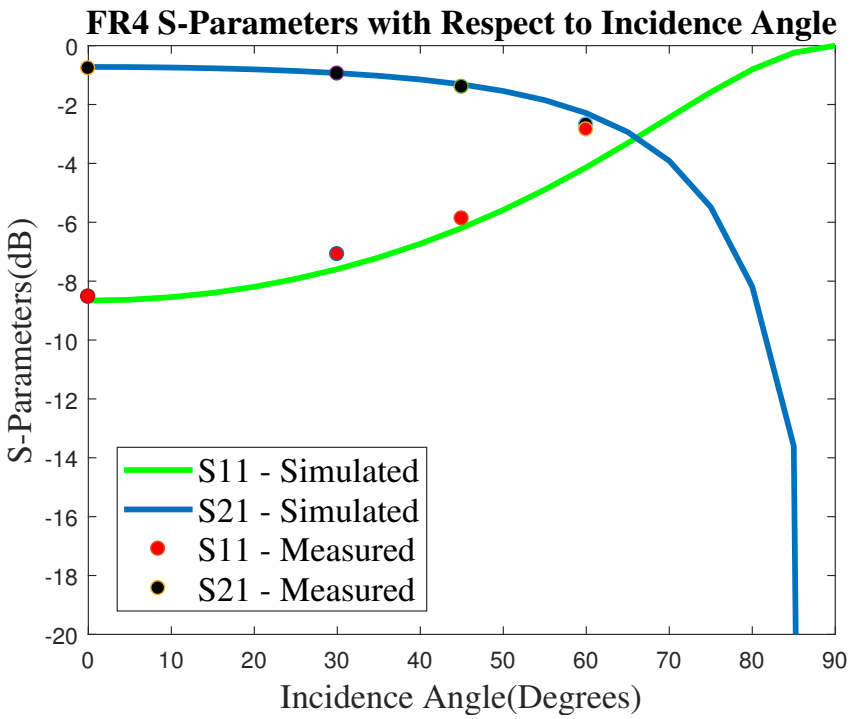

Figure 4.40: FR4 measured and simulated S-parameters with respect to incidence angle.

The results of the oblique incidence testing for the custom frequency selective surface are presented below in Figures 4.41. These results show the measured and simulated S-parameters of the frequency selective surface at 7.5 GHz with respect to incidence angle. These measurements were made at 0^o, 15^o, 30^o, 45^o, and 60^o.

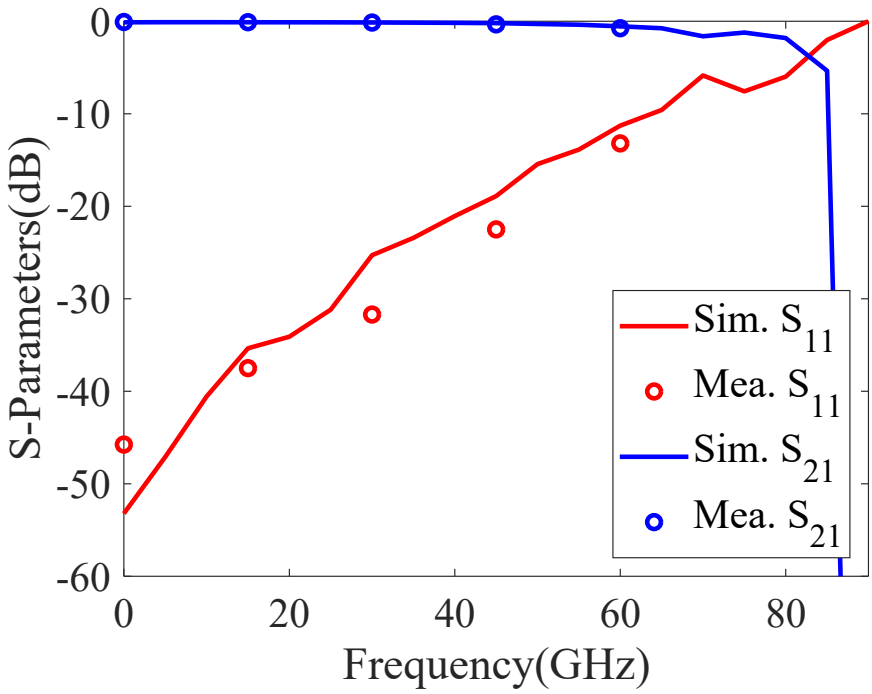

Figure 4.41: Frequency selective surface measured and simulated S-parameters with respect to incidence angle.

For both FR4 (isotropic medium) and the frequency selective surface (anisotropic medium), the oblique incidence measurements and observed data trends match the simulated values very well. These results are extremely promising, and demonstrate (in conjunction with the findings of [89], [90], [91], [92], [93], and [94]) the ability of the system to fully characterize both isotropic and anisotropic materials at oblique angles of incidence.

4.8 Summary

In this chapter, the new system developed for this thesis was presented. This began with a discussion of the issues that exist with current systems that drove the

development of this new system, followed by an overview of the method being proposed. The design and assembly of the newly developed system was then described. This included discussions of the intial concept drawing, each major design iteration, and the fully assembled system. The proof of concept testing was then described, including descriptions of the samples that were tested as well as the calibration procedures, test procedures, and extraction/post-processing that was applied. Finally, the results of the proof of concept testing were presented. These results were very positive, demonstrating the capabilities of the system and successfully proving the concept.

Chapter 5

Conclusion

5.1 Conclusion

This thesis project focused on the conceptualization, design, assembly, and initial testing of a novel system for the electromagnetic characterization of materials. The purpose of this system is to allow for free space characterization of the electrical permittivity and magnetic permeability of materials at both normal and oblique angles of incidence, with the ultimate goal of being able to characterize anisotropic metamaterials. At this stage of the project, the testing was limited to proof of concept testing conducted on several isotropic dielectrics and one anisotropic medium (a frequency selective surface). Additional testing will be conducted on anisotropic materials in future stages of the project, after the system has been thoroughly characterized.

The conceptualization and design of the new system were completed successfully. This design consisted of a central mounting structure with an elevated rotary table and attached sample holder. Connected to the central mounting structure are three rotatable antenna mounts each consisting of one horizontal and one vertical linear actuator. Each antenna mount supports one waveguide fed polyrod antenna connected to a vector network analyzer. This system design allows for automated

control of the height and seperation of the antennas, as well as manual control of the incidence angle of the propagating wave. The use of the polyrod antennas means that the system can directly operate in the far-field range without the need to use focussing lenses for plane wave approximation. The use of a three antenna design allows for the measurement of both the transmitted energy and the specular reflection in the case of oblique incidence, both of which are necessary for the characterization of a samples' permeability and permittivity. The combination of the linear actuators, polyrod antennas, and three antenna design have not previously been used together in this type of test system, making it a novel test system.

After completion and approval of the design, a budget of $10,000 was allotted for its development. The rotary table, VNA, and RF cables/components were provided by OU's PAARD team, and the remainder of the system was sourced for $6,000. Assembly and wiring of the system have both been successfully completed, and it is currently set up in OU's ARRC facility. The system successfully underwent proof of concept testing involving the characterization of four materials (FR4, 4350B, 5880, and Rohacell) at normal incidence, and the measurement of the transmission and reflection parameters of FR4 and a frequency selective surface at oblique incidence. During this testing, all measurements matched simulated results well, with only one significant source of error. This error was clearly caused by a phase offset in S_{11} almost certainly related to minor calibration path and sample offset errors. Such phase errors are common and well documented in free space material characterization test setups, and will be trivial to resolve in the next stages of the project. From

these results it is clear that the system performs as required and can be used for the full electromagnetic characterization of materials at oblique angles of incidence.

5.2 Future Work

At this stage in the project, the system has been designed, assembled, and successfully undergone proof of concept testing using isotropic dielectric materials. These are excellent results, and serve to demonstrate the potential of this novel system, but in order to fully utilize this system and extend it to the accurate characterization of anisotropic metamaterials at oblique incidence angles, additional work is required. In the next stage of the project, the observed phase error in S_{11} needs to be characterized and removed. Additionally, a Labview program should be developed to fully automate testing. This would help to reduce test times and limit potential user error.

The system should be augmented with the automated ability to rotate either the antennas or the sample under test. This could be accomplished using either small rotary tables or stepper motors. This would allow for reliable characterization along multiple ϕ cuts, which is necessary when the sample of interest is anisotropic. The system should also be improved with a better sample holder, ideally one that completely frames test samples and helps to ensure that they are perfectly flat and properly oriented. This would help to mitigate alignment errors caused by bending of the sample.

Additional work will also be required to improve the calibration procedure and extraction algorithm. The implementation of a 4-parameter calibration would help to limit the impact of alignment errors, as would the use of isolation standards. An iterative extraction algorithm should be implemented to help improve accuracy when testing materials whose approximate parameters are known. Also, NRW and Smith algorithms currently used should be improved with the incorporation of the Kramers-Kronig approximation in order to allow for thicker samples to be reliably tested.

Bibliography

[1] "Basics of Measuring the Dielectric Properties of Materials," tech. rep., Application Note 5989-2589EN, Keysight Technologies, 2017.

[2] J.-Y. Chung, *Broadband Characterization Techniques for RF Materials and Engineered Composites*. PhD thesis, Ohio State University, 2010.

[3] K. Saeed, R. D. Pollard, and I. C. Hunter, "Substrate integrated waveguide cavity resonators for complex permittivity characterization of materials," *IEEE Transactions on Microwave Theory and Techniques*, vol. 56, pp. 2340–2347, oct 2008.

[4] K. Buell, *Development of Engineered Magnetic Materials for Antenna Applications*. PhD thesis, University of Michigan, 2005.

[5] Baker-Jarvis and James, "Transmission/reflection and short-circuit line permittivity measurements," tech. rep., NIST, Washington, DC, 1990.

[6] S. Roberts and A. Von Hippel, "A New Method for Measuring Dielectric Constant and Loss in the Range of Centimeter Waves," *Journal of Applied Physics*, vol. 17, pp. 610–616, jul 1946.

[7] U. Lundgren, *Characterization of Components and Materials for EMC Barriers*. PhD thesis, Lulea University of Technology, 2004.

[8] A. G. Knisely, *Biaxial Anisotropic Material Development and Characterization using Rectangular to Square Waveguide*. PhD thesis, AIR FORCE INSTITUTE OF TECHNOLOGY, 2015.

[9] A. G. Knisely, M. W. Hyde, M. J. Havrilla, and P. J. Collins, "Uniaxial anisotropic material measurement using a single port waveguide probe," in *AMTA 2016 Proceedings*, (Austin, TX, USA), pp. 1–6, IEEE, oct 2016.

[10] B. Crowgey, J. Tang, O. Tuncer, L. Kempel, E. Rothwell, and B. Shanker, "Measurement of anisotropic material properties for antenna applications," in *2012 Loughborough Antennas & Propagation Conference (LAPC)*, pp. 1–4, IEEE, nov 2012.

[11] F. Costa, M. Borgese, M. Degiorgi, and A. Monorchio, "Electromagnetic Characterisation of Materials by Using Transmission/Reflection (T/R) Devices," *Electronics*, vol. 6, p. 95, nov 2017.

[12] R. A. Fenner, E. J. Rothwell, and L. L. Frasch, "A comprehensive analysis of free-space and guided-wave techniques for extracting the permeability and permittivity of materials using reflection-only measurements," *Radio Science*, vol. 47, feb 2012.

[13] J. Obrzut, A. M. Hassan, and E. J. Garboczi, "Free Space Microwave Non Destructive Characterization of Composite Materials — NIST," in *NDT of Composites 2015*, vol. 2015, NIST, may 2015.

[14] D. Ghodgaonkar, V. Varadan, and V. Varadan, "A free-space method for measurement of dielectric constants and loss tangents at microwave frequencies," *IEEE Transactions on Instrumentation and Measurement*, vol. 38, pp. 789–793, jun 1989.

[15] D. R. Smith, D. C. Vier, T. Koschny, and C. M. Soukoulis, "Electromagnetic parameter retrieval from inhomogeneous metamaterials," *Physical Review E - Statistical, Nonlinear, and Soft Matter Physics*, vol. 71, p. 11, mar 2005.

[16] Ó. García-Pérez, F. Tercero, and S. López-Ruiz, "Free-space W-band setup for the electrical characterization of materials and mm-wave components," tech. rep., 2017.

[17] D. Zaluški, A. Grbic, and S. Hrabar, "Analytical and experimental characterization of metasurfaces with normal polarizability," *Physical Review B*, vol. 93, p. 155156, apr 2016.

[18] H.-C. Yin, Z.-M. Chao, and Y.-P. Xu, "A new free-space method for measurement of electromagnetic parameters of biaxial materials at microwave frequencies," *Microwave and Optical Technology Letters*, vol. 46, pp. 72–78, jul 2005.

[19] C. E. Kintner, *Free-Space Measurements of Dielectrics and Three-Dimensional Periodic Metamaterials*. PhD thesis, University of Arkansas, 2017.

[20] W. Fwen, S. Ping, M. F. Abd Malek, and N. Hasss, "Alternatives for PCB Laminates: Dielectric Properties' Measurements at Microwave Frequencies," in *Dielectric Material* (M. I. Silaghi, ed.), ch. 5, InTech, oct 2012.

[21] M. A. Silaghi, ed., *Dielectric Material*. InTech, oct 2012.

[22] J. W. Schultz, *Focused Beam Methods Measuring Microwave Materials in Free Space*. 2012.

[23] L. E. Rickard Petersson and G. S. Smith, "On the use of a Gaussian beam to isolate the edge scattering from a plate of finite size," *IEEE Transactions on Antennas and Propagation*, vol. 52, pp. 505–512, feb 2004.

[24] Z. Cui, Y. Han, and H. Zhang, "Scattering of an arbitrarily incident focused Gaussian beam by arbitrarily shaped dielectric particles," *Journal of the Optical Society of America B*, vol. 28, pp. 2625–2632, nov 2011.

[25] R. J. Wylde, G. S. Bell, and A. Murk, "Sample size limitations for frequency-swept free-space material characterization," in *2012 37th International Conference on Infrared, Millimeter, and Terahertz Waves*, pp. 1–1, IEEE, sep 2012.

[26] P. F. Goldsmith, *Quasioptical systems: Gaussian beam quasioptical propagation and applications*. IEEE Press, 1998.

[27] J. L. Vedral, *Analysis, Characterization and Application of Microwave Metamaterials*. PhD thesis, University of Colorado at Colorado Springs, 2016.

[28] A.-S. Popescu, I. Bendoym, T. Rexhepi, and D. Crouse, "ANISOTROPIC ZERO INDEX MATERIAL: A METHOD OF REDUCING THE FOOTPRINT OF VIVALDI ANTENNAS IN THE UHF RANGE," *Progress In Electromagnetics Research C*, vol. 65, pp. 33–43, 2016.

[29] C. E. Kriegler, M. S. Rill, S. Linden, and M. Wegener, "Bianisotropic Photonic Metamaterials," *IEEE Journal of Selected Topics in Quantum Electronics*, vol. 16, no. 2, pp. 367–375, 2010.

[30] R. W. Ziolkowski, "Design, fabrication, and testing of double negative metamaterials," *IEEE Transactions on Antennas and Propagation*, vol. 51, pp. 1516–1529, jul 2003.

[31] J. Shin, A. Akyurtlu, M. Deshpande, and R. W. Ziolkowski, "Comments on "design, fabrication, and testing of double negative metamaterials"," feb 2005.

[32] R. W. Ziolkowski, "Author reply to comments on "Design, fabrication, and testing of double negative metamaterials"," *Antennas and Propagation, IEEE Transactions on*, vol. 53, pp. 891–892, feb 2005.

[33] S. K. Ghosh, S. K. Parui, and A. Chatterjee, "Development of novel engineered metamaterial: Structure, extraction of various parameters and applications," in *2017 1st International Conference on Electronics, Materials Engineering and Nano-Technology, IEMENTech 2017*, pp. 1–6, IEEE, apr 2017.

[34] S. J. Orfanidis, *Electromagnetic Waves and Antennas*. 2004.

[35] C. C. Njoku, W. G. Whittow, and J. C. Vardaxoglou, "Simulation Methodology for Synthesis of Antenna Substrates With Microscale Inclusions," *IEEE Transactions on Antennas and Propagation*, vol. 60, pp. 2194–2202, may 2012.

[36] A. Dalkiliç, *ANALYSIS AND DESIGN OF CONFORMAL FREQUENCY SELECTIVE SURFACES A THESIS SUBMITTED TO THE GRADUATE SCHOOL OF NATURAL AND APPLIED SCIENCES OF MIDDLE EAST TECHNICAL UNIVERSITY*. PhD thesis, MIDDLE EAST TECHNICAL UNIVERSITY, 2014.

[37] D. Seetharamdoo, R. Sauleau, K. Mahdjoubi, and A. C. Tarot, "Anomalous frequency range of effective parameters of resonant negative refractive index metamaterials," in *ANTEM 2005 - 11th International Symposium on Antenna Technology and Applied Electromagnetics, Conference Proceedings*, pp. 1–4, IEEE, jun 2005.

[38] M. G. Silveirinha, "Generalized Lorentz-Lorenz formulas for microstructured materials," *Physical Review B*, vol. 76, p. 245117, dec 2007.

[39] H. S. Sehmi, W. Langbein, and E. A. Muljarov, "Optimizing the drude-lorentz model for material permittivity: Examples for semiconductors," in *Progress in Electromagnetics Research Symposium*, pp. 994–1000, 2017.

[40] C. A. Gonano and R. E. Zich, "Drude-Lorentz model in circuit form," in *8th European Conference on Antennas and Propagation, EuCAP 2014*, pp. 1518–1521, IEEE, apr 2014.

[41] H. Wei, S. Lihua, X. Qiwei, and L. Feng, "Shielding effectiveness estimation for concrete slabs based on measured frequency dependent dielectric constant," in *2015 7th Asia-Pacific Conference on Environmental Electromagnetics (CEEM)*, pp. 309–312, IEEE, nov 2015.

[42] A. Solovey, M. Wasson, and R. Mittra, "Measurement of Conductive Magneto-Dielectric Material Parameters in High Noise Environment," in *2011 41st European Microwave Conference*, (Manchester, UK), IEEE, 2011.

[43] A. Solovey and R. Mittra, "Measurement of thin conductive dielectric coating material parameters in a high noise environment," *International Journal of RF and Microwave Computer-Aided Engineering*, vol. 23, pp. 452–458, jul 2013.

[44] A. Solovey, M. Wasson, and R. Mittra, "Free space transmission loss measurement of magneto-dielectric materials: Solution uniqueness and measurement tolerance tradeoffs," in *The 40th European Microwave Conference*, (Paris, France), IEEE, 2010.

[45] J. Schultz, J. Maloney, K. Maloney, and R. Schultz, "A Comparison of Material Measurement Accuracy of RF Spot Probes to a Lens-Based Focused Beam System," in *AMTA 36th Annual Meeting and Symposium*, 2014.

[46] R. Fenner and E. Rothwell, "Deficiency in the error propagation method for sensitivity analysis of free space material characterization," in *Antenna Technology and Applied Electromagnetics (ANTEM), 2012 15th International Symposium on*, no. 1, pp. 1–3, IEEE, jun 2012.

[47] M. Kaniecki, E. Saenz, L. Rolo, R. Appleby, and O. Breinbjerg, "Scattering-parameter extraction and calibration techniques for RF free-space material characterization," in *8th European Conference on Antennas and Propagation, EuCAP 2014*, pp. 1093–1097, IEEE, apr 2014.

[48] G. F. Engen and C. A. Hoer, "Thru-Reflect-Line: An Improved Technique for Calibrating the Dual Six-Port Automatic Network Analyzer," *IEEE Transactions on Microwave Theory and Techniques*, vol. 27, pp. 987–993, dec 1979.

[49] A. M. Hassan, J. Obrzut, and E. J. Garboczi, "A Q-Band Free-Space Characterization of Carbon Nanotube Composites," *IEEE Transactions on Microwave Theory and Techniques*, vol. 64, pp. 3807–3819, nov 2016.

[50] I. Rolfes and B. Schiek, "Calibration methods for microwave free space measurements," *Advances in Radio Science*, vol. 2, pp. 19–25, may 2005.

[51] P. G. Bartley and S. B. Begley, "A new free-space calibration technique for materials measurement," in *2012 IEEE International Instrumentation and Measurement Technology Conference Proceedings*, (Graz, Austria), pp. 47–51, IEEE, may 2012.

[52] H. J. Eul and B. Schiek, "A Generalized Theory and New Calibration Procedures for Network Analyzer Self-Calibration," *IEEE Transactions on Microwave Theory and Techniques*, vol. 39, pp. 724–731, apr 1991.

[53] H. J. Eul and B. Schiek, "Reducing the Number of Calibration Standards for Network Analyzer Calibration," *IEEE Transactions on Instrumentation and Measurement*, vol. 40, no. 4, pp. 732–735, 1991.

[54] U. Stumper, "Uncertainties of VNA S-Parameter Measurements Applying the TAN Self-Calibration Method," *IEEE Transactions on Instrumentation and Measurement*, vol. 56, pp. 597–600, apr 2007.

[55] U. Stumper and T. Schrader, "Influence of different configurations of non-ideal calibration standards on vector network analyzer performance," *IEEE Transactions on Instrumentation and Measurement*, vol. 61, pp. 2034–2041, jul 2012.

[56] U. Stumper and T. Schrader, "Calibration method for vector network analyzers using one or two known reflection standards," *IEEE Transactions on Instrumentation and Measurement*, vol. 63, pp. 1648–1655, jun 2014.

[57] A. H. Muqaibel, *Characterization of Ultra Wideband Communication Channels*. PhD thesis, Virginia Polytechnic Institute and State University, 2003.

[58] S. Arslanagić, T. V. Hansen, N. A. Mortensen, A. H. Gregersen, O. Sigmund, R. W. Ziolkowski, and O. Breinbjerg, "A review of the scattering-parameter extraction method with clarification of ambiguity issues in relation to metamaterial homogenization," *IEEE Antennas and Propagation Magazine*, vol. 55, pp. 91–106, apr 2013.

[59] L. J. Olule, G. Gnanagurunathan, and T. Nandha Kumar, "Electromagnetic metamaterial parameter retrieval methods: A review," in *RFM 2015 - 2015 IEEE International RF and Microwave Conference*, pp. 213–217, IEEE, dec 2016.

[60] A. M. Nicolson and G. F. Ross, "Measurement of the Intrinsic Properties Of Materials by Time-Domain Techniques," *IEEE Transactions on Instrumentation and Measurement*, vol. 19, pp. 377–382, nov 1970.

[61] W. B. Weir, "Automatic Measurement of Complex Dielectric Constant and Permeability at Microwave Frequencies," *Proceedings of the IEEE*, vol. 62, no. 1, pp. 33–36, 1974.

[62] A. N. Vicente, G. M. Dip, and C. Junqueira, "The step by step development of NRW method," in *2011 SBMO/IEEE MTT-S International Microwave and Optoelectronics Conference (IMOC 2011)*, pp. 738–742, IEEE, oct 2011.

[63] D. R. Smith, S. Schultz, P. Markoš, and C. M. Soukoulis, "Determination of effective permittivity and permeability of metamaterials from reflection and transmission coefficients," *Physical Review B*, vol. 65, no. 19, p. 5, 2002.

[64] X. Chen, B.-I. Wu, J. A. Kong, and T. M. Grzegorczyk, "Retrieval of the effective constitutive parameters of bianisotropic metamaterials," *Physical Review E*, vol. 71, p. 046610, apr 2005.

[65] B. P. Mishra, S. Sahu, S. K. Pathak, and S. K. Parashar, "An investigation on cross-shaped fishnet metamaterial for W-band radar application," in *2017 IEEE Calcutta Conference, CALCON 2017 - Proceedings*, vol. 2018-Janua, pp. 314–317, IEEE, dec 2018.

[66] A. N. Plastikov, "About two approaches to automation of a process of calculating metamaterial parameters according to the scattering-parameter extraction method using modern full-wave simulators," in *2017 Progress In Electromagnetics Research Symposium - Spring (PIERS)*, pp. 3763–3767, IEEE, may 2017.

[67] V. V. Varadan and R. Ro, "Unique retrieval of complex permittivity and permeability of dispersive materials from reflection and transmitted fields by enforcing causality," *IEEE Transactions on Microwave Theory and Techniques*, vol. 55, pp. 2224–2230, oct 2007.

[68] S. Kim, D. Novotny, J. Gordon, and J. Guerrieri, "A differential form of the Kramers-Kronig relation for determining a Lorentz-type of refractive index," in *IEEE Antennas and Propagation Society, AP-S International Symposium (Digest)*, vol. 2015-Octob, pp. 1174–1175, IEEE, jul 2015.

[69] I. B. Brezeanu, P. A. Paraschivoiu, R. Negroiu, and L. A. Chiva, "Applications of Kramers-Kronig Relations," in *2017 IEEE 23rd International Symposium for Design and Technology in Electronic Packaging (SIITME)*, pp. 82–85, IEEE, oct 2017.

[70] Z. Szabó, G. H. Park, R. Hedge, and E. P. Li, "A unique extraction of metamaterial parameters based on Kramers-Kronig relationship," *IEEE Transactions on Microwave Theory and Techniques*, vol. 58, pp. 2646–2653, oct 2010.

[71] J. J. Barroso and U. C. Hasar, "Comments on "A Unique Extraction of Metamaterial Parameters Based on Kramers-Kronig Relationship"," *IEEE Transactions on Microwave Theory and Techniques*, vol. 60, pp. 1743–1744, jun 2012.

[72] Z. Szabo, G. H. Park, R. Hedge, and E. P. Li, "Authors' Reply to "Comments on Unique Extraction of Metamaterial Parameters Based on Kramers–Kronig Relationship"," *IEEE Transactions on Microwave Theory and Techniques*, vol. 60, pp. 3634–3635, nov 2012.

[73] J. J. Barroso and U. C. Hasar, "Constitutive Parameters of a Metamaterial Slab Retrieved by the Phase Unwrapping Method," *Journal of Infrared, Millimeter, and Terahertz Waves*, vol. 33, pp. 237–244, feb 2012.

[74] A. Elhawil, G. Koers, L. Zhang, J. Stiens, and R. Vounckx, "Reliable method for material characterisation using quasi-optical free-space measurement in W-band," *IET Science, Measurement & Technology*, vol. 3, pp. 39–50, jan 2009.

[75] U. C. Hasar, G. Buldu, Y. Kaya, and G. Ozturk, "Determination of effective constitutive parameters of inhomogeneous metamaterials with bianisotropy," *IEEE Transactions on Microwave Theory and Techniques*, vol. 66, pp. 3734–3744, aug 2018.

[76] H. Esteban, J. M. Catala, S. Cogollos, and V. E. Boria, "Characterization of complex dielectric properties of materials using a hybrid iterative method," in *IEEE Antennas and Propagation Society International Symposium: Wireless Technologies and Information Networks, APS 1999 - Held in conjunction with USNC/URSI National Radio Science Meeting*, vol. 10, pp. 186–188, may 2000.

[77] P. Paul, F. G. Guimarães, and J. P. Webb, "Reducing the computational cost of inverse scattering problems with evolutionary algorithms," *IEEE Transactions on Magnetics*, vol. 45, pp. 1514–1517, mar 2009.

[78] I. T. Rekanos, T. V. Yioultsis, and C. S. Hilas, "An inverse scattering approach based on the differential E-formulation," *IEEE Transactions on Geoscience and Remote Sensing*, vol. 42, pp. 1456–1461, jul 2004.

[79] R. A. Fenner and S. Keilson, "Free space material characterization using genetic algorithms," in *2014 16th International Symposium on Antenna Technology and Applied Electromagnetics (ANTEM)*, pp. 1–2, IEEE, jul 2014.

[80] X. Zhang, T. Chang, H. L. Cui, Z. Sun, C. Yang, X. Yang, L. Liu, and W. Fan, "A Free-Space Measurement Technique of Terahertz Dielectric Properties," *Journal of Infrared, Millimeter, and Terahertz Waves*, vol. 38, pp. 356–365, mar 2017.

[81] I. Zivkovic and A. Murk, "Free-Space Transmission Method for the Characterization of Dielectric and Magnetic Materials at Microwave Frequencies," in *Microwave Materials Characterization*, ch. 5, InTech, nov 2012.

[82] E. Kemptner and S. Thurner, "Free space material characterization for microwave frequencies," in *2012 6th European Conference on Antennas and Propagation (EUCAP)*, pp. 3513–3515, IEEE, mar 2012.

[83] T. Ozturk, M. Hudlička, and Uluer, "Development of Measurement and Extraction Technique of Complex Permittivity Using Transmission Parameter S 21 for Millimeter Wave Frequencies," *Journal of Infrared, Millimeter, and Terahertz Waves*, vol. 38, pp. 1510–1520, dec 2017.

[84] T. Martin and B. Vallhagen, "A novel method to increase the accuracy of material characterization using free space transmission measurements," in *2017 International Conference on Electromagnetics in Advanced Applications (ICEAA)*, pp. 1608–1611, IEEE, sep 2017.

[85] R. Feio, *Material Parameter Extraction from Reflection Measurements*. PhD thesis, Universidade do Porto, 2017.

[86] V. V. Varadan, S. Puligalla, and R. Ro, "S-parameter measurements for oblique angles of incidence and Brewster angle studies for metamaterial samples," *Microwave and Optical Technology Letters*, vol. 48, pp. 2619–2624, dec 2006.

[87] Kai Du, *Permittivity Measurement of Circular Shell Using a Spot-Focused Free-Space System and Reflection Analysis of Open-ended Coaxial Line Radiating into a Chiral Medium*. PhD thesis, Pennsylvania State University, 2001.

[88] R. Johnk and A. Ondrejka, "Electrical material properties from a free-space time-domain RF absorber reflectivity measurement system," in *IEEE 1997, EMC, Austin Style. IEEE 1997 International Symposium on Electromagnetic Compatibility. Symposium Record (Cat. No.97CH36113)*, pp. 537–542, IEEE, 1997.

[89] D. Cohen and R. Shavit, "Bi-anisotropic Metamaterials Effective Constitutive Parameters Extraction Using Oblique Incidence S-Parameters Method," *IEEE Transactions on Antennas and Propagation*, vol. 63, pp. 2071–2078, may 2015.

[90] C. Menzel, C. Rockstuhl, T. Paul, F. Lederer, and T. Pertsch, "Retrieving effective parameters for metamaterials at oblique incidence," *Physical Review B*, vol. 77, p. 195328, may 2008.

[91] T. D. Karamanos and N. V. Kantartzis, "Effective parameter retrieval of 3D bianisotropic scatterer arrays for oblique propagation," in *2016 10th International Congress on Advanced Electromagnetic Materials in Microwaves and Optics, METAMATERIALS 2016*, pp. 154–156, IEEE, sep 2016.

[92] Y. Si and Z. Zhan, "Extraction of metamaterial parameters," in *2015 IEEE 6th International Symposium on Microwave, Antenna, Propagation, and EMC Technologies, MAPE 2015*, pp. 608–610, IEEE, oct 2016.

[93] A. Castanié, J.-F. Mercier, S. Félix, and A. Maurel, "Generalized method for retrieving effective parameters of anisotropic metamaterials," *Optics Express*, vol. 22, no. 24, 2014.

[94] H. J. Lee, H. S. Lee, P. S. Ma, and Y. Y. Kim, "Effective material parameter retrieval of anisotropic elastic metamaterials with inherent nonlocality," *Journal of Applied Physics*, vol. 120, p. 104902, sep 2016.

[95] J. Qi, H. Kettunen, H. Wallen, and A. Sihvola, "Different homogenization methods based on scattering parameters of dielectric-composite slabs," *Radio Science*, vol. 46, no. 5, pp. 1–7, 2011.

[96] C. Menzel, C. Rockstuhl, T. Paul, T. Pertsch, and F. Lederer, "Effective Parameters For Anisotropic Metamaterials," in *Conference on Lasers and Electro-Optics/International Quantum Electronics Conference*, (Washington, D.C.), pp. 1–2, OSA, 2009.

[97] C. A. Balanis, *Advanced engineering electromagnetics*. John Wiley & Sons, second edi ed., 2012.

[98] X. Huang, S. Yu, J. Chen, and H. Yang, "Ultra broadband metamaterial absorber with oblique incidence based on effective medium theory," in *ISAPE 2016 - Proceedings of the 11th International Symposium on Antennas, Propagation and EM Theory*, pp. 1–4, IEEE, oct 2017.

[99] L. C. Paul, M. A. Haque, M. A. Haque, M. M. U. Rashid, M. F. Islam, and M. M. Rahman, "Design a slotted metamaterial microstrip patch antenna by creating three dual isosceles triangular slots on the patch and bandwidth enhancement," in *2017 3rd International Conference on Electrical Information and Communication Technology (EICT)*, pp. 1–6, IEEE, dec 2017.

[100] S. Kim, E. F. Kuester, C. L. Holloway, A. D. Scher, and J. R. Baker-Jarvis, "EFFECTIVE MATERIAL PROPERTY EXTRACTION OF A METAMATERIAL BY TAKING BOUNDARY EFFECTS INTO ACCOUNT AT TE/TM POLARIZED INCIDENCE," *Progress In Electromagnetics Research B*, vol. 36, pp. 1–33, 2012.

[101] A. Alù, "First-principles homogenization theory for periodic metamaterials," *Physical Review B*, vol. 84, p. 075153, aug 2011.

[102] L. S. Bobrow, *Elementary linear circuit analysis*. New York: Holt, Rinehart, and Winston, 2nd ed. ed., 1987.

[103] F. Caspers, "RF Engineering Basic Concepts : S - Parameters," tech. rep., CERN, 2010.

[104] A. G. Knisely and M. J. Havrilla, "Material characterization de-embedding for rectangular to square waveguide," in *Antennas and Propagation (EuCAP), 2015 9th European Conference on.*, (Lisbon, Portugal), pp. 1–5, IEEE, 2015.

[105] Raenita Fenner, *Error Analysis of Reflection-Only Material Characterization Methods*. PhD thesis, Michigan State University, 2011.

[106] A. Mancini, J. L. Salazar, R. M. Lebron, and B. L. Cheong, "A novel technique to characterize the effect of rain over a radome for radar applications," in *2017 IEEE Radar Conference (RadarConf)*, pp. 0470–0475, IEEE, may 2017.

[107] A. Mancini, J. L. Salazar, R. M. Lebrón, B. L. Cheong, A. Mancini, J. L. Salazar, R. M. Lebrón, and B. L. Cheong, "A Novel Instrument for Real-Time Measurement of Attenuation of Weather Radar Radome Including Its Outer Surface. Part I: The Concept," *Journal of Atmospheric and Oceanic Technology*, vol. 35, pp. 953–973, may 2018.

[108] A. Mancini, J. L. Salazar, R. M. Lebrón, B. L. Cheong, A. Mancini, J. L. Salazar, R. M. Lebrón, and B. L. Cheong, "A Novel Instrument for Real-Time Measurement of Attenuation of Weather Radar Radome Including Its Outer Surface. Part II: Applications," *Journal of Atmospheric and Oceanic Technology*, vol. 35, pp. 975–991, may 2018.

[109] V. V. Varadan and Z. Sheng, "Direct Comparison of the Magnitude and Phase of Measured S-parameters of Metamaterials with Finite Element Simulation," in *2006 IEEE Antennas and Propagation Society International Symposium*, pp. 4587–4590, IEEE, 2006.

[110] X. Chen, T. M. Grzegorczyk, B. I. Wu, J. Pacheco, and J. A. Kong, "Robust method to retrieve the constitutive effective parameters of metamaterials," *Physical Review E - Statistical Physics, Plasmas, Fluids, and Related Interdisciplinary Topics*, vol. 70, no. 1, p. 7, 2004.